PhD

PROGRAM IN TRANSLATIONAL

AND MOLECULAR MEDICINE

DIMET

Functional analysis of AFG3L2 mutations causing spinocerebellar ataxia type 28 (SCA28)

Coordinator: Prof. Andrea Biondi
Tutor: Dr. Valeria Tiranti
Cotutor: Dr. Franco Taroni

Dr. Valentina Fracasso
Matr. No. 037096

XXIII CYCLE

ACADEMIC YEAR

2009-2010

A Andre

Table of Contents

Chapter 1: General Introduction

Ataxia 6

SCA28 14

Clinical Features 15

Linkage analysis 16

AFG3L2 20

Paraplegin…… 21

AFG3L1 22

m-AAA complex 24

The AAA+ superfamily 25

Structure of AAA metalloproteases 27

Role of AAA complexes in yeast 29

Function 30

Phenotype of mutations in yeast Saccharomyces cerevisiae 33

Substrates 34

Human *m*-AAA 38

Mouse models 40

Scope of the thesis 44

Reference list of chapter 1 45

Chapter 2:

Mutations in the mitochondrial protease gene AFG3L2 cause dominant hereditary ataxia SCA28 50

Supplementary Information for Mutations in the mitochondrial protease gene *AFG3L2* cause dominant hereditary ataxia SCA28 101

Co-immunoprecipitation of human mitochondrial proteases AFG3L2 and paraplegin heterologously expressed in yeast cells 138

Preparation of yeast mitochondria and in vitro assay of respiratory chain complex activities 147

Chapter 3:

Spinocerebellar ataxia type 28: identification and functional analysis of novel AFG3L2 mutations 158

Chapter 4: Summary, conclusions and future perspectives 203

Chapter 5: Publications 211

Chapter 1: General Introduction

Ataxia

Ataxia is a neurological dysfunction of motor coordination that can affect gaze, speech, gait and balance. The aetiology of ataxia encompasses toxic causes, metabolic dysfunction, autoimmunity, paraneoplastic and genetic factors. Hereditary forms are classified as: autosomal recessive and autosomal dominant. Two main mechanisms manifest autosomal recessive ataxias. Inactivating mutations result in loss of protein function, which affects control of energy output and oxidative stress (Friedreich ataxia (FRDA), ataxia with isolated vitamin E deficiency (AVED), Cayman ataxia) and control of DNA maintenance and the cell cycle (ataxia telangiectasia (AT), ataxia-OCULOMOTOR APRAXIA 1 and 2 (AOA1 and 2), spinocerebellar ataxia with axonal neuropathy (SCAN1)) (Taroni, & Di Donato, 2004).

Autosomal dominant spinocerebellar ataxias (SCAs, previously named ADCAs) are a clinically and genetically heterogeneous group of neurological disorders caused by degeneration of the cerebellum and its afferent and efferent connections (Taroni, & Di Donato, 2004-Koeppen, 2005). Patients exhibit a cerebellar syndrome characterized by imbalance, progressive gait and limb ataxia, and dysarthria (Schols, et al., 2004, Harding, 2004). Since the degenerative process is often not limited to the cerebellum, the clinical phenotype may appear complicated by

the presence of additional neurological signs (pyramidal and extrapyramidal signs, ophthalmoparesis, dementia, pigmentary retinopathy, peripheral neuropathy, cognitive decline, and psychiatric manifestations), which are highly variable among and within families (Schols, et al., 2004).

Since the identification of the first gene responsible for spinocerebellar ataxia type 1 (SCA1) in 1993 (Zoghbi, & Orr, 2000), an increasing number of genes and chromosomal loci have been characterized, demonstrating large genetic heterogeneity in these hereditary disorders (Duenas, et al, 2006). Thirty-one SCA loci are currently known: SCA1-8, SCA10-15, SCA 17-23, SCA25-28, SCA30-31 and the genetic form designated as dentato-rubral-pallido-luysian atrophy (DRPLA) which is also commonly classified within this group of disorders (Duenas, et al, 2006)
(http://neuromuscular.wustl.edu/ataxia/domatax.html).

Eighteen unrelated disease genes have been identified thus far. In approximately 50% of cases with dominant ataxia (SCA1-2-3-6-7-17 and DRPLA), the molecular mutation is a CAG-triplet repeats in the coding region of the disease gene, which results in production of a mutant protein with a longer-than-normal polyglutamine stretch (Schols, et al., 2004, Brusco, et al, 2004, Orr & Zoghbi, 2007) The predominant effect of this mutation is thought to be a toxic gain-of-function of the aberrant protein (Taroni & Di Donato, 2004). In most polyQ diseases there is microscopic evidence of pathogenic protein aggregates in the cytoplasm and nucleus of affected neurons. These neuronal

intranuclear inclusions are hallmarks of neurodegeneration in the brains of patients with SCA1, SCA3, SCA7, SCA17 and DRPLA (Taroni & Di Donato, 2004). Longer expansions are associated with earlier onset and more severe disease in subsequent generations.

Disorder	Chromosomal Location	Gene	Mutations	Main clinical features
Polyglutamine expansions SCAs				
SCA 1	6p23	*ATXN1*ataxin-1	CAG repeats	Ataxia, extrapyramidal symptoms, spasticity, ophthalmoparesis, slow saccades, axonal polyneuropathy, cognitive impairment
SCA 2	12p24	*ATXN2* ataxin-2	CAG repeats	Ataxia, parkinsonism, extrapyramidal symptoms, spasticity, ophthalmoparesis, slow saccades, axonal polyneuropathy

Disorder	Chromosomal Location	Gene	Mutations	Main clinical features
SCA 3	14q32.1	*ATXN3* ataxin-3	CAG repeats	Ataxia, parkinsonism, extrapyramidal features, spasticity (severe), ophthalmoparesis, disease axonal polyneuropathy
SCA 6	19p13	*CACNA1A* P/Q-type calcium channel a1A subunit	CAG repeats	Prominent cerebellar features (ataxia, dysarthria, nystagmus, tremor)
SCA 7	3p14	*ATXN7* ataxin-7	CAG repeats	Ataxia, retinal degeneration, ophthalmoplegia, pyramidal signs, hearing loss, no peripheral nerve pathology. Infantile variant (hypotonia, development delay, microcephaly, visual loss, fatal cardiac failure)
SCA 17	6q27	TBP TATA box-binding protein	CAG repeats	Ataxia, psychosis and behavioural changes, dystonia, parkinsonism, mental deterioration, seizures

Disorder	Chromosomal Location	Gene	Mutations	Main clinical features
DRPLA	12p13.31	*ATN1* atrophin-1	CAG repeats	Myoclonus epilepsy, ataxia, chorea, dementia, subcortical demyelination (Haw-River syndrome)
Non-coding expansion SCAs				
SCA 8	13q21	*ATXN8* and *ATXN8OS*	CTG repeat (3´UTR)	Ataxia, spasticity, sensory neuropathy
SCA10	22q13	*ATXN10* Ataxin 10	ATTCT repeat (intronic)	Prominent cerebellar features (ataxia, dysarthria, nystagmus, tremor), seizures
SCA 12	5p31	*PPP2R2B* regulatory subunit b protein phosphatase 2	CAG repeats (5´UTR)	Ataxia, extrapyramidal features, polyneuropathy, facial myokimia, dementia
SCA31=16qlinked	16q22.1	*BEAN-TK2*	TGGAA repeat	Ataxia, dysmetria, dysarthria, abnormal fine finger movements, hypotonia
Conventional mutations SCAs				
SCA5	11q13	*SPTBN2* β-III Spectrin	Missense, in-frame deletion	Ataxia, nystagmus, dysarthria, facial myokymia

Disorder	Chromosomal Location	Gene	Mutations	Main clinical features
SCA11	15q14	*TTBK2* tau tubulin kinase 2	Frameshift	Ataxia, nystagmus, dysarthria , hyperreflexia
SCA13	19q13.3-q13.4	*KCNC3* Potassium channel, voltage-gated, shaw-related subfamily, member 3	Missense mutations	Ataxia, dysarthria, nystagmus, mental retardation
SCA14	19q13.4	*PRKCG* protein kinase Cg	Missense mutations	Ataxia, myoclonus, dystonia, peripheral neuropathy
SCA15/16	3p26-p25	*ITPR1* Inositol 1,4,5-triphosphate receptor, type 1	Missense, deletion	Ataxia, dysarthria, nystagmus
SCA 23	20p13	*PDYN* Prodynorphin	Missense mutations	Ataxia, pyramidal signs
SCA27	13q34	*FGF14* fibroblast growth factor 14	Missense, frameshift	Ataxia, tremor, orofacial dyskinesia, psychiatric manifestations, cognitive impairment,axonal peripheral neuropathy

Table 1: Genes and mutations that cause autosomal dominant cerebellar ataxias, according to locus and mutation type

Noncoding repeat expansions (SCA8-10-12-31) and other dominant mutations [missense mutations (SCA5-13-14-23-27), frameshift mutations (SCA11), and deletions (SCA15)] have been identified in a smaller group of cases (Taroni & Di Donato, 2004, Duenas et al, 2006).

Little is known about the genes that currently cause the majority of genetically defined SCA subtypes and have revealed the complex heterogeneity of the pathogenic mechanisms leading to cerebellar degeneration and ataxia.

In the rest of SCAs, the genes and, therefore, the mutations remain to be identified and characterized. We only know the chromosome location (Duenas et al, 2006).

Disorder	**Chromosomal Location**
SCA 18	7q31-q32
SCA 19	1p21-q21
SCA 20	11p13-q11
SCA21	7p21.3-p15.1
SCA 22	1p21-q23
SCA 25	2p21-p13
SCA 26	19p13.3
SCA30	4q34.3-q35.1

Table 2: chromosome location autosomal dominant cerebellar ataxias

The prevalence of SCAs has been estimated to be approx. 3 in 100,000, but the relative frequency of specific genotypes may vary in different geographical areas and in populations of different ethnic origins (Schols et al., 2004, Brusco et al, 2004, Duenas et al, 2006).

The distribution of SCA gene mutations is peculiar in Italy. A relatively high frequency of SCA1 and SCA2 gene expansions; SCA3, SCA6, SCA7 and SCA17 and DRPLA mutations were rare, compared with other European countries. No SCA10 or SCA12 and only a few SCA8 and SCA17 families are detected (Brusco et al, 2004).

SCA28

In the last two decades, the Unit of Genetics of Neurodegenerative and Metabolic Diseases of the Fondazione IRCCS Carlo Besta Neurological Institute has been responsible for the analysis of currently known SCA gene mutations. The population screening for the currently known SCA gene mutations has demonstrated that ~40% of the clinically identified ADCA families remain genetically unassigned, indicating further genetic heterogeneity, in agreement with literature data (Schols et al., 2004- Brusco et al, 2004).
Research studies are necessary to identify genes involved in the pathogenesis of the disease.

We have analysed 225 families negative for the known SCA genes (SCA 1-2, SCA3, SCA6, SCA7, SCA17 and DRPLA). The families selected for this research had to meet the following selection criteria: ataxia as the principal neurological symptom, disease progression, and a positive family history.
In these families, the Repeat Expansion Detection (RED) analysis excluded the presence CAG/CTG expansions >40 repeats, and linkage exclusion tests showed no evidence of linkage to most of the known SCA loci (SCA4, SCA5/20, SCA11, SCA13-16, SCA18, SCA19/22, SCA21, SCA25 and SCA27), suggesting a genetically distinct form of SCA.
A four-generation Italian family had been identified with a total of 30 members, including 14 affected individuals. This family

was sufficient informative for statistical analysis and that it was possible to find the genetic material to performed a linkage analysis, to identification the locus involved in the pathogenesis of this form of ataxia (Cagnoli et al., 2006).

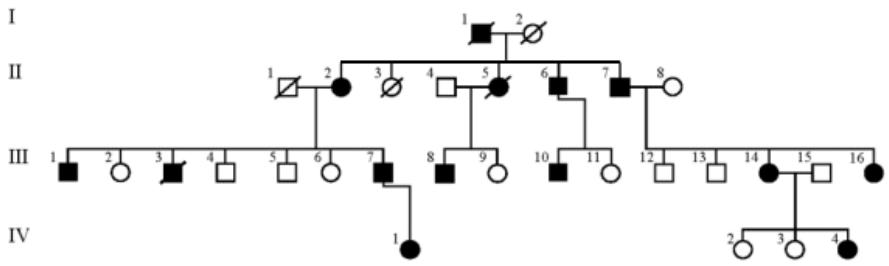

Figure. 1 Pedigree of the family with autosomal dominant spinocerebellar ataxia.

Clinical Features

This disease occurs in all affected members of the family as a dominant ataxia with juvenile-onset (The mean age at onset was 19.5 years, range 12–36). There is no anticipation in subsequent generations. The initial symptoms are unstable standing and ataxia and incoordination of limbs and gait. The disease is also characterized by abnormal eye movements: ophthalmoparesis and lateral and vertical gaze nystagmus, Babinski sign, hyperreflexia and pyramidal signs. Disease progression is very slow.

The clinical features were characteristic of ADCA type I as defined by Harding (Harding 1982), except for an unusually slow disease course (Mariotti et al, 2008).

Biochemical assays on muscle homogenates demonstrated normal activities of the respiratory chain enzymes (complexes I-V), and Southern blot analysis excluded the presence of mitochondrial DNA deletions (Cagnoli et al., 2006).

Linkage analysis

We have analyzed the entire genome of patients available for analysis (II-1-2-4-5-6-7-8, III-1-6-7-8-10-14-15-16-IV -1-4) using 383 fluorescent-labelled microsatellite commercial markers. Chromosome X was excluded because a male-to-male transmission was present, excluding automatically the presence of the mutation on this chromosome. The most suggestive evidence of linkage was obtained at two distinct non-consecutive markers on chromosome 18, one on the short arm (D18S53) and one on the long arm (D18S474). To confirm linkage in one of the two regions and for fine mapping, we tested 11 additional polymorphic markers (D18S843, D18S1418, D18S1150, D18S453, D18S1104, D18S1107, D18S66, D18S1143, D18S1126, D18S1127 and D18S69). The highest LOD scores were found in the first region between markers D18S1418 and D18S1104 with a maximum of $Z = 4.77$ at marker D18S453 in multipoint analysis. LOD scores in the second region, spanning markers D18S1102 and D18S69, were below the threshold of $Z = 3.3$ both in two point and multipoint tests. Two key recombination events, centromeric to D18S1418 in patient II-6 and to D18S1104 in patient III-8, defined the minimal in-linkage interval of 7.9 Mb on the short

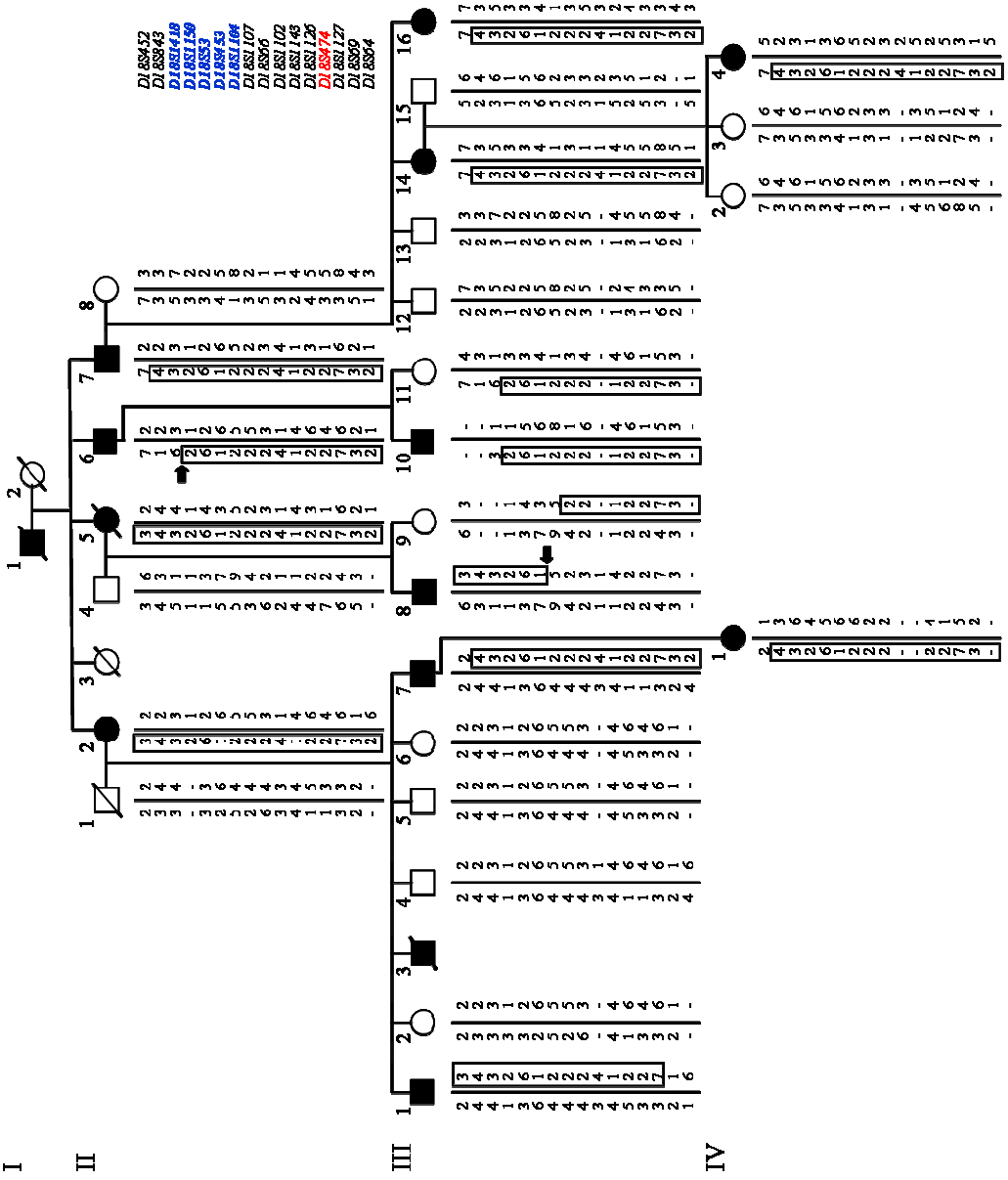

Figure. 2 Pedigree of the family with 16 non-consecutive markers on chromosome 18.

arm (18p11.22-q11.2). This genome-wide linkage analysis allowed us to map a new locus on chromosome region 18p11.22–q11.2, thus confirming that the disorder observed in this family represents a novel form of autosomal dominant SCA. Chromosome 18 has never been associated with hereditary cerebellar ataxias. This new locus has been assigned the SCA28 symbol by the Human Genome Nomenclature Committee (www.gene.ucl.ac.uk/hugo) (Cagnoli et al., 2006) (Mariotti et al., 2008).

This region contains approximately 70 genes (Human Genome Assembly NCBI35.1), none of which exhibits obvious similarity with any of the currently known genes causing dominant ataxias. A candidate gene approach based on expression in disease-affected tissues reduced the number of candidate genes to 12, including the gene encoding the mitochondrial metalloprotease AFG3L2 (ATPase family gene 3-like 2). Although no dominant ataxia has been thus far associated with mitochondrial dysfunction, we focused on this gene because of its partnership with paraplegin, a cognate mitochondrial protease, the loss of which causes a distinct neurodegenerative disorder, the recessively-inherited form of hereditary spastic paraplegia SPG7 (Banfi et al., 1999).

Genetic analysis of the critical region of the SCA28 locus has been conducted in all patients in this family; all the affected subjects are characterized by a missense mutation (E691K) in the exon 16 of the *AFG3L2* gene. In addition, the mutation is not found to be present in approximately 200 alleles of control

of the normal population. Showing that point mutations in *AFG3L2* are associated with dominant hereditary ataxia SCA28.

AFG3L2

ATPase Family Gene 3-Like 2 (AFG3L2) gene is composed of 17 exons, which encode a protein of 797 amino acids.

It was shown by immunofluorescence that AFG3L2 is a mitochondrial protein. This protein is present in the inner membrane of mitochondria and active on the matrix side (Banfi et al., 1999).

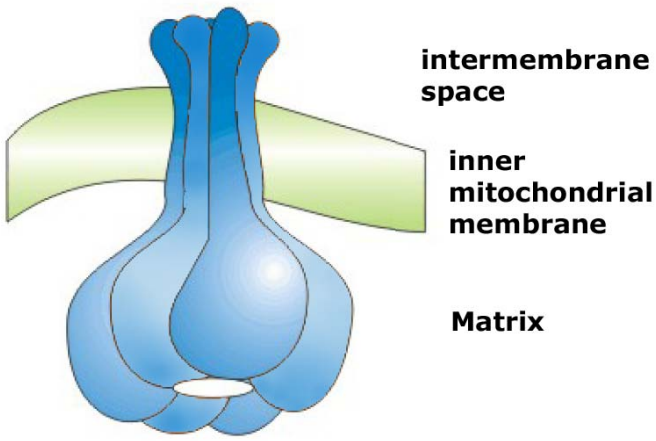

Figure 3: Localizing AFG3L2

The protein is evolutionarily highly conserved, particularly in certain domains characteristic.

Paraplegin

AFG3L2 is highly homologous to paraplegin (58.3% similarity and 49% identity), the product of the SPG7 gene. Mutations in the SPG7 gene are responsible for an autosomal recessive form of hereditary spastic paraplegia.

Hereditary spastic paraplegias (HSPs) are a group of neurodegenerative disorders characterized by progressive spasticity and weakness of the lower limbs, resulting from a length-dependent “dying back” axonopathy of the corticospinal tract. HSP may be pure or complex, depending on whether spastic paraplegia is the only symptom or whether it is associated with other clinical features such as peripheral neuropathy or cerebellar atrophy. These diseases are genetically heterogeneous and can be autosomal dominant, autosomal recessive, or X-linked. The SPG7 gene is located on chromosome 16q24.3, it is composed of 17 exons and encodes a 795 amino acid protein (Wilkinson et al 2004, Elleuch et al. 2006).

Both AFG3L2 and paraplegin are metalloproteases that are components of the mitochondrial AAA (*m*-AAA) protease. These proteases are known to exert chaperon-like activity and to participate in protein quality control.

It is very interesting to note the importance of *m*-AAA in humans, underlined by the evidence that mutations in both genes are responsible for important neurodegenerative diseases: mutations in AFG3L2 cause an autosomal dominant

spinocerebellar ataxia type 28 (SCA28) while mutations in the *SPG7* gene encoding paraplegin cause an autosomal recessive form of hereditary spastic paraparesis.

AFG3L1

Mouse AFG3L1. The expression of a third *m*-AAA protease subunit, Afg3l1, makes the situation more complex in mice. Murine Afg3l1 and Afg3l2 share 68% sequence identity, suggesting similar activities of both proteins. Coimmunoprecipitation experiments demonstrated that all the subunits are able to interact with each other and that, like Afg3l2, Afg3l1 can form homo-oligomeric complexes that are able to rescue the respiratory phenotype of yeast cells lacking Yta10 or Yta12 (Koppen et al., 2007). Experiments in mouse tissues have demonstrated that Afg3l2 accumulated at ~10-fold higher levels in brain than in liver. Paraplegin was also ~4-fold more abundant in brain than in liver mitochondria. By contrast, Afg3l1 was present at lower molar concentrations than those of Afg3l2 and paraplegin in murine brain mitochondria.

Knockdown experiments in MEFs (Mouse Embrionic Fibroblasts), heterologous expression in yeast, and in vitro processing assays have demonstrated processing of various mouse *m*-AAA protease subunits upon import into mitochondria. Two processing steps are required to generate mature paraplegin: after formation of an intermediate form by

MPP, Afg3l1 and/or Afg3l2 mediate maturation of paraplegin. Both intermediate and mature forms of paraplegin were detected in *m*-AAA protease complexes, indicating that maturation is not required for assembly after completion of import.

Afg3l1 and Afg3l2 can be autocatalytically processed when expressed in yeast. Although Afg3l2 appears to be cleaved initially by another peptidase before autocatalytic processing, there is no evidence for an involvement of MPP in the formation of the intermediate form. On the contrary, the precursor form of Afg3l1 is directly converted into the mature form. It is interesting to note that the yeast *m*-AAA protease subunits Yta10 and Yta12 do not undergo autocatalytic processing. (Koppen et al., 2009).

Human AFG3L1. The third *m*-AAA subunit paralogue, Afg3L1, that is expressed in mouse is encoded by a pseudogene in humans. In human, the *AFG3L1* gene is located on chromosome 16q24. The AFG3L1 gene appears to be transcribed but is probably not translated. Four AFG3L1 mRNA isoforms have been identified, but none of them contain an open reading frame (Kremmidiotis et al. 2001). Abrogation of AFG3L1 translation in humans is likely to be the result of nucleotide changes affecting the splicing of some exons and/or the open reading frame.

m-AAA complex

Cell survival critically depends on the integrity and functionality of mitochondria. These organelles evolved from an endosymbiontic relationship of aerobic bacteria and primordial eukaryotic cells and are the major energy production site in “modern” eukaryotic cells (Wallace, 2005).

The most important role of mitochondria is the production of ATP by respiratory chain. Much of the activity of the mitochondria occurs within the inner mitochondrial membrane (IMM); the most protein-rich cellular membrane of cell. The reactive oxygen species (ROS) are an inevitable by-product of oxidative phosphorylation, with inner membrane proteins being primary targets of oxidative damage. Mitochondria must be able to eliminate excess, non-assembled polypeptides to avoid potential deleterious effects on organellar functions.

Elaborate proteolytic systems which carry out the quality surveillance of mitochondrial proteins are present within different subcompartments of the organelle. A number of these proteases also exert essential housekeeping functions and control crucial steps during mitochondrial biogenesis. The maintenance of the mitochondrial genome, mitochondrial gene expression, and mitochondrial fusion and fission are examples for processes which are under proteolytic control (Koppen & Langer, 2007, Rugarli & Langer, 2006). On the other hand, mitochondrial proteases serve as gatekeepers for programmed cell death upon release from the organelle (Koppen & Langer,

2007). Many mitochondrial proteins are synthesized in a precursor form on cytosolic ribosomes and undergo proteolytic maturation upon import into mitochondria. The integrity of the inner membrane is maintained by members of the membrane-bound FtsH/AAA protease family, which specifically degrade misfolded and non-assembled inner membrane proteins and thereby ensure inner membrane integrity (Koppen & Langer, 2007).

The AAA+ superfamily

The AAA metalloproteases are a family of ATP-dependent protease belonging to the AAA^+ superfamily. The AAA^+ superfamily, ATPases associated with various cellular activities, is composed of several members employed in control of many vital cellular processes including membrane fusion, the cell cycle regulation, organelle biogenesis, folding and degradation of proteins. The activity of AAA^+ proteins is based on ability to use the energy released by hydrolysis of ATP to generate mechanical power. The binding and hydrolysis of ATP is mediated by a conserved AAA domain which promotes the oligomerization of AAA^+ proteins and the formation of a pore with a central channel.

The proteins of the superfamily can be divided into two distinct group based on the number of AAA domains present: AAA proteins of class I, containing two AAA domains called AAA-1 and AAA-2 and separated by a segment of variable length. AAA

proteins of class II, which contain only one AAA domain homologous to AAA-2. The different functions of these proteins is the presence of additional domains adjacent to or included in the AAA domain (Ogura & Wilkinson, J.2001).

AAA metalloproteases form a large complex of identical or homologous subunits with a mass of 70-80 kDa. They are ubiquitous in bacteria and eukaryotes, but have not been found in archaea, They are highly conserved: with sequence identities of >40% between the bacterial, yeast and human members (Langer, 2000).

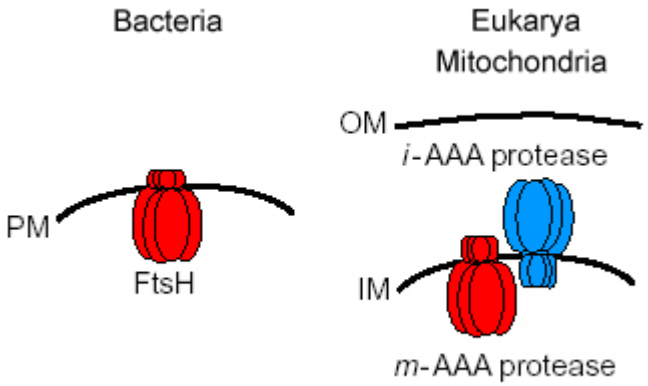

Fig 4: AAA proteases of Bacteria and Eukarya.
PM = plasma membrane, OM = outer mitochondrial membrane
IM = inner mitochondrial membrane (Langer T., 2000).

Most bacteria have only one AAA protease, called FtsH in *Escherichia coli*, which forms a homo-oligomeric complex in the plasma membrane. Eukaryotes have rather different orthologs that appear to be localized exclusively in mitochondria and

chloroplasts. The mitochondrial AAA metalloproteases are termed *i*-AAA and *m*-AAA.

Structure of AAA metalloproteases

AAA proteases form a ring structure consisting of homo-or hetero-hexamers characterized by an highly conserved structure.

To N-terminal, after the sequence of mitochondrial localization, there are one or two transmembrane domains. All the AAA protease, except the *i*-AAA Yme1p and its orthologs, have two transmembrane regions. Yme1 has only one transmembrane domain and exposes the catalytic sites in the intermembrane space. Like all members of the AAA^+ superfamily, proteases have the AAA domain consisted of two discrete structural domains: a domain α/β nucleotide-binding domain and an α helical bundle. The nucleotide-binding domain is composed by Walker A, Walker B, and SRH.

The Walker A motif, also called P-loop, is the consensus sequence GXXXXGKT and is located between β2 and α2. The Walker B sequence ψψψψDE, where ψ represents a hydrophobic amino acid, is associated with the β4 strand.

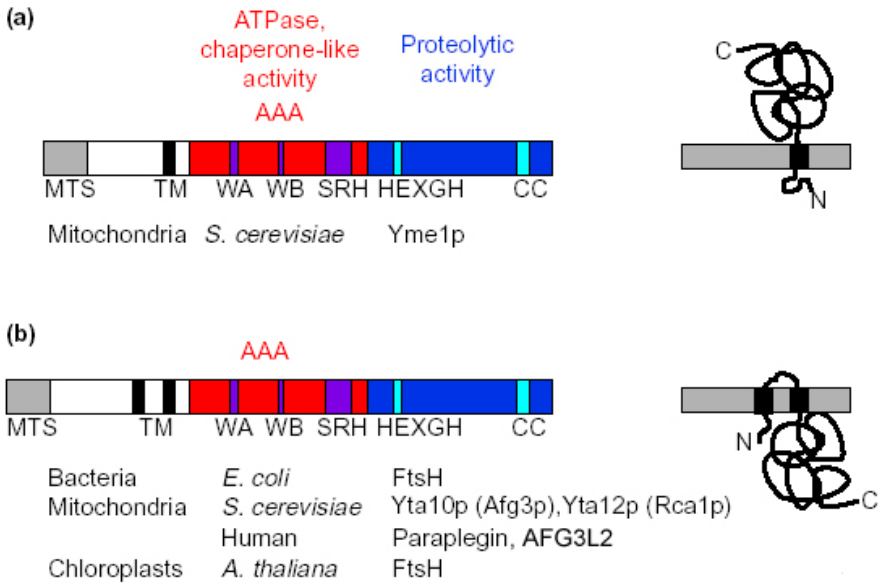

Fig 5: Structure of the AAA protease:
AAA = ATPase domain, MTS = mitochondrial localization sequence; TM = transmembrane domains; WA = Walker A box; WB = Walker B box; SRH = second region of homology; HEXGH = sequence of the binding site to metal; CC = coiled-coil region (Langer, 2000).

The SRH region is present in all AAA protease and differs from all other members of the AAA + superfamily, it consists of 19 highly conserved amino acids, in particular an asparagine (N301), an aspartate (D307) and two arginines (R312 and R315) are essential for the activity of the complex. This region seems to be involved in the interaction between different subunits. N301 forms a hydrogen bond with K201 of Walker A

and E255 of Walker B. D307 and R312 form a salt bridge that stabilizes the conformation of the SRH and contributes to positioning and orientation of R315 (Karata, 2001). This arginine termed “arginine finger” is localized in the ATP binding pocket to form interactions with the γ phosphate of ATP bound to adjacent subunits (Ogura et al., 2004).

The AAA domain is followed by a highly-conserved proteolytic domain. Analysis of the primary structure of the protease domain has revealed the presence of a consensus sequence motif HEXXH for binding to zinc, which prompted to term this family of zinc metalloprotease as “zincin” (Hooper, 1994). At the C-terminal region, there is another highly-conserved helical region of unknown function presumably forming leucine zipper-like coiled-coil structure (Langer, 2000)

Role of AAA complexes in yeast

The mitochondrial *m*-AAA protease has been first described and studied in yeast *Saccharomyces cerevisiae*.

Several members of the class of ATP-dependent proteases, the AAA proteases, are present within the inner membrane of mitochondria: Afg3p (Yta10p), Yme1p (Yta11p) e Rca1p (Yta12p). They form two AAA protease complexes: one, termed i-AAA, which protrudes into the intermembrane space and one, termed *m*-AAA, active on the matrix side (Wilkinson et al, 2004). AAA protease complexes are composed of closely related or

identical subunits of 70 to 80 kDa (Arlt et al., 1996; Leonhard et al., 1996)

The homo-oligomeric i-AAA protease, composed of Yme1 subunit only, was first identified in a genetic screen for yeast mutants resulting in an increased rate of DNA escape from mitochondria to the nucleus. Yme1 is required for respiratory growth of yeast cells at high temperatures and for fermenting growth at low temperature. The i-AAA protease present in yeast is also present in mammalian mitochondria, where is composed of YME1L (Leonhard et al., 1996, Tatsuta & Langer, 2009).

In yeast, the *m*-AAA protease is a hetero-oligomeric complex composed by highly homologous subunits Yta10 (Afg3) and Yta12 (Rca1), which assemble in an ATP-dependent manner into *m*-AAA protease complexes (Arlt et al., 1996).

Function

Both mitochondrial AAA proteases are part of a quality control system in the inner membrane and ensure the removal of non-native membrane proteins. (Korbel et al., 2004).

Studies in the yeast *Saccharomyces cerevisiae* have demonstrated a dual role for the *m*-AAA protease. First, it is a crucial component of the mitochondrial quality control system, selectively degrading improperly folded or unassembled inner membrane proteins (Esser et al., 2002) Second, it plays a regulatory role in mitochondrial protein synthesis and

antioxidant defense by participating in the processing and maturation of some mitochondrial proteins including cytochrome c peroxidase (Ccp1) in yeast (Nolden et al., 2005) and the ribosomal subunit Mrpl32 in both yeast and mammals (Arlt et al., 1996).

Two models have been proposed for the degradation of integral membrane proteins: “shedding model” and “pulling model”.

The first model requires that solvent-exposed loops or domains from membrane-embedded polypeptides may be cleaved off by AAA proteases present at the membrane surfaces. This may result in a concomitant destabilization of hydrophobic segments allowing their proteolysis from the membrane surface. The protein is cleaved at both membrane surfaces by either AAA proteases (Leonhard et al., 1996). The “pulling model” suggests that AAA proteases may act by exerting a pulling force on membrane embedded polypeptides and actively mediate membrane extraction. Authors favour this second model where the membrane proteins are not degraded by the joint action of AAA proteases on the two sides of the membrane, as predicted by the shedding model. Rather, each AAA protease can mediate the proteolytic breakdown of the complete polypeptide chain from either membrane surface.

This hypothesis is supported by evidence that the *m*-AAA protease is essential for viability of cells lacking i-AAA protease. This indicates the existence of common substrate polypeptides that can be degraded by either protease but can become

deleterious for cell growth if accumulation occurs (Leonhard et al. 2000).

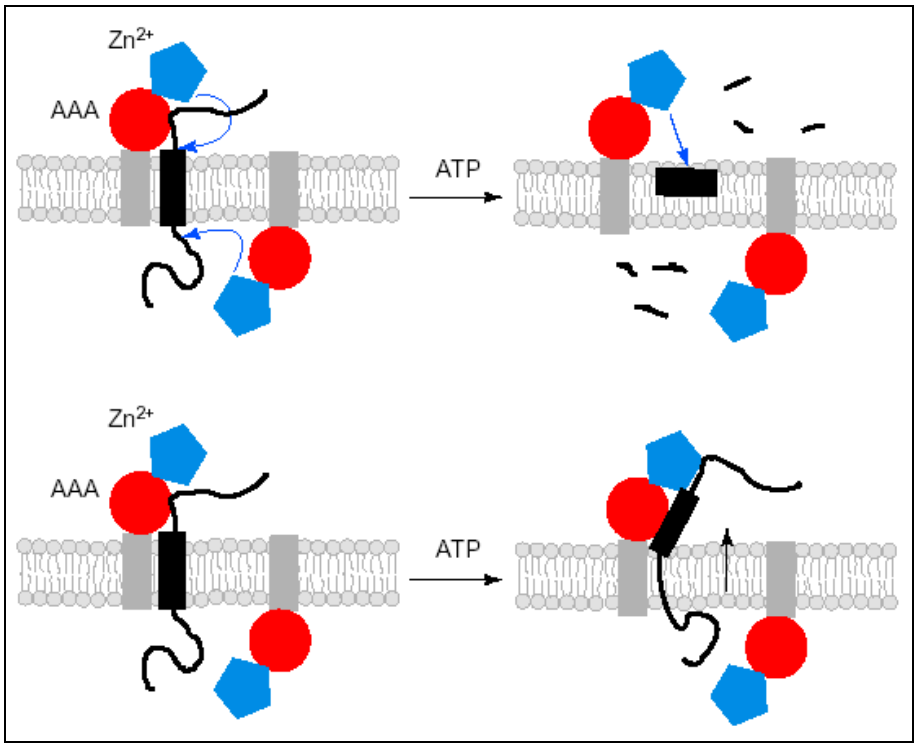

Figure 6: Two models for the destruction of integral membrane proteins the shedding model (top panel) and the pulling model (bottom panel). The AAA module (AAA) and the proteolytic domain (Zn^{2+}) are shown in red and blue, respectively. Blue arrows show sites of proteolytic attack and the black arrow indicates the direction of the pulling force (Langer, 2000).

Phenotype of mutations in the yeast *Saccharomyces cerevisiae*

Yeast cells lacking either Yta10 (yta10Δ) or Yta12 (yta12Δ) grow on glucose but exhibit impaired growth on a nonfermentable carbon source such as glycerol, indicating a defect in respiration (OXPHOS phenotype) (Nolden et al., 2005).

Yta10p and Yta12p contain a consensus binding site for divalent metal ions, HEXXH, which is characteristic of the proteolytic centre of metal-dependent peptidases. The glutamic acid residue is dispensable for binding and play exclusively a catalytic role during proteolysis. If glutamic acid residues in the metal-binding sites of Yta10p (yta10^{E559Q}) and Yta12p (yta12^{E614Q}) were replaced by glutamine, the expression of Yta10^{E559Q}p or Yta12^{E614Q}p did not affect the respiratory competence (Arlt et al., 1998).

The protease activity of the complex *m*-AAA is essential for respiratory growth (Koppen & Langer, 2007). Yeast cells expressing proteolytically inactive variants of both subunits (yta10^{E559Q} yta12^{E614Q}) are respiratory deficient, lack assembled respiratory chain and F_1F0-ATP-synthase complexes in the inner membrane, and show an increased tendency to lose mitochondrial DNA (Arlt et al., 1998).

It has been demonstrated that the transmembrane domain of either *m*-AAA protease subunit is dispensable for assembly and proteolytic activity, but deletion of the transmembrane domain

of one *m*-AAA protease subunit impairs the ability of the protease to degrade integral membrane proteins. The lack of transmembrane domain of both subunits impair the respiratory competence (Korbel et al., 2004).
In the absence of both *m*- and *i*-AAA proteases, yeast cells are not viable indicating an overlap of substrate specificity (Leonhard et al. 2000).

Substrates

AAA proteases degrade non-assembled subunits preventing their potentially harmful accumulation within mitochondria. No evidence for sequence-specific cleavage by AAA proteases does exist. Rather, AAA proteases have chaperone-like activities and recognize the solvent-exposed domains of membrane proteins. The chaperone activity resides within the AAA domains of AAA protease subunits, which have been demonstrated to bind unfolded model substrates *in vitro*. N- or C-terminal tails of ~20 amino acids protruding from the membrane are sufficient to allow the proteolytic attack of a membrane protein by an AAA protease (Leonhard et al. 2000).
Coimmunoprecipitation studies and functional inactivation have allowed the identification of some substrates of *m*-AAA complex. *m*-AAA is able to degrade either misfolded or non-assembled inner membrane proteins. For example, nonassembled subunits of respiratory chain and F_1F_0-ATP

synthase complexes belong to this group of substrate proteins (Arlt et al., 1998).

Inactivation of the *m*-AAA protease impairs the synthesis of the mitochondrially-encoded respiratory chain subunits Cox1 oxidase and the bc1 complex in the inner membrane. The proteolytic activity of the *m*-AAA protease is crucial for the expression of the intron-containing COX1 and COB genes in mitochondria. The dependence on the *m*-AAA protease is alleviated in cells harbouring an intronless mitochondrial genome, indicating that the protease regulates the processing and/or stability of COX1 and COB precursor transcripts (Arlt et al., 1998).

m-AAA protease can also act as processing enzymes of specific mitochondrial proteins. Another substrate is cytochrome *c* peroxidase (Ccp1). Ccp1 is a soluble protein of the yeast mitochondrial intermembrane space that plays a role as peroxide and toxic radical scavenger (Jiang & English, 2006). Ccp1 precursor (pCcp1) contains a bipartite N-terminal targeting sequence which is processed by the consecutive action of the *m*-AAA protease, which yields intermediate Ccp1 (iCcp1), and the intramembrane rhomboid protease Pcp1, which releases mature Ccp1 (mCcp1) into the intermembrane space (Esser et al., 2002; Michaelis et al. 2005; Tatsuta et al, 2007).

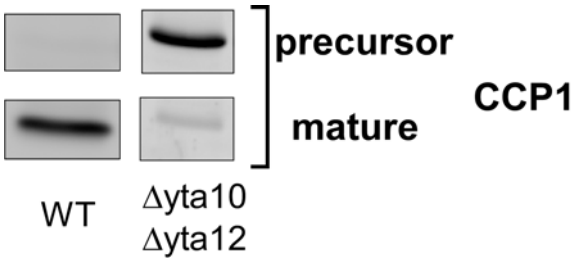

Figure 7: Ccp1 processing in wt and lacking *m*-AAA (Δyta10/Δyta12) yeast cells (Di Bella et al., unpublished).

Recent studies have suggested that *m*-AAA is required to mediate the ATP-dependent dislocation of precursor form of Ccp1 to the matrix side. The correct positioning of Ccp1 relative to the membrane allows intramembrane cleavage by rhomboid. Ccp1 cleavage by rhomboid is abolished if mutations are introduced into the AAA domains of *m*-AAA protease subunits, whereas the maturation of Ccp1 by rhomboid is observed in yeast cells harboring a proteolytically inactive variant of the *m*-AAA protease (Tatsuta et al, 2007).

The latest resuts would appear to indicate that the maturation of Ccp1 depends only on the ATPase but not the proteolytic activity of the *m*-AAA protease and therefore represents the first known non-proteolytic function of the *m*-AAA protease within mitochondrial biogenesis (Tatsuta et al., 2007).

The *m*-AAA protease mediates maturation of MrpL32. MrpL32 is a component of the large mitochondrial ribosome subunit which, unlike Ccp1, is present in both yeast and mammalian

cells. Removal of the N-terminal targeting sequence of MrpL32 by the *m*-AAA protease allows its assembly into ribosomes and subsequent protein synthesis within mitochondria, thus controlling the assembly of respiratory complexes in the inner membrane (Nolden et al., 2005)

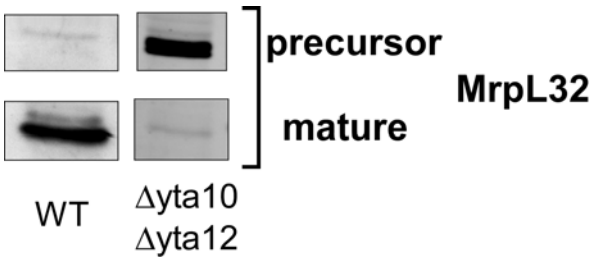

Figure 8: MrpL32 processing in wt and lacking *m*-AAA (Δyta10/Δyta12) yeast cells (Di Bella et al., 2010)

That the processing of MrpL32 indeed represents a key function of the *m*-AAA protease in yeast is demonstrated by complementation experiments. Expression of an MrpL32 variant,
which harbors an unrelated presequence and is matured by MPP, maintains respiratory growth of *m*-AAA protease-deficient cells (Nolden et al., 2005)

Human *m*-AAA

The human *m*-AAA protease has a native molecular mass of approximately 900 kDa (Banfi et al., 1999). The *m*-AAA exist as homo-oligomeric AFG3L2 complexes as well as hetero-oligomeric assemblies of AFG3L2 with homologous paraplegin subunits. (Koppen et al., 2007).

m-AAA complexes are structured to form a hexameric ring located on the inner mitochondrial membrane and active on its matrix side.

It is thought that the homocomplex is composed of six molecules of AFG3L2 and heterocomplex would have a stoichiometry of three molecules of AFG3L2 and three molecules of paraplegin.

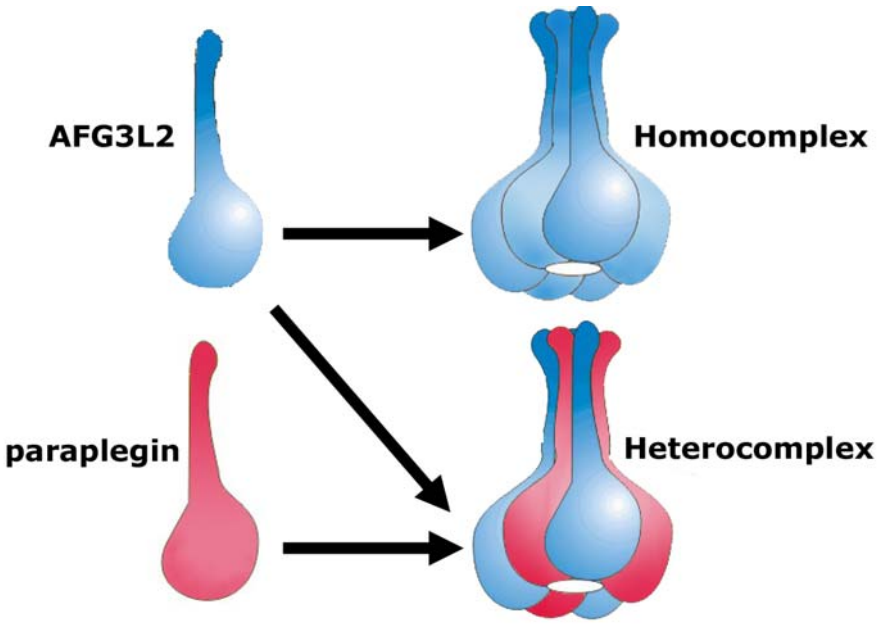

Figure 9: The stoichiometry and topology of human homocomplex and heterocomplex *m*-AAA

Paraplegin mutations affect only the heterooligomeric complex, whereas mutations in AFG3L2 affect both *m*-AAA complex. This explain the fact that recessive mutations of paraplegin cause a rather mild phenotype, while only heterozygous missense mutations of AFG3L2 appear to be tolerated. Fibroblasts of HSP patients have an increased sensitivity to oxidative damage. The increased sensitivity to ROS of mitochondria lacking the AFG3L2-paraplegin complex was indicated by the reduction of ATP synthesis and an impairment of complex I activity in HSP cells compared to control cells (Atorino et al., 2003).

Both AFG3L2 and paraplegin are highly homologous (40-45% amino-acid identity) to two yeast mitochondrial proteins Yta10 and Yta12, respectively (Arlt et al., 1996 and Banfi et al.1999). Complementation studies in yeast have demonstrated the functional conservation of the human *m*-AAA complex. Yeast cells lacking both proteins (Δyta10/Δyta12 cells) are respiratory deficient. The human AFG3L2 homocomplex or AFG3L2/paraplegin heterocomplex, but not paraplegin homocomplex, are able to functionally replace the Yta10p/Yta12p complex and to restore the respiratory competence. A glutamic acid residue is present at position 575 in the highly conserved consensus metal binding site of human AFG3L2 and paraplegin; replacing this residue with glutamine

(E575Q) abolishes the proteolytic activity of the complex (Koppen et al., 2007). All mammalian *m*-AAA isoenzymes can functionally substitute for the yeast *m*-AAA protease upon expression in yeast, indicating that at least essential housekeeping functions of the yeast enzyme are conserved and demonstrating functional conservation (Nolden et al., 2005; Koppen et al., 2007). We have used the yeast *Saccharomyces cerevisiae* model to investigate the functional consequences of the SCA28 mutations and to validate their pathogenicity.

Mouse models

There are several mouse models created to understand the function and pathogenesis of the *m*-AAA.

Spg7$^{-/-}$ mice were generated by deleting the .first two exons of the gene. They showed motor impairment and abnormal movements of the hindlimbs with increasing age. Neuropathologic analysis revealed a late-onset retrograde axonal degeneration in long descending motor spinal tracts, long ascending sensory spinal tracts, peripheral and optic nerves, resembling the HSP phenotype (Ferreirinha et al., 2004).

They are two different null Afg3l2 mouse models. The first one is the spontaneous mouse mutant *paralysé*, that carries a missense mutation (a C to G transversion) in exon 10 of the Afg3l2 gene causing the substitution of an arginine by a glycine (R389G) in the highly conserved AAA domain of the molecule (Duchen et al., 1983).

The second model termed Afg3l2^{Emv66} originated after ecotropic murine leukemia proviral reinsertion in the MEV/2TyJ strain in intron 14 of the gene. The reinsertion causes a premature stop codon at residue 592 deleting the final 210 amino acids following instability of the protein product (Maltecca et al,2008)

Both mouse null models show an extremely severe neuromuscular syndrome which progresses until complete tetraparesis and do not survive over 16 days of age.

Afg3l2 mutants show a severe defect in axonal development and widespread morphological alterations in both the CNS and PNS. Purkinje cells were normal in number but failed to develop a branched dendritic tree. Mitochondrial morphology abnormalities are detected in motor and sensory neurons, more frequently in proximity of the nucleus. The enzymatic activities of the respiratory chain complexes are strikingly impaired in these two Afg3l2 models, thus resulting in highly reduced ATP production (Maltecca et al, 2008).

Another mouse model is the heterozygous Afg3l2$^{+/Emv66}$. Mice carrying this background appear normal at birth and do not show a remarkable phenotype up to 3 months of age. These

defects appear at 4 months and worsen with age, and mutants older than 12 months present abnormal gait characterized by uncoordinated hindlimb movement. Mutant mice have been monitored up to 18 months and observed that none developed other signs of neurological disease such as tremor, rigidity, or kyphosis. They instead seem to have strictly an ataxic phenotype of cerebellar origin, as clinical features of SCA28 patients. This evidence, together with the severe cerebellar phenotype previously observed in Afg3l2 homozygous mutants (Maltecca et al., 2008), prompted authors to evaluate cerebellar degeneration in Afg3l2 heterozygous mice. It was observed progressive degeneration and loss of Purkinje cells in $Afg3l2^{Emv66/+}$ cerebella between 4 and 12 months. Dramatic defects in mitochondrial morphology, distribution, and cristae organization were detected at 4 months, contemporary to the onset of motor coordination defects. Moreover it was detected marked reduction of ATP synthesis associated with a reduced activity of respiratory complexes I and III. (Maltecca et al, 2009)

Last mouse model is double mutant with a background $Spg7^{-/-}$ /$Afg3l2^{+/Emv66}$. The phenotype of $Afg3l2^{+/Emv66}$ markedly worsens when placed on a paraplegin-null background

These mice showed a severe neurological phenotype from 6 weeks of age, characterized by reduced cage activity, loss of balance, uncoordinated gait, tremor and ataxia. These animals display anticipation and increased severity of motoneuron degeneration found in Spg7 knock-out mice, suggesting that

Afg3l2 is able to partially compensate the lack of paraplegin in the spinal cord. Later, they lost significant weight, became paralysed, and finally died within the 4th month of life (Martinelli et al., 2009).

Moreover, as expected from the reduced amount of AFG3L2 containing *m*-AAA complexes, these animals undergo anticipated degeneration of Purkinje cells with respect to $Afg3l2^{+/Emv66}$ mice. Mitochondria from affected tissues have abnormal structural, tend to lose mt-DNA and display reduced levels of assembled respiratory complexes, especially of complexes I, III, and IV (Martinelli et al., 2009).

Scope of the thesis

The aim of this work was to demonstrate that mutations in *AFG3L2* cause dominant SCA type 28 evaluating the frequency of mutation in AFG3L2 gene in a large cases of ataxic individuals. A second aspect concerned the functional characterization of the protein involved in SCA28 pathogenesis using a yeast cellular model. We have analysed the respiratory competence and the proteolytic activity of human mutant AFG3L2 expressed in yeast to evaluate the functional effects and the pathogenic role of the amino acid substitutions identified in AFG3L2.

Reference list of chapter 1

- Arlt, H., Tauer, R., Feldmann, H., Neupert, W. & Langer, T. The YTA10-12 complex, an AAA protease with chaperone-like activity in the inner membrane of mitochondria. *Cell* **85**, 875-885 (1996).
- Arlt H., Steglich G., Perryman R., Guiard B., Neupert W., and Langer T. The formation of respiratory chain complexes in mitochondria is under the proteolytic control of the *m*-AAA protease. *EMBO Journal* **17**, 4837-4847. (1998).
- L. Atorino, L. Silvestri, M. Koppen, L. Cassina, A. Ballabio, R. Marconi, T. Langer, G. Casari, Loss of *m*-AAA protease in mitochondria causes complex I de.ciency and increased sensitivity to oxidative stress in hereditary spastic paraplegia, *J. Cell Biol*. **163** 777–787(2003).
- Banfi, S. et al. Identification and characterization of AFG3L2, a novel paraplegin-related gene. *Genomics* **59**, 51-58 (1999).
- Brusco, A. et al. Molecular genetics of hereditary spinocerebellar ataxia: mutation analysis of spinocerebellar ataxia genes and CAG/CTG repeat expansion detection in 225 Italian families. *Arch Neurol* **61**, 727-733 (2004).
- Cagnoli, C. et al. SCA28, a novel form of autosomal dominant cerebellar ataxia on chromosome 18p11.22-q11.2. *Brain* **129**, 235-242 (2006).
- Duenas, A. M., Goold, R. & Giunti, P. Molecular pathogenesis of spinocerebellar ataxias. *Brain* **129**, 1357-1370 (2006).
- Duchen L.W., S. Gomez, J.L. Guénet, S. Love, Paralysé: a new neurological mutant mouse with progressive atrophy and loss of motor nerve terminals, J. *Physiol*. **345** (1983) .
- Elleuch, N. et al. Mutation analysis of the paraplegin gene (SPG7) in patients with hereditary spastic paraplegia. *Neurology* **66**, 654-659 (2006).
- Esser, K., Tursun, B., Ingenhoven, M., Michaelis, G. & Pratje, E. A novel two-step mechanism for removal of a mitochondrial signal sequence

involves the AAA complex and the putative rhomboid protease Pcp1. *J. Mol. Biol.* **323**, 835–843 (2002).

- F. Ferreirinha, A. Quattrini, M. Pirozzi, V. Valsecchi, G. Dina, V. Broccoli, A. Auricchio, F. Piemonte, G. Tozzi, L. Gaeta, G. Casari, A. Ballabio, E.I. Rugarli, Axonal degeneration in paraplegin-de.cient mice is associated with abnormal mitochondria and impairment of axonal transport, *J. Clin. Invest*. **113** 231–242. (2004)
- Harding, A. E. The clinical features and classification of the late onset autosomal dominant cerebellar ataxias. A study of 11 families, including descendants of the 'the Drew family of Walworth'. *Brain* **105**, 1-28 (1982)
- Hooper, N.M. Families of zinc metalloproteases. *FEBS Lett*. **354**, 1–6. (1994).
- Jiang, H. & English, A. M. Phenotypic analysis of the ccp1Delta and *ccp1Delta-ccp1W191F* mutant strains of *Saccharomyces cerevisiae* indicates that cytochrome *c* peroxidase functions in oxidative-stress signaling. *J Inorg Biochem* **100**, 1996-2008 (2006).
- Koeppen, A. H. The pathogenesis of spinocerebellar ataxia. *Cerebellum* **4**, 62-73 (2005).
- Koppen, M. & Langer, T. Protein degradation within mitochondria: versatile activities of AAA proteases and other peptidases. *Crit Rev Biochem Mol Biol* **42**, 221-242 (2007).
- Koppen, M., Metodiev, M. D., Casari, G., Rugarli, E. I. & Langer, T. Variable and tissue-specific subunit composition of mitochondrial *m*-AAA protease complexes linked to hereditary spastic paraplegia. *Mol Cell Biol* **27**, 758-767 (2007).
- Koppen M., Bonn F., Ehses S., Langer T. Autocatalytic Processing of *m*-AAA Protease Subunits in Mitochondria *Molecular Biology of the Cell* **20**, 4216–4224 (2009)
- Korbel D., Wurth S., Käser M., and Langer T. Membrane protein turnover by the *m*-AAA protease in mitochondria depends on the transmembrane domains of its subunits. *EMBO Reports* **5**, 698-703. (2004).

- Kremmidiotis, G. et al. Molecular and functional analyses of the human and mouse genes encoding AFG3L1, a mitochondrial metalloprotease homologous to the human spastic paraplegia protein. *Genomics* **76**, 58-65 (2001).
- Langer T. AAA proteases: cellular machines for degrading membrane proteins *TIBS* **25** 247-251 (2000)
- Leonhard K., Herrmann J. M., Stuart R. A., Mannhaupt G., Neupert W., and Langer T. AAA proteases with catalytic sites on opposite membrane surfaces comprise a proteolytic system for the ATP-dependent degradation of inner membrane proteins in mitochondria. *EMBO Journal* **15**, 4218-4229(1996).
- Leonhard, K. et al. Membrane protein degradation by AAA proteases in mitochondria: extraction of substrates from either membrane surface. *Mol Cell* **5**, 629-638 (2000).
- Maltecca F., A. Aghaie, D.G. Schroeder, L. Cassina, B.A. Taylor, S.J. Phillips, M. Malaguti, S. Previtali, J.L. Guenet, A. Quattrini, G.A. Cox, G. Casari, The mitochondrial protease AFG3L2 is essential for axonal development*, J. Neurosci.* **28** 2827–2836 (2008)
- Maltecca F., et al. Haploinsufficiency of AFG3L2, the Gene Responsible for Spinocerebellar Ataxia Type 28, Causes Mitochondria-Mediated Purkinje Cell Dark Degeneration *J. Neurosci*. **29** 9244 –9254 (2009)
- Mariotti C, Brusco A, Di Bella D, Cagnoli C, Seri M, Gellera C, Di Donato S, Taroni F. Spinocerebellar ataxia type 28: a novel autosomal dominant cerebellar ataxia characterized by slow progression and ophthalmoparesis. *Cerebellum* **7**:184–188 (2008).
- P. Martinelli, V. LaMattina, A. Bernacchia, R. Magnoni, F. Cerri, G. Cox, A. Quattrini, G. Casari, E.I. Rugarli, Genetic interaction between the *m*-AAA protease isoenzymes reveals novel roles in cerebellar degeneration, *Hum. Mol. Genet*. **18** 2001–2013 (2009)
- Michaelis, G. et al. Mitochondrial signal peptidases of yeast: the rhomboid peptidase Pcp1 and its substrate cytochrome C peroxidase. *Gene* **354**, 58-63 (2005).

- Nolden, M. *et al.* The *m*-AAA protease defective in hereditary spastic paraplegia controls ribosome assembly in mitochondria. *Cell* **123**, 277–289 (2005).
- Ogura, T. & Wilkinson, A. J. AAA+ superfamily ATPases: common structure--diverse function. *Genes Cells* **6**, 575-597 (2001).
- Ogura, T., Whiteheart S. W., Wilkinson, A. J Conserved arginine residues implicated in ATP hydrolysis, nucleotide-sensing, and inter-subunit interactions in AAA and AAA+ ATPases *Journal of Structural Biology* **146** 106–112 (2004)
- Orr, H. T. & Zoghbi, H. Y. Trinucleotide repeat disorders. *Annu Rev Neurosci* **30**, 575-621 (2007).
- Rugarli1 E. I. and Langer T. Translating *m*-AAA protease function in mitochondria to hereditary spastic paraplegia *TRENDS in Molecular Medicine* **12** 262-269 (2006).
- Schols, L., Bauer, P., Schmidt, T., Schulte, T. & Riess, O. Autosomal dominant cerebellar ataxias: clinical features, genetics, and pathogenesis. *Lancet Neurol* **3**, 291-304 (2004).
- Taroni, F. & Di Donato, S. Pathways to motor incoordination: the inherited ataxias. *Nature Rev Neurosci* **5**, 641-655 (2004).
- Tatsuta, T., Augustin, S., Nolden, M., Friedrichs, B. & Langer, T. *m*-AAA protease-driven membrane dislocation allows intramembrane cleavage by rhomboid in mitochondria. *EMBO J* **26**, 325-335 (2007).
- Tatsuta T., Langer T. AAA proteases in mitochondria: diverse functions of membrane-bound proteolytic machines. *Research in Microbiology* **160** 711-717 (2009)
- Wilkinson P. A., Crosby A. H., Turner C., Bradley L. J., Ginsberg L., Wood N. W., Schapira A. H., Warner T. T. A clinical, genetic and biochemical study of SPG7 mutations in hereditary spastic paraplegia. *Brain* **127**, 973-980 (2004).
- Wallace, D.C.. A mitochondrial paradigm of metabolic and degenerative diseases, aging, and cancer: a dawn for evolutionary medicine. *Annu Rev Genet* **39**:359–407 (2005).

- Zoghbi, H. Y. & Orr, H. T. Glutamine repeats and neurodegeneration. *Annu Rev Neurosci* **23**, 217-247 (2000).

Chapter 2:

Mutations in the mitochondrial protease gene AFG3L2 cause dominant hereditary ataxia SCA28

Di Bella D, Lazzaro F, Brusco A, Plumari M, Battaglia G, Pastore A, Finardi A, Cagnoli C, Tempia F, Frontali M, Veneziano L, Sacco T, Boda E, Brussino A, Bonn F, Castellotti B, Baratta S, Mariotti C, Gellera C, Fracasso V, Magri S, Langer T, Plevani P, Di Donato S, Muzi-Falconi M, Taroni F.

Nature Genetics 42:313–321.2010

Abstract

Autosomal dominant spinocerebellar ataxias (SCAs) are genetically heterogeneous neurological disorders characterized by cerebellar dysfunction mostly due to Purkinje cell degeneration. Here we show that AFG3L2 mutations cause SCA type 28. Along with paraplegin, which causes recessive spastic paraplegia, AFG3L2 is a component of the conserved m-AAA metalloprotease complex involved in the maintenance of the mitochondrial proteome. We identified heterozygous missense mutations in five unrelated SCA families and found that AFG3L2 is highly and selectively expressed in human cerebellar Purkinje cells. m-AAA–deficient yeast cells expressing human mutated AFG3L2 homocomplex show respiratory deficiency, proteolytic impairment
and deficiency of respiratory chain complex IV. Structure homology modeling indicates that the mutations may affect AFG3L2 substrate handling. This work identifies AFG3L2 as a novel cause of dominant neurodegenerative disease and indicates a previously unknown role for this component of the mitochondrial protein quality control machinery in protecting the human cerebellum against neurodegeneration.

Introduction

Autosomal dominant SCAs are a clinically and genetically heterogeneous group of neurological disorders primarily characterized by imbalance, progressive gait and limb ataxia, and dysarthria[1–3], caused by degeneration of the cerebellum and its afferent and efferent connections[2–5]. Twenty-eight SCA loci are currently known, and 16 seemingly unrelated disease genes have been identified thus far[3] (http://neuromuscular.wustl.edu/ataxia/domatax.html). In ten types of ataxia, the disease is caused by dynamic expansions of polyglutamine-encoding CAG repeats[4,6] (SCA types 1, 2, 3, 6, 7 and 17, and dentatorubral-pallidoluysian atrophy) or repeats falling outside the coding region[7] (SCA types 10, 12 and 31) in genes whose function is still largely unknown. In recent years, a group of SCAs have emerged that are caused by conventional mutations in specific genes (SCA types 5, 11, 13, 14, 15/16/29 and 27). The distinct functions of these disease genes have revealed the complex heterogeneity of the pathogenic mechanisms leading to cerebellar degeneration and ataxia[3].

We had mapped a previously unidentified SCA locus (*SCA28*) on chromosome 18p11.22–q11.2 in a four-generation Italian family with an autosomal dominant form of cerebellar ataxia[8] (ADCA type I (ref. 1)). On the basis of expression profiles in the nervous system, we selected 12 genes within the 7.9-megabase critical region, including that encoding the mitochondrial metalloprotease AFG3L2 (ATPase family gene 3-like 2). Although no dominant ataxia has thus far been associated with

mitochondrial dysfunction, we focused on this gene because of its partnership with paraplegin, a cognate mitochondrial protease, the loss of which causes a distinct neurodegenerative disorder, the recessively inherited form of hereditary spastic paraplegia SPG7 (ref. 9).

AFG3L2 and paraplegin are highly homologous (40–45% amino acid identity) to two yeast mitochondrial proteins, Yta10p (Afg3p) and Yta12p (Rca1p), respectively, belonging to the superfamily of P-loop ATPases known as ATPases associated with various cellular activities, or AAA+ (ref. 10). They contain an ATP-binding/ATPase domain (AAA domain), the structural hallmark of the AAA-protease subfamily[11,12], and a zinc-dependent metalloprotease domain in a single polypeptide (**Fig. 1**), and they form large proteolytic complexes in the mitochondrial inner membrane that are active on the matrix side (*m*-AAA protease)[12]. In humans, *m*-AAA is composed of paraplegin and AFG3L2. A third *m*-AAA subunit paralog, AFG3L1, is expressed in mouse but is encoded by a pseudogene in humans[13]. In yeast, the *m*-AAA is a hetero-oligomer composed of Yta10p and Yta12p subunits. By contrast, both homo-oligomeric AFG3L2-AFG3L2 and hetero-oligomeric AFG3L2-paraplegin complexes exist in mammalian mitochondria[13]. Yeast studies have demonstrated that *m*-AAA is a crucial component of the mitochondrial protein quality-control system[14]. It also has a regulatory role in mitochondrial protein synthesis and antioxidant defence, participating in protein processing and maturation both in yeast and mammals[15,16].

We report that heterozygous missense mutations in *AFG3L2* cause dominant hereditary spinocerebellar ataxia type 28 (SCA28).

Expression of mutant human AFG3L2 in yeast demonstrated that the mutations alter the proteolytic competence of the *m*-AAA complex, ultimately resulting in defective activity of cytochrome *c* oxidase (COX, also known as complex IV) and impairment of cell respiration. SCA28 is, to our knowledge, the first autosomal dominant spinocerebellar ataxia shown to be caused by alterations in a mitochondrial protein. Consistent with the clinicopathological phenotype, *AFG3L2* is highly and selectively expressed in cerebellar Purkinje cells. Our results indicate a specialized role for this component of the *m*-AAA complex in protecting the human cerebellum from neurodegeneration.

Results

Missense mutations affect functional domains of AFG3L2

Human AFG3L2 is an ~80-kDa protein encoded by a 17-exon gene (**Fig. 1**). Sequence analysis of *AFG3L2* in proband III-7 of the original kindred MI-A0091 (ref. 8) revealed a single G2071A change in exon 16 (**Supplementary Fig. 1**), resulting in the amino acid substitution E691K within the proteolytic domain, in a region that is highly conserved in m-AAA and m-AAA–related proteins from eubacteria to humans (**Fig. 1**). The mutation was found in heterozygosis in all the affected subjects

(**Supplementary Fig. 1**), consistent with the dominant pattern of inheritance, but in none of >400 unrelated ethnically matched controls.

We then examined 337 unrelated people with ataxia (Online Methods) for the presence of AFG3L2 mutations. The pattern of inheritance was dominant in 136 affected individuals and consistent with recessive transmission in 51. The disease was apparently sporadic in 150 individuals. Numerous sequence variants were identified in both affected and control subjects (**Supplementary Table 1**). Five missense mutations (**Supplementary Fig. 1**), all in heterozygous form, were detected in affected individuals only, suggesting that they may be causative mutations. Three amino acid substitutions (S674L, A694E and R702Q) found in affected individuals with dominant inheritance occurred within a portion of the proteolytic domain encoded in exon 16 (**Fig. 1**), close to the E691K substitution identified in kindred MI-A0091. R702Q was found in family MI-A0762 in the fully symptomatic index patient and in her mother and maternal uncle, both negative at neurological examination but with moderate cerebellar atrophy at magnetic resonance imaging, suggesting reduced expressivity of the mutation (**Supplementary Fig. 2**). A fourth substitution (N432T) was found in the sequence encoded by exon 10, within a highly conserved region of the ATPase domain (**Fig. 1**), in the six living affected members from a three-generation family (MI-A2473/RM-DS) presenting an ADCA type 1 phenotype. Finally, one substitution (H126Q) outside the proteolytic domain, in a

region of the protein with unknown function encoded by exon 4 (**Supplementary Note**), was found in one affected individual in the possibly recessive group.

AFG3L2 substitutions impair respiration in yeast

As *in silico* predictions and analysis of *AFG3L2* mRNA in the cells of affected individuals ruled out possible effects of the mutations on pre-mRNA splicing (**Supplementary Note**), we investigated the functional consequences of the disease-segregating mutations in the facultative aerobic yeast *Saccharomyces cerevisiae*. Yeast cells lacking the Yta10p (*yta10*Δ) or Yta12p (*yta12*Δ) *m*-AAA subunit grow on glucose but show impaired growth on a nonfermentable carbon source such as glycerol, indicating a respiratory defect[16] (OXPHOS phenotype), and they also do not process substrate proteins of the *m*-AAA complex[13,15–17]. Notably, this phenotype can be rescued by the expression of mammalian AFG3L2 alone, which, unlike paraplegin, can homo-oligomerize into a functional *m*-AAA complex[13]. We therefore tested the identified AFG3L2 variants for their ability to support respiration in an *m*-AAA–defective strain (*yta10*Δ*yta12*Δ) obtained by targeted deletion of both the *YTA10* and *YTA12* genes (**Fig. 2**). Overexpression of human AFG3L2 was necessary to fully restore respiration (**Fig. 2a**). *yta10*Δ*yta12*Δ cells were transformed with wild-type AFG3L2 (AFG3L2WT), the six identified mutants and AFG3L2E575Q, used as a positive control for inactivation of proteolytic activity13,16 (**Fig.2b**). When

glycerol (YPG) was the only carbon source, the yta10Δyta12Δ OXPHOS phenotype was rescued by both AFG3L2WT and AFG3L2H126Q, suggesting that this substitution, located outside the conserved functional domains, probably represents a rare or private variant of no or limited pathological relevance. By contrast, despite the high levels of expression (**Fig. 2g** and **Supplementary Fig. 3**), the four variants with substitutions in the protease domain (AFG3L2E691K, AFG3L2S674L, AFG3L2A694E and AFG3L2R702Q) as well as the one with a substitution in the ATPase domain (AFG3L2N432T) did not restore respiration (**Fig. 2b**), indicating that these substitutions are deleterious. Given the missense nature of the mutations, we examined whether haploinsufficiency or negative dominance was the mechanism underlying these effects by coexpressing wild-type AFG3L2 with each mutant (**Fig. 2c** and **Supplementary Fig. 4**). Notably, introducing $AFG3L2^{WT}$ into cells carrying mutant $AFG3L2^{E691K}$ (**Fig. 2c**) or $AFG3L2^{N432T}$ (**Supplementary Fig. 4**) resulted in only a limited correction of the *yta10Δyta12Δ* respiratory phenotype, with an intermediately reduced growth rate of $AFG3L2^{WT}$-$AFG3L2^{mut}$ cells, clearly indicating a dominant negative effect of these fully penetrant mutations. By contrast, coexpression of $AFG3L2^{WT}$ with mutant $AFG3L2^{S674L}$, $AFG3L2^{A694E}$ or $AFG3L2^{R702}$Q fully rescued the defective growth phenotype, suggesting that haploinsufficiency or weak negative dominance may be the disease-causing mechanism for these mutations.

To recapitulate the physiological organization of *m*-AAA in human cells, we performed a further set of experiments in which AFG3L2 and paraplegin were coexpressed (**Fig. 2d**–**g**). *yta10*Δ*yta12*Δ cells carrying AFG3L2^{E691K} (**Fig. 2d**,**f**) or the AFG3L2^{E575}Q control (data not shown) still had a respiratory-deficient phenotype, which is consistent with a dominant negative effect of these mutations. Rescue of the AFG3L2^{N432T} phenotype by paraplegin appeared to be temperature sensitive, with moderate growth at 28 °C that was progressively reduced and abolished at higher temperatures (**Fig. 2e**). By contrast, coexpression of paraplegin in the 28–37 °C range always restored respiration in cells harbouring the mutant AFG3L2^{S674L}, AFG3L2^{A694E} or AFG3L2^{R702}Q, suggesting that hetero-oligomeric complexes may form between mutant AFG3L2 and paraplegin. We confirmed this with co-immunoprecipitation experiments showing that both paraplegin-responsive and paraplegin-nonresponsive mutants of AFG3L2 interact with paraplegin in a quantitative fashion (**Fig. 2g**).

AFG3L2 substitutions impair cytochrome *c* oxidase activity in yeast

The *m*-AAA protease is an integral protein of the inner mitochondrial membrane that has a crucial role in the quality control of mitochondrial membrane proteins, participating in both the degradation of loosely folded polypeptides and the correct assembly of other integral components of the inner membrane, including complexes of the respiratory chain[14,17,18].

To elucidate the mechanism responsible for the OXPHOS phenotype induced by SCA28 mutations, we investigated respiratory-chain activity. Whereas complex III (ubiquinol:ferricytochrome-*c* oxidoreductase) and complex V (ATPase) activities were less severely affected (data not shown), the five SCA28 mutations caused a marked reduction (≥90%) of COX activity and reduction in the levels of COX subunit proteins (**Fig. 3a**,**b** and **Supplementary Note**), as observed in cells (*yta10*A*yta12*A) lacking endogenous *m*-AAA (ref. 18). The severe COX defect provides a direct explanation for the respiratory-deficient phenotype associated with AFG3L2 SCA28 mutations. In the presence of paraplegin, COX enzyme activity and subunit protein levels are restored in cells expressing AFG3L2^{S674L}, AFG3L2^{A694E} or AFG3L2^{R702}Q (paraplegin-responsive mutants) but not in cells expressing AFG3L2^{E691K} or AFG3L2^{N432T} or the control proteolytic mutant AFG3L2^{E575}Q (**Fig. 3c**,**d**). Persistent COX deficiency upon expression of paraplegin confirms the dominant effects of the AFG3L2^{E691K} and AFG3L2^{N432T} mutants in both the homo- and the hetero-oligomeric assembly of the complex.

The mutations alter the proteolytic activity of AFG3L2

As an indicator of the overall proteolytic competence of mutant AFG3L2, we analyzed the processing and maturation of the yeast nuclear-encoded ribosomal protein MrpL32 (**Fig. 4**), a known substrate of both the mammalian and yeast *m*-AAA

proteases[13,16], evolutionarily conserved from yeast to mammals[16].

In *m*-AAA–deficient yeast cells (*yta10*A*yta12*A), the processing of MrpL32 is completely abolished, and the precursor species (pMrpL32) accumulates (**Fig. 4a**). Expression of AFG3L2^{WT} or AFG3L2^{H126}Q substantially reduced pMrpL32 accumulation (**Fig. 4b**). Some mature MrpL32 was produced in cells carrying the disease-associated mutants AFG3L2^{S674L} and AFG3L2^{E691K}, and, to a lesser extent, in those carrying AFG3L2^{A694E}, AFG3L2^{R702}Q and AFG3L2^{N432T}; however, for all mutants, the accumulation of unprocessed precursor, expressed as the ratio of pMrpL32 levels to total MrpL32 levels, indicated a statistically significant impairment of proteolytic activity ($P \leq 0.01$, $n = 4$; **Fig. 4b**).

When AFG3L2 and paraplegin were coexpressed (**Fig. 4c**), higher levels of pMrpL32 were observed in all transformed strains, suggesting increased MrpL32 expression in cells expressing both heterologous proteins. No statistically significant difference ($P > 0.05$, $n = 4$) was observed between the ratio of precursor to total MrpL32 in AFG3L2^{WT} harbouring cells (**Fig. 4c**) and that in SCA28 mutant strains harbouring AFG3L2^{S674L}, AFG3L2^{A694E} or AFG3L2^{R702}Q, whose defective respiration is rescued by paraplegin coexpression (**Fig. 2d**). By contrast, the respiratory-deficient strains expressing AFG3L2^{E691K}, AFG3L2^{E575}Q (ref. 13) and AFG3L2^{N432T}, whose OXPHOS phenotype is not rescued by paraplegin (**Fig. 2**), still showed proteolytic dysfunction, with a precursor- to-total ratio

significantly higher than that of the AFG3L2^{WT} strain ($P \leq 0.005$, $n = 4$). Together, the results clearly indicate that the identified mutations affect AFG3L2 proteolytic activity and that alteration of this activity correlates with impairment of cellular respiratory competence.

Structural modeling of AFG3L2 mutants

To analyze the impact of the identified mutations on the structure of AFG3L2, we built a three-dimensional model using the structure of the Thermus thermophilus AAA protease FtsH (refs. 11,19) as a template (**Fig. 5**). A more detailed description of the modeling can be found in the **Supplementary Note**. AFG3L2 Glu691 is also a glutamate (Glu537) in *T. thermophilus* FtsH (ref. 19) but is not conserved in other orthologs, including paraplegin (**Fig. 1**). This residue sits in the middle of the central pore formed by the six subunits surrounding the exit from the proteolytic chamber on the matrix side of the complex (**Fig. 5a**,**b**, and **Supplementary Figs. 5a**,**b** and **6a**). Substitution of this residue to a lysine, as in AFG3L2^{E691K}, drastically changes the electrostatic potential and the chemical characteristics of the pore (**Fig. 5c**–**g** and **Supplementary Fig. 5c**–**g**). The change is evident in the AFG3L2^{WT}-AFG3L2^{E691K} compound homohexamer but is greatest in both the homohexameric mutant AFG3L2^{E691K}-AFG3L2^{E691K} and the heterohexameric AFG3L2^{E691K}-paraplegin (**Supplementary Fig. 5e**,**d**,**g**, respectively), in which paraplegin's neutral Gln693 residue, substituting for AFG3L2 Glu691, does not counteract the charge reversal of E691K.

Asn432 is located within the ATPase domain in an evolutionarily conserved region and is absolutely conserved from *T. thermophilus* FtsH to human AFG3L2 (**Fig. 1**). In the hexameric assembly of FtsH, the side chain of the corresponding residue Asn280 is located in the pore and is near (~6 Å) Phe229 (Phe381 in AFG3L2) of the alternate monomer (**Supplementary Fig. 6b**), the crucial aromatic residue in the central pore loop motif @XG (pore-1 motif, where @ is an aromatic residue and X is any residue) that is conserved in all subfamilies of the AAA family[20].

Protein expression studies in cells from affected individuals

We raised polyclonal antibodies that specifically recognize AFG3L2 and paraplegin (**Supplementary Fig. 7**). Immunoblot analysis of lymphoblastoid cells showed similar levels of AFG3L2 and paraplegin in affected and control subjects (**Supplementary Fig. 8a**). Furthermore, nondenaturing blue native gel electrophoresis revealed normal levels of a high-molecular-mass (~1 MDa) immunoreactive protein (**Supplementary Fig. 8b**). The results are consistent with co-immunoprecipitation experiments performed in yeast (**Fig. 2g**) and indicate that the mutant protein is stable and competent for supramolecular assembly and does not induce secondary depletion of paraplegin.

To examine whether AFG3L2 substitutions could induce secondary abnormalities of other proteins known to be either

partners or substrates of the *m*-AAA complex, we also investigated the expression of prohibitin-1 (PHB1) and prohibitin-2 (PHB2)[12,21], MRPL32, described above, and OPA1 (ref. 22), observing no differences either in the protein levels or in the migration patterns as compared to normal controls (**Supplementary Fig. 9**).

Expression of AFG3L2 and paraplegin in the nervous system

Confocal immunofluorescence analysis (**Fig. 6a**–**h**) showed that in the human cerebellum both AFG3L2 and paraplegin are highly and selectively expressed in the Purkinje cell layer (**Fig. 6a**–**d**) and the large neurons of the deep cerebellar nuclei (data not shown), with negligible labelling in all other cerebellar structures, including the molecular layer (**Fig. 6a**–**b**). Furthermore, the intensity of staining clearly outlined not only the cell body but also the dendritic arbor of all Purkinje neurons (**Fig. 6c**,**d**). A similar staining pattern was present in neurons of the cerebellar dentate nuclei (data not shown). AFG3L2 and paraplegin were also expressed in the motor system (pyramidal cortical neurons and spinal motor neurons; **Fig. 6e**–**h**). However, in contrast with observations in the cerebellum, paraplegin staining was more evident than that of AFG3L2 in both layer-V cortical neurons (compare **Fig. 6e**,**g)** and lamina-IX motor neurons (compare **Fig. 6f**,**h**). AFG3L2 staining of most spinal motor neurons was just above background levels (**Fig. 6f**, inset).

We confirmed the pattern of expression observed in the human cerebellum through *in situ* hybridization analysis of *Afg3l2* and *Spg7* transcripts in mouse (**Fig. 6i**–**k** and **l**–**n**, respectively). Both genes were strongly expressed in the Purkinje cell layer and in deep nuclei neurons. By contrast, almost no labeling was observed in the molecular layer, and in the granule cell layer, cells were labeled at an intermediate level for *Afg3l2* (**Fig. 6i**,**j)** and weakly for *Spg7* (**Fig. 6l**,**m**). Labeling of Golgi cells was strong for *Afg3l2* (**Fig. 6j**) and weak for *Spg7* (**Fig. 6m**).

Discussion

The genetic and functional data presented here demonstrate that missense mutations of *AFG3L2* are responsible for the autosomal dominant spinocerebellar ataxia SCA28 that we previously mapped on chromosome 18p11.22 (ref. 8). Furthermore, they indicate an unexpectedly essential role for AFG3L2 in protecting the human cerebellum from neurodegeneration and expand the spectrum of molecular mechanisms underlying the overlapping features of hereditary ataxias.

The finding that substitutions in AFG3L2, a metalloprotease of the mitochondrial protein quality control system[12,14], cause a dominant form of cerebellar ataxia is remarkable for several reasons. First, the vast majority of disorders of nuclear genes encoding mitochondrial proteins are recessively inherited[23]. In this group, a number of defects are known to cause different

forms of early-onset ataxia, the most important of which is Friedreich's ataxia[4]. By contrast, no autosomal dominant spinocerebellar degeneration has thus far been associated with mutations affecting proteins targeted to the mitochondria, and the relatively few mitochondrial disorders having an autosomal dominant pattern of inheritance are characterized by noncerebellar phenotypes, such as progressive external ophthalmoplegia (associated with *SLC25A4* (*ANT1*; MIM 609283), *C10orf2* (*TWINKLE*; MIM 609286) and *POLG* (MIM 157640)), optic atrophy (*OPA1*; MIM 165500), peripheral neuropathy (*MFN2* (CMT2A2; MIM 609260)) and spastic paraplegia (*HSPD1* (SPG13; MIM 605280) and *REEP1* (SPG31; MIM 610250))[23]. Second, alterations of paraplegin, a cognate AAA protease partner of AFG3L2 in the *m*-AAA metalloprotease complex, cause a distinct neurodegenerative disorder, SPG7 hereditary spastic paraplegia, by a loss-of-function recessive mechanism[9].

In total, we identified six heterozygous missense mutations in affected individuals that were absent in controls. Notably, five of them are located in highly conserved regions of the two functional domains (**Fig. 1**). Four substitutions (E691K, S674L, A694E and R702Q) reside close to each other in the proteolytic domain. Although none of these substitutions affects the catalytic zinc-binding motif HEAGH, their clustering in this small region suggests that it may be crucial in proteolysis, possibly in substrate recognition and/or handling. Expression studies in an *m*-AAA–deficient *S. cerevisiae* strain (*yta10*A*yta12*A) showed

that all the substitutions except H126Q, the only one found outside the two functional domains, affect protein activity, causing a respiratory-deficient phenotype that correlates with the accumulation of unprocessed *m*-AAA substrates.

Analysis of the respiratory phenotype of cells coexpressing both normal and mutant AFG3L2 suggests that two classes of *AFG3L2* mutations exist. A first group of dominant negative mutants, exemplified by AFG3L2^{E691K} and AFG3L2^{N432T}, would affect both the homo-oligomeric (AFG3L2^{WT}-AFG3L2^{mut}) and the hetero-oligomeric (AFG3L2^{mut} paraplegin^{WT}) assemblies, as also suggested by structural models. These two mutations are expected to be highly penetrant, and the number of affected subjects observed in both families MI-A0091 (E691K) and MI-A2473/RM-DS (N432T) is consistent with this hypothesis. By contrast, haploinsufficiency or a weak dominant negative effect, as no evidence of ataxia has been reported in individuals with familial syndromes caused by chromosome 18p deletion[24] could be the mechanism for a second group of AFG3L2 mutants (AFG3L2^{S674L}, AFG3L2^{A694E} and AFG3L2^{R702}Q), which are rescued in yeast by coexpression of wild-type AFG3L2 or paraplegin. In human cells, assembly of normal AFG3L2 or paraplegin with one of these mutant AFG3L2 forms might variably mitigate the effect of the mutation, resulting in variably reduced penetrance and/or expressivity in affected people, as observed in the family bearing AFG3L2^{R702}Q (**Supplementary Fig. 2**). This hypothesis would be consistent with the limited number of affected individuals reported in families MI-A1948

(S674L), MI-A0650 (A694E) and MI-A0762 (R702Q). Whichever the mechanism, however, all the clinically affected individuals showed a substantially homogeneous phenotype regardless of the mutation. Thus, taken together, the results point to a model in which the cerebellar degeneration and the consequent clinical phenotype arise from the perturbation of a specific function of AFG3L2 in the Purkinje neurons, which is essentially independent from the presence of paraplegin. The selective and intense expression of both AFG3L2 and paraplegin in human and murine Purkinje cells (**Fig. 6**) is consistent with this hypothesis.

How could the identified mutations affect AFG3L2 function? Polypeptide processing by AAA proteases involves substrate recognition and ATP-dependent unfolding and disassembly of the substrate as it is threaded through the ATPase central pore into the catalytic chamber[25,26]. Analysis of both yeast and affected individuals' cells (**Supplementary Fig. 8**) indicates that there is no substantial effect on protein stability and that the mutants are competent for supramolecular assembly. The hypothesis that the mutations may disrupt specialized function(s) of AFG3L2 gains support from molecular modeling of mutants into the crystal structure of the eubacterial FtsH metalloprotease[19]. The most intriguing mutations are those affecting Glu691 (E691K) in the proteolytic domain and Asn432 (N432T) in the ATPase domain, both of which behave in a dominant negative fashion. Both affect central pore structures, either on the proteolytic side (E691K) or on the ATPase side (N432T), that may be crucial for

the recognition, unfolding, translocation or release of substrate proteins. E691K drastically changes the electrostatic potential and the chemical characteristics of the pore in both the homo- and heterohexameric complexes (**Fig. 5c**–**g**), which explains why the respiratory-deficient phenotype of the AFG3L2^{E691K} strain is not rescued by AFG3L2^{WT} or paraplegin coexpression. Although several studies have investigated the structural and functional role of the central pore in the ATPase domain[26–28], very little is known concerning the pore on the proteolytic side. On the basis of our results (**Fig. 4**), one might speculate that the mutation(s) affecting this functional domain hamper the release of processed substrate(s), thus causing upstream accumulation of unprocessed species, although one could also consider an effect on substrate recognition, on binding of adaptor proteins[21,29,30] if there are any such proteins, or even on ATPase activity[31].

The N432T substitution in the ATPase domain is also noteworthy in that it affects an absolutely conserved residue in the central pore region on the membrane side of the barrel, the channel through which substrates are translocated into the proteolytic chamber. Molecular modeling in *T. thermophilus* FtsH reveals that Asn432 is semi-exposed and in proximity to Phe381 (Phe229 in FtsH), the crucial aromatic residue in the highly conserved central pore loop motif F/YVG (ref. 20) proposed to be essential for substrate recognition and ATP-dependent translocation of proteins into the proteolytic chamber[27,28,32]. Although Asn432 does not appear to make direct contact with Phe381, its extreme conservation, along with

the deleterious effects of its substitution with an amino acid of the same class (uncharged polar), strongly suggest that Asn432 makes a functionally relevant contribution to forming interactions with substrates. In this case, the involvement of residues from alternate chains (monomers; **Supplementary Fig. 6b**) would be perfectly consistent with the dominant negative mechanism proposed for this mutation.

We have shown a clear correlation between respiratory deficiency and a severe defect of respiratory chain complex IV in *m*-AAA–deficient yeast cells expressing human AFG3L2 mutants. As both essential proteolytic functions and chaperone-like activity of the *m*-AAA complex have been implicated in the biogenesis and maintenance of respiratory chain complexes[17,18], the possibility exists that substitutions in the proteolytic domain may affect an activity of AFG3L2 that is poorly dependent on the proteolytic function[31]. However, we have found a good correlation between respiration and proteolytic competence of AFG3L2 (**Fig. 4**). A significant accumulation of MrpL32 precursor species was indeed observed in yeast cells expressing mutant AFG3L2. Notably, though, these cells did not respire despite the fact that some mature MrpL32 was still produced. It is possible that mature-sized

MrpL32 generated by mutant AFG3L2 does not support respiration because it is not appropriately released from the mutant protease or does not attain a proper conformation. Whichever the mechanism, however, the accumulation of pMrpL32 indicates a general impairment of AFG3L2's substrate

processing activity. As the *m*-AAA protease can act as both a processing enzyme in the biogenesis of specific mitochondrial proteins and a component of the mitochondrial protein quality control system for the degradation of misfolded polypeptides[14,33], even a partial reduction of its proteolytic competence may result in a generalized impairment of these crucial activities, with potentially lethal pleiotropic effects on mitochondrial function.

Thus, although the human pathology caused by AFG3L2 substitutions could be the result of a general impairment of the 'mitochondrial proteasome', the specificity of the lesions, particularly if compared with those associated with paraplegin substitutions, suggests that specific substrate(s) may be affected in the neurons of individuals with SCA28. No biochemical phenotype could be identified in non-neuronal cell lines and tissue obtained from affected individuals. Both MRPL32 (refs. 13,16) and OPA1, another protein recently proposed to be regulated by AFG3L2 (ref. 22), are processed normally in lymphoblasts of affected individuals (**Supplementary Fig. 9**). Similarly, there is no evidence for a defect of autocatalytic processing of *m*-AAA subunits by AFG3L2 (ref. 34; **Supplementary Fig. 8**). Furthermore, despite the high *AFG3L2* expression levels in human skeletal muscle[35], analysis of muscle biopsies from four affected individuals in families MI-A0091 and MI-A1948 did not reveal any abnormality of respiratory chain activity nor characteristic histopathological signs of mitochondrial involvement (data not shown). The lack of

mitochondrial abnormalities in nonneuronal tissues is not surprising and has been observed in other disease conditions showing neuronal specificity[36]. It is conceivable that, in non-neuronal cells, the presence of one mutant *AFG3L2* allele might be insufficient to impair housekeeping functions of the *m*-AAA protease that can be carried out by proteolytic complexes with both homo- and hetero-oligomeric subunit composition[13]. By contrast, it might be deleterious in a cellular context (such as the Purkinje neuron) more susceptible to perturbations of AFG3L2 activity or in which AFG3L2 homocomplex would perform unique or predominant functions. Thus, the data together are consistent with the purely neurological phenotype observed in all affected individuals and further support the hypothesis that specific substrates for AFG3L2 exist whose normal processing is essential to protect the cerebellum from neurodegeneration.

A specialized role of AFG3L2—both in the homo- and in the hetero- complex configuration—in the human cerebellum would well account for the phenotypic differences between SCA28, in which pyramidal dysfunction is clinically negligible, and the recessive form of hereditary spastic paraplegia (SPG7) caused by paraplegin deficiency, which is characterized by degeneration of the corticospinal tract[37]. Consistent with this model, expression analysis of AFG3L2 and paraplegin indicates a much lower expression of AFG3L2 relative to paraplegin in the human motor system (**Fig. 6**). Contrasting with the human disease, two recently described *Afg3l2*-null mouse models have a lethal motor phenotype characterized by early-onset

tetraparesis leading to death at postnatal day 16 (ref. 38). In these models, however, the disease is recessive and is characterized by the complete inactivation of Afg3l2. Given the severe phenotype of *Afg3l2*-null mice and the lack of the third *m*-AAA component, Afg3l1, in human cells, we predict that complete loss of AFG3L2 is embryonically lethal in humans. Heterozygous *Afg3l2*$^{+/-}$ animals are apparently unaffected[38]. However, a recent re-evaluation of these mice based on our findings has revealed Purkinje cell degeneration associated with a subtle late onset decline of some motor performance[39].

In conclusion, we have identified *AFG3L2* as the gene responsible for SCA28, which appears to account for at least 3% of SCAs with unknown defects. The discovery that dominant mutations cause cerebellar ataxia by affecting AFG3L2 activity and that AFG3L2 is highly and selectively expressed in human Purkinje cells reveals its essential role in protecting the human cerebellum against neurodegeneration. The identification of neuron-specific substrates or adaptor proteins[25] of AFG3L2 will shed more light on the normal function of this versatile component of the mitochondrial protein quality control and activation machinery and will pave the road to understanding the specificity of neuronal death in human disease.

Refence

1. Harding, A.E. The clinical features and classification of the late onset autosomal dominant cerebellar ataxias. A study of 11 families, including descendants of the 'the Drew family of Walworth'. *Brain* **105**, 1–28 (1982).
2. Schöls, L., Bauer, P., Schmidt, T., Schulte, T. & Riess, O. Autosomal dominant cerebellar ataxias: clinical features, genetics, and pathogenesis. *Lancet Neurol.* **3**, 291–304 (2004).
3. Matilla-Duenas, A. *et al.* Cellular and molecular pathways triggering neurodegeneration in the spinocerebellar ataxias. Cerebellum published online, doi:10.1007/s12311- 009-0144-2 (5 November 2009).
4. Taroni, F. & Di Donato, S. Pathways to motor incoordination: the inherited ataxias. *Nat. Rev. Neurosci.* **5**, 641–655 (2004).
5. Koeppen, A.H. The pathogenesis of spinocerebellar ataxia. *Cerebellum* **4**, 62–73 (2005).
6. Orr, H.T. & Zoghbi, H.Y. Trinucleotide repeat disorders. *Annu. Rev. Neurosci.* **30**, 575–621 (2007).
7. Soong, B.W. & Paulson, H.L. Spinocerebellar ataxias: an update. *Curr. Opin. Neurol.* **20**, 438–446 (2007).
8. Cagnoli, C. *et al.* SCA28, a novel form of autosomal dominant cerebellar ataxia on chromosome 18p11.22-q11.2. *Brain* **129**, 235–242 (2006).
9. Casari, G. *et al.* Spastic paraplegia and OXPHOS impairment caused by mutations in paraplegin, a nuclear-encoded mitochondrial metalloprotease. *Cell* **93**, 973–983 (1998).
10. Hanson, P.I. & Whiteheart, S.W. AAA+ proteins: have engine, will work. *Nat. Rev. Mol. Cell Biol.* **6**, 519–529 (2005).
11. Ito, K. & Akiyama, Y. Cellular functions, mechanism of action, and regulation of FtsH protease. *Annu. Rev. Microbiol.* **59**, 211–231 (2005).

12. Koppen, M. & Langer, T. Protein degradation within mitochondria: versatile activities of AAA proteases and other peptidases. *Crit. Rev. Biochem. Mol. Biol.* **42**, 221–242 (2007).
13. Koppen, M., Metodiev, M.D., Casari, G., Rugarli, E.I. & Langer, T. Variable and tissue-specific subunit composition of mitochondrial m-AAA protease complexes linked to hereditary spastic paraplegia. *Mol. Cell. Biol.* **27**, 758–767 (2007).
14. Tatsuta, T. & Langer, T. Quality control of mitochondria: protection against neurodegeneration and ageing. *EMBO J.* **27**, 306–314 (2008).
15. Esser, K., Tursun, B., Ingenhoven, M., Michaelis, G. & Pratje, E. A novel two-step mechanism for removal of a mitochondrial signal sequence involves the mAAA complex and the putative rhomboid protease Pcp1. *J. Mol. Biol.* **323**, 835–843 (2002).
16. Nolden, M. *et al.* The m-AAA protease defective in hereditary spastic paraplegia controls ribosome assembly in mitochondria. *Cell* **123**, 277–289 (2005).
17. Arlt, H., Tauer, R., Feldmann, H., Neupert, W. & Langer, T. The YTA10–12 complex, an AAA protease with chaperone-like activity in the inner membrane of mitochondria. *Cell* **85**, 875–885 (1996).
18. Arlt, H. *et al.* The formation of respiratory chain complexes in mitochondria is under the proteolytic control of the m-AAA protease. *EMBO J.* **17**, 4837–4847 (1998).
19. Suno, R. *et al.* Structure of the whole cytosolic region of ATP-dependent protease FtsH. *Mol. Cell* **22**, 575–585 (2006).
20. Yamada-Inagawa, T., Okuno, T., Karata, K., Yamanaka, K. & Ogura, T. Conserved pore residues in the AAA protease FtsH are important for proteolysis and its coupling to ATP hydrolysis. *J. Biol. Chem.* **278**, 50182–50187 (2003).
21. Tatsuta, T. & Langer, T. AAA proteases in mitochondria: Diverse functions of membrane-bound proteolytic machines. *Res. Microbiol.* **160**, 711–717 (2009).

22. Ehses, S. *et al.* Regulation of OPA1 processing and mitochondrial fusion by m-AAA protease isoenzymes and OMA1. *J. Cell Biol.* **187**, 1023–1036 (2009).
23. DiMauro, S. & Schon, E.A. Mitochondrial disorders in the nervous system. *Annu. Rev. Neurosci.* **31**, 91–123 (2008).
24. Nasir, J. *et al.* Unbalanced whole arm translocation resulting in loss of 18p in dystonia. *Mov. Disord.* **21**, 859–863 (2006).
25. Dougan, D.A., Mogk, A., Zeth, K., Turgay, K. & Bukau, B. AAA+ proteins and substrate recognition, it all depends on their partner in crime. *FEBS Lett.* **529**, 6–10 (2002).
26. Graef, M., Seewald, G. & Langer, T. Substrate recognition by AAA+ ATPases: distinct substrate binding modes in ATP-dependent protease Yme1 of the mitochondrial intermembrane space. *Mol. Cell. Biol.* **27**, 2476–2485 (2007).
27. Graef, M. & Langer, T. Substrate specific consequences of central pore mutations in the i-AAA protease Yme1 on substrate engagement. *J. Struct. Biol.* **156**, 101–108 (2006).
28. Okuno, T., Yamanaka, K. & Ogura, T. Characterization of mutants of the *Escherichia coli* AAA protease, FtsH, carrying a mutation in the central pore region. *J. Struct. Biol.* **156**, 109–114 (2006).
29. White, S.R. & Lauring, B. AAA+ ATPases: achieving diversity of function with conserved machinery. *Traffic* **8**, 1657–1667 (2007).
30. Dunn, C.D., Tamura, Y., Sesaki, H. & Jensen, R.E. Mgr3p and Mgr1p are adaptors for the mitochondrial i-AAA protease complex. *Mol. Biol. Cell* **19**, 5387–5397 (2008).
31. Tatsuta, T., Augustin, S., Nolden, M., Friedrichs, B. & Langer, T. m-AAA proteasedriven membrane dislocation allows intramembrane cleavage by rhomboid in mitochondria. *EMBO J.* **26**, 325–335 (2007).
32. Augustin, S. *et al.* An intersubunit signaling network coordinates ATP hydrolysis by m-AAA proteases. *Mol. Cell* **35**, 574–585 (2009).
33. Augustin, S. *et al.* Characterization of peptides released from

mitochondria: evidence for constant proteolysis and peptide efflux. *J. Biol. Chem.* **280**, 2691–2699 (2005).

34. Koppen, M., Bonn, F., Ehses, S. & Langer, T. Autocatalytic processing of m-AAA protease subunits in mitochondria. *Mol. Biol. Cell* **20**, 4216–4224 (2009).
35. Banfi, S. *et al.* Identification and characterization of AFG3L2, a novel parapleginrelated gene. *Genomics* **59**, 51–58 (1999).
36. Amiott, E.A. *et al.* Mitochondrial fusion and function in Charcot-Marie-Tooth type 2A patient fibroblasts with mitofusin 2 mutations. *Exp. Neurol.* **211**, 115–127 (2008).
37. Stevanin, G., Ruberg, M. & Brice, A. Recent advances in the genetics of spastic paraplegias. *Curr. Neurol. Neurosci. Rep.* **8**, 198–210 (2008).
38. Maltecca, F. *et al.* The mitochondrial protease AFG3L2 is essential for axonal development. *J. Neurosci.* **28**, 2827–2836 (2008).
39. Maltecca, F. *et al.* Haploinsufficiency of AFG3L2, the gene responsible for spinocerebellar ataxia type 28, causes mitochondria-mediated Purkinje cell dark degeneration. *J. Neurosci.* **29**, 9244–9254 (2009).

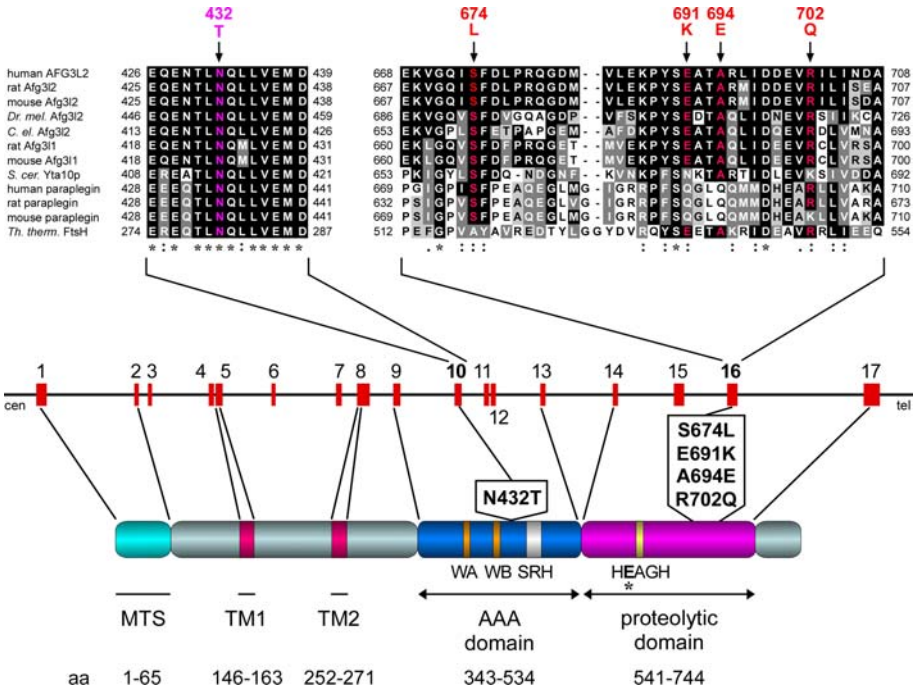

Figure 1 *AFG3L2* mutations cause amino acid substitutions in highly conserved regions of the protein. Bottom, genomic organization of the human *AFG3L2* gene and domain structure of the protein. *AFG3L2* consists of 17 exons spanning 48 kb on chromosome 18p11.21 (5'—>3′ map position: 12319108–12367194). The identified mutations in exon 10 and in exon 16 are boxed. Top, ClustalW2 multiple alignments of the human AFG3L2 regions encoded by exon 10 (residues 426–439) or exon 16 (residues 668–708) with members of the *m*-AAA family from different organisms (*Dr. mel.*, *Drosophila melanogaster*; *C. el.*, *Caenorhabditis elegans*; *S. cer.*, *S. cerevisiae; T. therm.*, *T. thermophilus*).

The mutated residues are indicated in red (proteolytic domain) or magenta (ATPase domain) above the alignment. Residues identical to AFG3L2 are framed in black. Conserved, semiconserved and nonconserved substitutions are framed in gray, light gray and white boxes, respectively. The following consensus symbols are used in the alignment to denote the degree of conservation, as defined by the Gonnet Pam250 matrix scores observed in each column: (*), residue is identical in all sequences in the alignment;(:), conserved substitutions have been observed; (.), semiconserved substitutions have been observed. MTS, mitochondrial targeting sequence; TM1 and TM2, transmembrane domains 1 and 2, respectively (TMHMM Server v2.0); WA, Walker-A motif (GPPGTGKT, residues 348–355); WB, Walker-B motif (ILFIDEID, residues 403–410); SRH, second region of homology (TNRPDILDPALLRPGRFD, residues 453–470); HEAGH (residues 574–578), protease catalytic site (Pfam 24.0, October 2009; http://pfam.sanger.ac.uk/; the asterisk on the HEAGH site indicates the catalytic Glu575 that is mutated to glutamine in the control proteolytic mutant AFG3L2^{E575Q}; ref. 13).

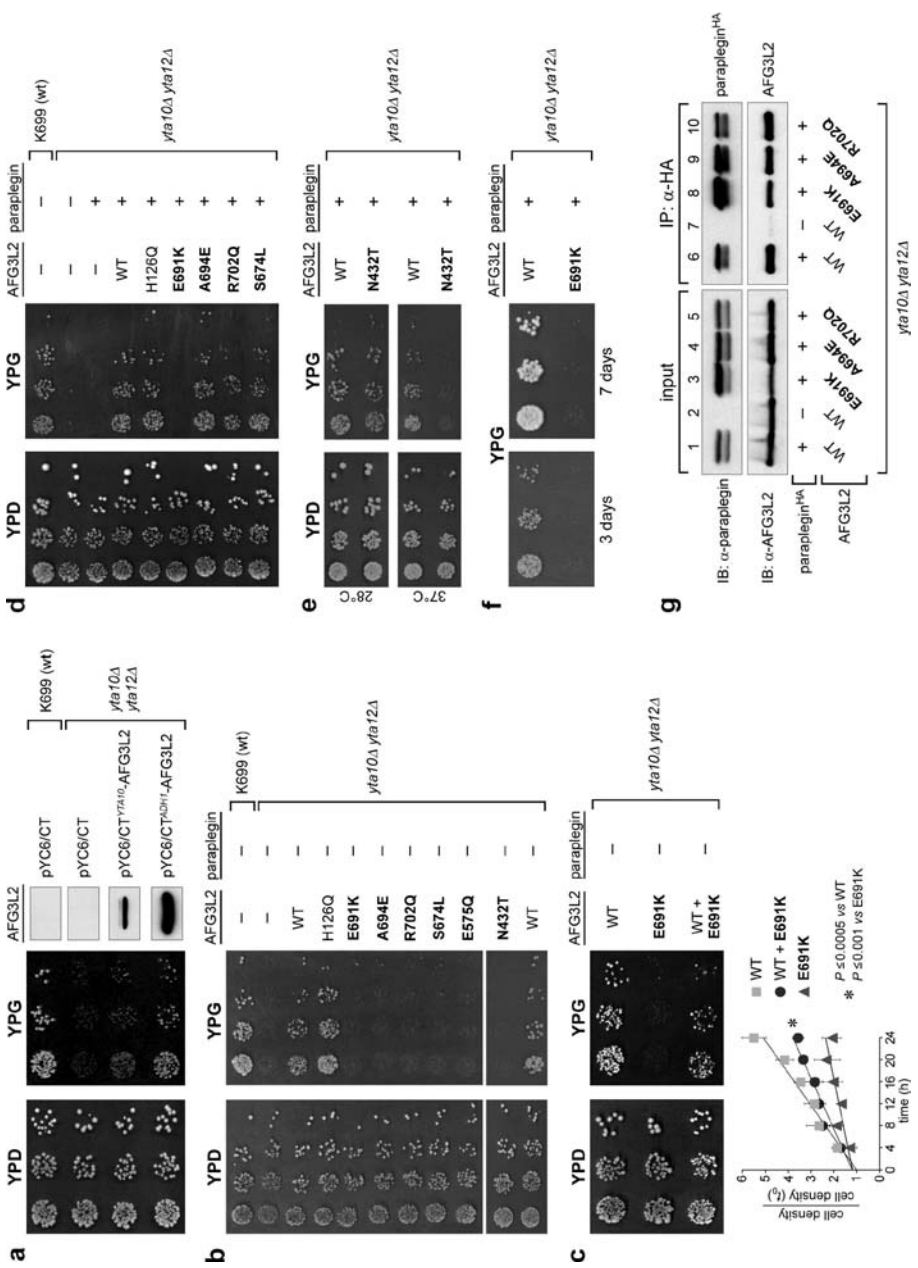

Figure 2 Complementation studies in *S. cerevisiae*. Serial dilutions of exponentially growing yeast cultures spotted on plates show oxidative growth phenotype of *yta10*Δ*yta12*Δ

cells expressing normal and mutant human AFG3L2. Substitutions affecting respiration are in bold. Respiratory competence is deduced by the ability to grow on 2% glycerol (YPG). Except where indicated, we scored growth after 3 d incubation at 28 °C. YPD and YPG, YEP plates containing 2% glucose or 2% glycerol, respectively. (**a**) AFG3L2 was expressed under control of the strong *ADH1* promoter (pYC6/ CT^{ADH1}-AFG3L2) or the endogenous *YTA10* promoter (pYC6/CT^{YTA10}-AFG3L2). Right panels, AFG3L2 levels assessed by immunoblotting. K699, WT yeast strain; pYC6/CT, empty plasmid. (**b**) Respiratory phenotype of *yta10*Δ*yta12*Δ cells expressing either normal (WT) or mutant human AFG3L2. Similar results were obtained after incubation at 37 °C (data not shown). (**c**) Coexpression of AFG3L2^{WT} (WT) and AFG3L2^{E691K} (E691K) results in a limited correction of the respiratory-deficient phenotype, suggesting a dominant negative effect of the mutation. The graph below shows the growth rates of cells expressing either AFG3L2^{WT} or AFG3L2^{E691K} or coexpressing both forms (WT+E691K). We grew cells for 24 h with cell counting every 4 h. Values on the *y* axis represent the ratio between cell density (cells/ml) at a given time and cell density at start (*t*0). Growth rates are calculated by linear regression analysis (trend line). Each value represents the mean of three independent experiments. Error bars indicate ± 1 s.d. We determined statistical significance ($P \leq 0.0005$ or $P \leq 0.001$) by Student's *t*-test. (**d**) Respiratory phenotype of

*yta10*Δ*yta12*Δ cells coexpressing either normal or mutant human AFG3L2 with human paraplegin. (**e**) Rescue of the AFG3L2^{N432T} respiratory-deficient phenotype by paraplegin is temperature sensitive, with moderate growth at 28 °C but no growth at 37 °C; no growth difference at 37 °C was observed for the other mutants (data not shown). (**f**) No rescue of the AFG3L2^{E691K} respiratory-deficient phenotype by paraplegin in long-term culture (7 d). (**g**) Both normal and mutant AFG3L2 interact with paraplegin. We immunoprecipitated hemagglutinin (HA)-tagged paraplegin (paraplegin^{HA}) with anti-HA from *yta10*Δ*yta12*Δ cells expressing AFG3L2^{WT} alone (lanes 2 and 7) or coexpressing either wild-type or mutant AFG3L2 with paraplegin^{HA}. We analyzed immunoprecipitates (IP) by SDS-PAGE and immunoblotting (IB) using anti-paraplegin (á-paraplegin) or anti-AFG3L2 (á-AFG3L2). AFG3L2 was detected in all the immunoprecipitates from yeast cells coexpressing paraplegin^{HA} (lanes 6 and 8–10). Lanes 1–5, immunoblot analysis of cell extracts before immunoprecipitation (input).

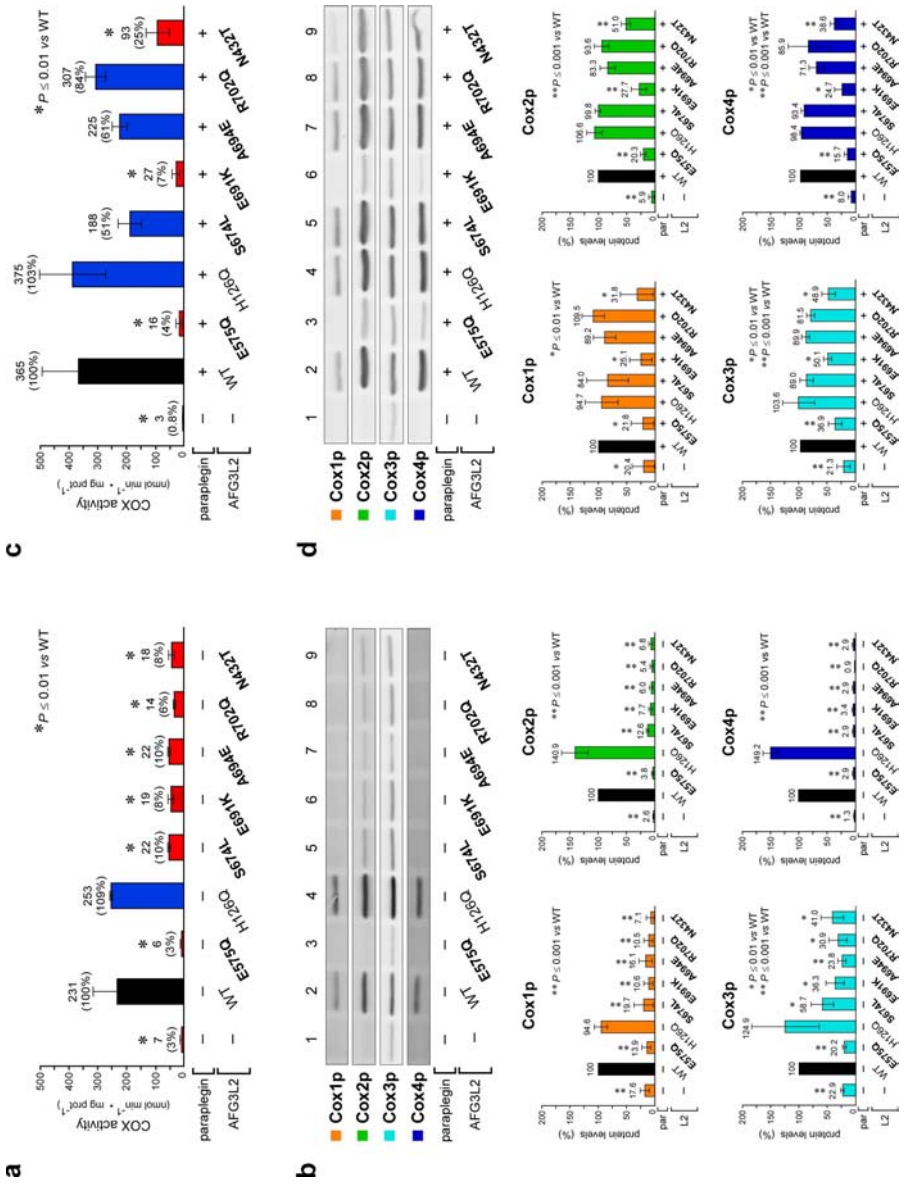

Figure 3 Cytochrome *c* oxidase enzyme activity and protein levels in yeast cells expressing mutant AFG3L2. Yeast strains and mutants are as described in **Figure 2**. Substitutions affecting respiration are in bold. (**a**) COX

activity measured in isolated mitochondria from *yta10*Δ*yta12*Δ *m*-AAA–deficient yeast cells expressing AFG3L2 alone, in the absence of paraplegin. Activity is expressed as nanomoles of cytochrome c^{red} oxidized per minute per milligram of protein. Values in parentheses indicate percentage of activity compared to that of cells expressing $AFG3L2^{WT}$ (black bars). Bars and vertical lines indicate mean and ± 1 s.d., respectively. Red bars and asterisk indicate a statistically significant ($P \leq 0.01$) difference from $AFG3L2^{WT}$, as determined by Student's *t*-test ($n = 4$). Absence of asterisk (blue bars) indicates $P > 0.05$. (**b**) Fluorescence immunoblot analysis and protein quantitation of mitochondria-encoded COX subunits Cox1p, Cox2p and Cox3p, and nuclear-encoded subunit Cox4p, in mitochondrial extracts from cells expressing AFG3L2 alone, in the absence of paraplegin. Single or double asterisk indicates a statistically significant difference from $AFG3L2^{WT}$ (black bars) with $P \leq 0.01$ or $P \leq 0.001$, respectively, as determined by Student's *t*-test ($n = 4$). Absence of asterisk indicate $P > 0.05$. (**c**,**d**) COX activity and fluorescence immunoblot analysis as in **a** and **b** for AFG3L2 in the presence of paraplegin.

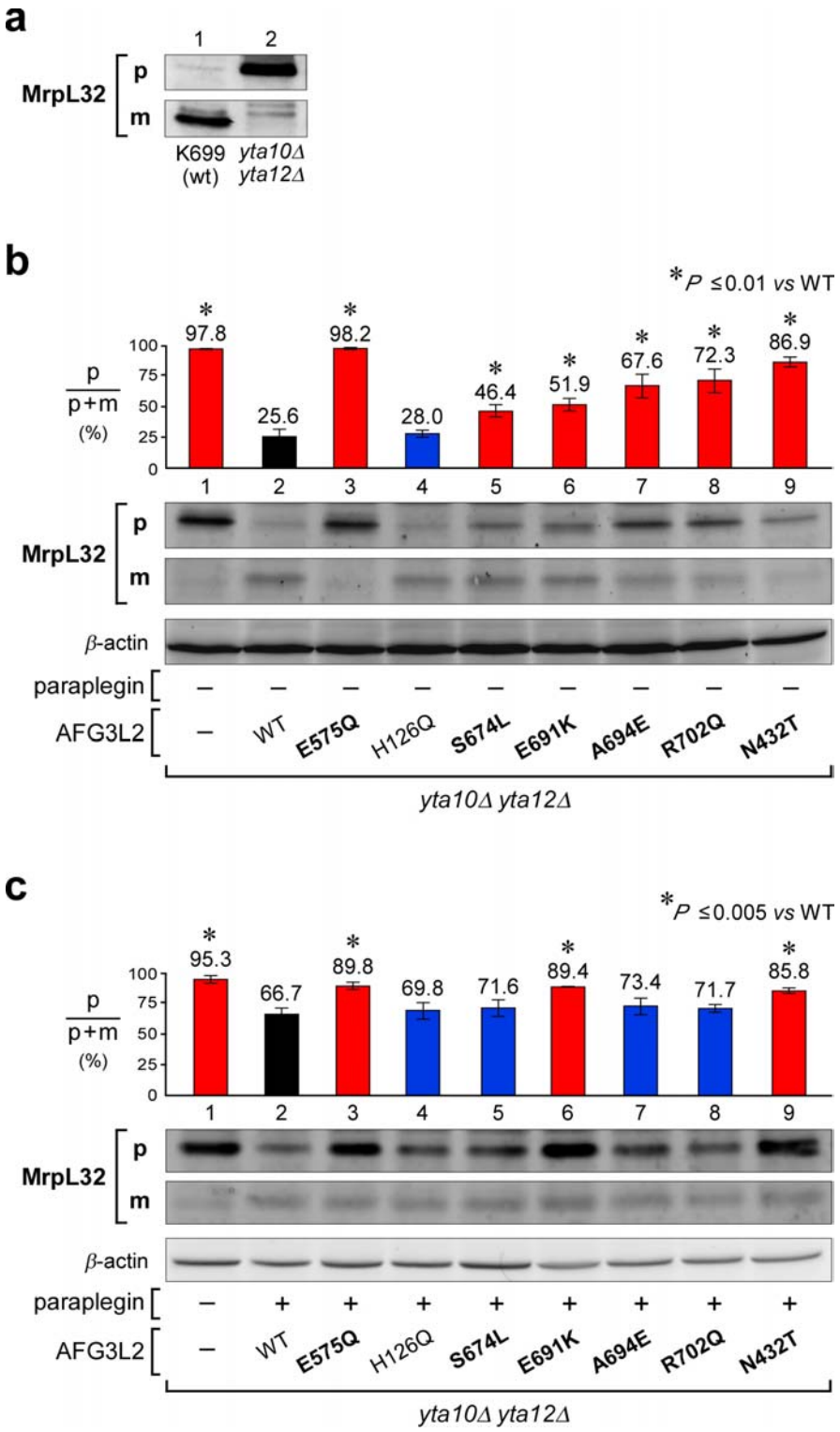
a
1
2
MrpL32
p
m
K699 (wt)
yta10Δ yta12Δ
b
*P ≤0.01 vs WT
p / p+m (%)
97.8
25.6
98.2
28.0
46.4
51.9
67.6
72.3
86.9
1 2 3 4 5 6 7 8 9
MrpL32
β-actin
paraplegin
AFG3L2
WT
E575Q
H126Q
S674L
E691K
A694E
R702Q
N432T
yta10Δ yta12Δ
c
*P ≤0.005 vs WT
95.3
66.7
89.8
69.8
71.6
89.4
73.4
71.7
85.8
1 2 3 4 5 6 7 8 9
MrpL32
β-actin
paraplegin
AFG3L2
WT
E575Q
H126Q
S674L
E691K
A694E
R702Q
N432T
yta10Δ yta12Δ

Figure 4 Proteolytic activity of normal and mutant AFG3L2 in yeast. Yeast strains and mutants are as in **Figure 2**. Substitutions affecting respiration are in bold. (**a**) Fluorescence immunoblot analysis with anti-MrpL32 shows that yeast MrpL32 precursor (p) accumulates in *yta10*A*yta12*A *m*-AAA–deficient cells (lane 2). m, mature MrpL32. (**b**) Fluorescence immunoblot analysis of MrpL32 in yeast cells expressing AFG3L2 homo-oligomeric *m*-AAA, showing accumulation of MrpL32 precursor in AFG3L2 mutants. Histograph reports quantitative results. AFG3L2 proteolytic competence is expressed as the ratio of pMrpL32 level to total (p + m) MrpL32 level. MrpL32 levels were normalized to the loading control protein f3-actin. Bars and vertical lines indicate mean and ± 1 s.d., respectively. Red bars and asterisks indicate a statistically significant (P ~ 0.01) difference from AFG3L2^{WT} (lane 2, black bar) as determined by Student's *t*-test (n = 4). Blue bars and absence of asterisk indicate P > 0.05. (**c**) Fluorescence immunoblot analysis of MrpL32 in *m*-AAA–deficient yeast cells, showing the effects of AFG3L2 and paraplegin coexpression on the accumulation of pMrpL32 (indicated by p/(p + m) ratio as in **b**). MrpL32 levels were normalized to the loading control protein f3-actin. Bars and vertical lines indicate mean and ± 1 s.d., respectively. No statistically significant difference (P > 0.05) was observed between AFG3L2^{WT}-harboring cells (lane 2, black bar) and strain AFG3L2^{H126Q} or mutant strains AFG3L2^{S674L}, AFG3L2^{A694E}

and AFG3L2^{R702Q} (lanes 4, 5, 7 and 8, blue bars). By contrast, asterisk (red bars) indicates a statistically significant difference (P ~ 0.005, n = 4; Student's t-test) between AFG3L2^{WT} cells and SCA28 mutants AFG3L2^{E691K} or AFG3L2^{N432T}, or the control mutant AFG3L2^{E575Q} (ref. 13).

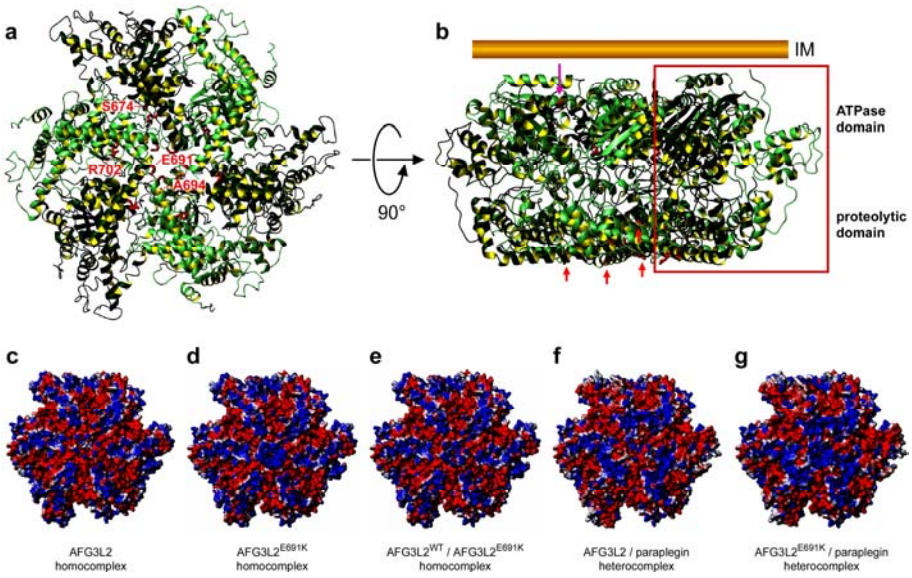

Figure 5 Molecular modeling of normal and mutant AFG3L2. (**a**,**b**) Orthogonal views of the hexameric ring of AFG3L2 built by homology using the coordinates of *T. thermophilus* FtsH (PDB 2DHR) as a template. Panel **a** shows the view from the protease domain (matrix) side. The monomers are alternately shown in light and dark green. The side chains of the proteolytic domain residues mutated in the affected individuals are shown in red. In **b**, it is clear that the hexamer adopts a flat-cylinderlike shape divided into two disks. The lower disk, containing the protease domain, forms a sixfold-symmetric structure with a zinc binding site. The upper disk is composed of six AAA domains, each of which contains ADP. Short red arrows indicate the locations of substitutions on the matrix side of the protease domain (lower disc); long magenta arrow indicates the location of the N432T

substitution in the ATPase domain (upper disc). The monomer (**Supplementary Fig. 5a**) is boxed in red. IM, inner mitochondrial membrane. (**c**–**g**) Surface representations of the protease side of the homo- and hetero-oligomeric homology models, showing the effect of the E691K substitution on the electrostatic potential of the complex (see also **Supplementary Fig. 5c–g**). Shown are electrostatic surfaces of wild-type AFG3L2 homohexamer (**c**); homohexamer of AFG3L2^{E691K} (**d**); homohexamer obtained by alternating wild-type AFG3L2 (AFG3L2^{WT}) and mutant AFG3L2^{E691K} (**e**); and heterohexamer obtained by alternating paraplegin with either AFG3L2^{WT} (**f**) or AFG3L2^{E691K} (**g**). Blue, positive charge; red, negative charge. The change induced by the E691K charge reversal in the central pore is greatest in the homohexameric mutant AFG3L2^{E691K}-AFG3L2^{E691K} (**d**) and in the heterohexameric complex of AFG3L2^{E691K} and paraplegin (**g**), in which the positively charged Lys691 of AFG3L2^{E691K} is not counteracted by the neutral Gln693 of paraplegin.

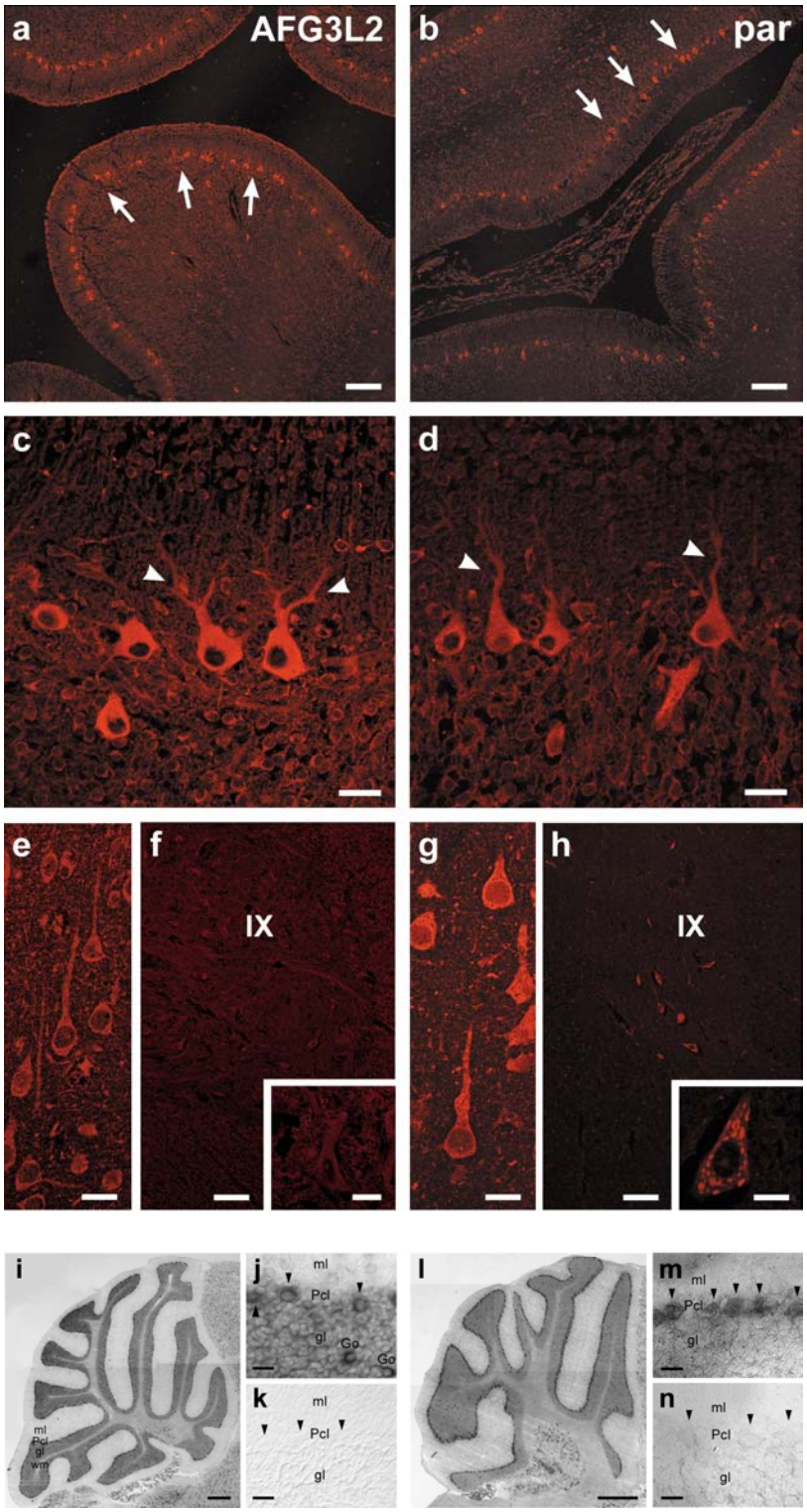
a
AFG3L2
b
par
c
d
e
f
IX
g
h
IX
i
ml
Pcl
gl
wm
j
ml
Pcl
gl
Go
Go
k
ml
Pcl
gl
l
m
ml
Pcl
gl
n
ml
Pcl
gl

Figure 6 Expression of AFG3L2 and paraplegin in human and mouse nervous systems. (**a**–**h**) Confocal immunofluorescence of human nervous tissue. In the cerebellum (**a**–**d**), both AFG3L2 (**a**,**c**) and paraplegin (**b**,**d**) are selectively expressed in the Purkinje cell layer (**a**,**b**, arrows). Note the intense expression in the soma and apical dendrites of Purkinje neurons (**c**,**d**, arrowheads). In the cerebral cortex (**e**,**g**) and spinal cord (**f**,**h**), as compared to AFG3L2 (**e**,**f**), paraplegin is more intensely expressed in layer-V pyramidal neurons (**g**) and lamina-IX motor neurons (**h**). AFG3L2 staining in spinal motor neurons (**f**) is just above background level. Insets in **f** and **h** show enlarged detail. Scale bars, 100 .tm (**a**,**b**,**f**,**h**) or 20 .tm (**c**–**e**,**g**, insets of **f** and **h**). (**i**–**n**) *In situ* hybridization of mouse cerebellum with *Afg3l2* (**i**–**k**) and *Spg7* (**l**–**n**) riboprobes. Low (**i**,**l**) and high (**j**,**m**) magnification of parasagittal sections of the cerebellar vermis showing a strong expression in Purkinje cells (**j**,**m**, arrowheads) and a weaker expression in granule and Golgi cells. (**k**,**n**) Control sections adjacent to **j** and **m**, hybridized with sense probes. Scale bars, 400 .tm (**i**,**l**) or 25 .tm (**j**,**k**,**m**,**n**). ml, molecular layer; Pcl, Purkinje cell layer; gl, granule cell layer; Go, Golgi cell; wm, white matter.

Online Methods

Affected individuals, DNA samples and cell lines.

Affected individuals and members from family MI-A0091 were as described[8]. We further studied 337 unrelated index cases (136 with autosomal dominant inheritance, 51 compatible with autosomal recessive inheritance because of parental consanguinity or occurrence of the disease in one or more siblings in a single generation, and 150 sporadic cases) selected from a large cohort of individuals with a diagnosis of ataxia referred to our center from throughout Italy. Inclusion criteria were the presence of a progressive clinical phenotype in which ataxia was the prominent symptom and a positive familial history, or, for sporadic cases, the absence of acquired causes of cerebellar dysfunction[40]. All affected individuals were of Italian origin and showed a progressive ataxic phenotype and cerebellar atrophy variably associated with additional features such as pyramidal signs and minor abnormalities in ocular movements. Autosomal dominant and sporadic cases were negative for SCA1 and SCA2, the most frequent Italian SCA mutations[41]. The genes associated with SCA3, SCA6, SCA7, SCA10, SCA12, SCA17 and DRPLA were tested whenever a suggestive phenotype was present[2]. In most of the dominant index cases, the presence of a CAG expansion had also been excluded by repeat expansion detection analysis[41]. Possibly recessive cases and sporadic cases were negative for *FRDA1*

GAA expansion. Control subjects were individuals who presented for work-up of unrelated neurologic conditions.

We prepared Epstein-Barr-virus-stabilized lymphoblastoid cell lines and genomic DNA from peripheral-blood lymphocytes and lymphoblastoid cells as previously described[42].

We obtained written informed consent from each individual providing a biological sample. All procedures involving human subjects were approved by the Institutional Review Board of the Fondazione IRCCS Istituto Neurologico “Carlo Besta”, Milan, Italy.

Mutation analysis.

All *AFG3L2* genotyping protocols took into account the presence, revealed by *in silico* analysis (NCBI Genome Assembly Build 36.2) and confirmed by genomic DNA sequencing, of a previously unrecognized *AFG3L2* pseudogene on chromosome 8p22 (5′→3′ map position: 13447603–13445733) encompassing *AFG3L2* exons 1–14. We analyzed sequences of the 17 exons of 18p11 *AFG3L2*, including flanking intron sequences and the 5′ and 3′ untranslated regions, on an automated capillary sequencer (ABI Prism 3100 Genetic Analyzer, Applied Biosystems) using the BigDyeDeoxy Terminator Cycle Sequencing Kit (Applied Biosystems) according to the manufacturer’s recommendations.

For mutation screening of the selected affected population, we analyzed PCR products by automated sequencing and/or denaturing HPLC (**Supplementary Note**).

PCR conditions and sequences of the oligonucleotide primers used for PCR amplification, sequencing and denaturing HPLC analysis are detailed in **Supplementary Table 2** online.

Nucleotides are numbered so that the first nucleotide of the first in-frame ATG codon is nucleotide +1. Amino acid residues are numbered so that the methionine encoded by the first in-frame ATG codon is Met1.

AFG3L2 and paraplegin yeast expression plasmids.

We generated plasmids for heterologous expression of human AFG3L2 and paraplegin in yeast as described in the **Supplementary Note**. We verified AFG3L2 and paraplegin protein expression levels in each strain by immunoblot analysis of trichloroacetic acid cell protein extracts (see 'Protein immunoblot analysis' below and **Supplementary Fig. 3**).

Yeast strains and growth conditions.

All the strains used in this study are derivatives of W303 (K699; **Supplementary Table 3** online). To generate the *yta10*Δ*yta12*Δ strain, we deleted *YTA10* and *YTA12* using the one-step PCR strategy[43]. We followed standard procedures for strain generation and cultures[44]. We transformed yeast strains with the described vectors and grew cells at 28 °C on YEP medium (1% yeast extract, 2% Bacto-peptone, 2% agar for plates) or selective medium supplemented with 2% (wt/vol) glucose according to standard procedures. We selected blasticidin-resistant transformants on YPD medium

supplemented with 50 µg of blasticidin S per ml. For complementation experiments, we spotted equal amounts of fivefold serial dilutions of cells from exponentially grown cultures onto YEP plates containing 2% (wt/vol) glucose (YPD) or 2% (vol/vol) glycerol (YPG) and incubated them at 28 °C or 37 °C.

For growth rate analysis, we precultured yeast cells from the stock cultures overnight in selective medium, inoculated at a standard density of approximately 1×10^6 cells/ml and then grew them in YEP medium supplemented with 2% (vol/vol) glycerol for 24 h. Except where indicated, we removed samples every 4 h and determined cell density, expressed as cells/ml, in a Bürker chamber.

Assay of cytochrome *c* oxidase activity.

For *in vitro* activity assay of COX, we prepared yeast cell mitochondria by differential centrifugations[45,46] (**Supplementary Note**) and determined COX activity spectrophotometrically as described in ref. 46 and **Supplementary Note**.

Antibodies. We raised polyclonal antisera directed against human AFG3L2 and paraplegin in rabbit using glutathione *S*-transferase fusion proteins that carried protein fragments of AFG3L2 (residues 67–305) and paraplegin (residues 89–304) showing no homology to each other (see **Supplementary Note**). The antisera against AFG3L2 and paraplegin showed no cross-reactivity against the two proteins (**Supplementary Fig. 7a**,**b**) and demonstrated colocalization of AFG3L2 and

paraplegin with the mitochondrial protein PHB1 (**Supplementary Fig. 7c**–**h**).

We prepared antibodies to HA from mouse hybridoma clone 12CA5. Anti-yeast MrpL32 (ref. 13) and anti–medium-chain acyl-CoA dehydrogenase (MCAD)[42] were as previously reported. Anti-human MRPL32 were polyclonal antibodies raised in rabbit (T.L., unpublished data). Anti-tubulin, anti-PHB1, anti-PHB2 and anti-OPA1 were from Santa Cruz Biotechnology. Anti–α-actin was from Abcam. Mouse monoclonal antibodies to Cox1p, Cox2p, Cox3p and Cox4p were from MitoSciences.

Protein immunoblot analysis.

For protein blot analysis of yeast cells, we prepared trichloroacetic acid protein extracts as described[43] and separated them by SDS-PAGE in 10% or 15% acrylamide gels. We performed protein blotting with anti-AFG3L2 (1:12,000 dilution) and anti-paraplegin (1:6,000 dilution) using standard techniques. We probed filters with anti-yMrpL32 (1:1,000 dilution; ref. 13) and anti–α-actin (1:1,500 dilution), and revealed them with Alexa Fluor 647-conjugated goat anti-rabbit IgG (H+L) and Alexa Fluor 488- conjugated goat anti-mouse IgG (H+L) (Molecular Probes). We normalized MrpL32 signal to that of α-actin as the loading control protein.

For protein blot analysis of respiratory chain complex IV (COX) subunits, we prepared yeast mitochondria as described above and in **Supplementary Note**. We electrophoresed equal

amounts of mitochondrial proteins on 15% SDS polyacrylamide gels and transferred them to a polyvinylidene difluoride membrane (PVDF; Immobilon FL, Millipore). We probed filters with antiCox1p (1:300 dilution), anti-Cox2p (1:1,500 dilution), anti-Cox3p (1:300 dilution) and anti-Cox4p (1:1,500 dilution), and revealed them with Alexa Fluor 488-conjugated goat anti-mouse IgG (H+L) (Molecular Probes). We acquired fluorescence signals using a VersaDoc Imaging System (Bio-Rad) and performed quantitative analysis using Quantity One software (Bio-Rad) in four independent experiments.

Co-immunoprecipitation of AFG3L2 and paraplegin.

For immunoprecipitation experiments[47], we grew cells of strains harboring the different AFG3L2 substitutions to late log phase, resuspended them in PBS, 1 mM PMSF, 1 mM $NaVO_4$ and 50 mM NaF supplemented with Complete Protease Inhibitor Cocktail (Roche), and homogenized them using the FastPrep System (Qbiogene-MP Biomedicals). We spun homogenates for 20 min at 16,000*g* and incubated the resulting supernatants with 12CA5 monoclonal anti-HA (2 h at 4 °C under gentle shaking). We then incubated antigen-antibody complexes with protein G–Sepharose (2 h at 4 °C under gentle shaking). After extensive washes, we eluted samples from beads and analyzed them by SDS-PAGE and immunoblotting.

Homology modeling.

We built a model of AFG3L2 using the automated homology modeling server SWISS-MODEL[48] and the structure of the cytosolic region of the ATP-dependent metalloprotease FtsH from *T. thermophilus*[19] (mutant G399L; PDB 2DHR; UniProt Q72IK4) as the coordinate template.

We first aligned the two sequences with the ClustalX program (http://www. clustal.org/) to optimize insertions and deletions, then visualized and analyzed the model with the Molmol program. We built a similar model for the heterohexameric complex, assuming that AFG3L2 and paraplegin form an alternating heterodimer.

Confocal immunofluorescence analysis of human nervous tissue.

We obtained autopsy paraffin sections from the cerebellum of an infant who died immediately after birth owing to respiratory failure, and from the spinal cords of a 6-month-old infant and an adult who died from respiratory failure and medulloblastoma, respectively. We also used cortical vibratome sections obtained from a temporal-lobe specimen of a 47-year-old individual during brain surgery for a low-grade glioma. We cut paraplast-embedded autopsy specimens in 5- to 10-µm sections with a rotary microtome (Leica), whereas we fixed the cortical sample by immersion in 4% (wt/vol) paraformaldehyde and then cut it in 50-µm

sections with a vibratome (Leica). We performed immunofluorescence assays with anti-AFG3L2 or anti-paraplegin (1:500 dilution) followed by incubation with biotinylated goat anti-rabbit IgG/rhodamine avidin D (Jackson ImmunoResearch Labs) essentially as previously described[49]. We acquired fluorescence images on a Radiance 2100 confocal microscope (Bio-Rad) at a resolution of 1,024 × 1,024 pixels.

In situ hybridization on mouse cerebellum.

We performed nonradioactive *in situ* hybridization with digoxigenin-labeled riboprobes spanning the transcripts of *Afg3l2* and *Spg7* on brains collected from adult CD-1 mice and prepared as previously described[50]. We cut sections (15 µm) with a cryostat, mounted them on glass slides, fixed them in 4% (wt/vol) paraformaldehyde and treated them with 0.5% Triton X-100 PBS and then with triethanolamineacetic anhydride solution. We carried out pre-hybridization and hybridization according to standard procedures[51]. Sense probes served as negative controls. We examined slides using a Zeiss Axiophot light microscope (Zeiss) equipped with a Nikon Coolpix 950 digital camera (Nikon).

URLs.

National Center for Biotechnology Information, http://www.ncbi.nlm.nih.gov/; Washington University

Neuromuscular Disease Center database (dominant ataxia section), http://www.neuro.wustl.edu/neuromuscular/ataxia/domatax.html ; ClustalW2, http://www.ebi.ac.uk/Tools/clustalw2/ index.html; ClustalX, http://www.clustal.org/; Pfam, http://pfam.sanger.ac.uk/; TMHMM Server v2.0, http://www.cbs.dtu.dk/services/TMHMM-2.0/; RCSB Protein Data Bank, http://www.rcsb.org/pdb/; SWISS-MODEL, http://swissmodel.expasy.org/; UniProt, http://www.uniprot.org/.

40. Manto, M. & Marmolino, D. Cerebellar ataxias. *Curr. Opin. Neurol.* **22**, 419–429 (2009).

41. Brusco, A. *et al.* Molecular genetics of hereditary spinocerebellar ataxia: mutation analysis of spinocerebellar ataxia genes and CAG/CTG repeat expansion detection in 225 Italian families. *Arch. Neurol.* **61**, 727–733 (2004).

42. Gellera, C. *et al.* Frataxin gene point mutations in Italian Friedreich ataxia patients. *Neurogenetics* **8**, 289–299 (2007).

43. Puddu, F. *et al.* Phosphorylation of the budding yeast 9–1-1 complex is required for Dpb11 function in the full activation of the UV-induced DNA damage checkpoint. *Mol. Cell. Biol.* **28**, 4782–4793 (2008).

44. Adams, A., Gottschling, D.E., Kaiser, C.A. & Stearns, T. *Methods in Yeast Genetics: A Cold Spring Harbor Laboratory Course Manual* (Cold Spring Harbor Laboratory Press, Cold Spring Harbor, New York, 1997).

45. Lemaire, C. & Dujardin, G. Preparation of respiratory chain complexes from *Saccharomyces cerevisiae* wild-type and mutant mitochondria: activity measurement and subunit composition analysis. *Methods Mol. Biol.* **432**, 65–81 (2008).

46. Magri, S., Fracasso, V., Rimoldi, M. & Taroni, F. Preparation of yeast mitochondria and *in vitro* assay of respiratory chain complex activities. *Nat. Protoc.* published online, doi:10.1038/nprot.2010.25 (7 March 2010).

47. Fracasso, V., Lazzaro, F. & Muzi-Falconi, M. Co-immunoprecipitation of human mitochondrial proteases AFG3L2 and paraplegin heterologously expressed in yeast cells. *Nat. Protoc.* published online, doi:10.1038/nprot.2010.26 (7 March 2010).

48. Schwede, T., Kopp, J., Guex, N. & Peitsch, M.C. SWISS-MODEL: An automated protein homology-modeling server. *Nucleic Acids Res.* **31**, 3381–3385 (2003).

49. Finardi, A. *et al.* NMDA receptor composition differs among anatomically diverse malformations of cortical development. *J. Neuropathol. Exp. Neurol.* **65**, 883–893 (2006).

50. Sacco, T., De Luca, A. & Tempia, F. Properties and expression of Kv3 channels in cerebellar Purkinje cells. *Mol. Cell. Neurosci.* **33**, 170–179 (2006).

51. Darby, I.A. & Hewitson, T.D. (eds) *In Situ Hybridization Protocols.* (Humana Press, Totowa, New Jersey, 2006).

Supplementary Information for

Mutations in the mitochondrial protease gene *AFG3L2*cause dominant hereditary ataxia SCA28

Genetic studies

RNA analysis

To verify that the mutations were present in the transcripts, when feasible, total RNA was extracted from transformed lymphoblastoid cell lines derived from affected individuals using the RNAeasy Mini Kit (Qiagen). cDNA synthesis was carried out using the Cloned AMV First-Strand Synthesis Kit (Invitrogen) with an *AFG3L2*-specific primer. PCR primer pairs were designed to amplify fragments spanning from exon 9 to exon 11 and exon 15 to exon 17.

In silico analysis of the identified *AFG3L2* mutations

The four mutations in exon 16 cause the amino acid substitutions S674L, E691K, A694E, and R702Q within the proteolytic domain, in a region that is highly conserved in *m*-AAA and *m*-AAA-related proteins of multiple species, ranging from eubacteria to humans (**Fig. 1**). In particular, conservation for Ser674, Arg702, Ala694, and Glu691 is 92%, 83%, 75%, and 66%, respectively. Notably, however, Glu691, Ala694, and Arg702 are conserved from the ancestral eubacterial protein FtsH[11]. The N432T substitution, found in the sequence

encoded by exon 10, occurs in the ATPase (AAA) domain and also resides within an evolutionarily highly conserved region. In particular, all *m*-AAA and *m*-AAA-related proteins from eubacteria to humans exhibit an absolute conservation of a 5-amino acid motif (TL**N**Q) encompassing AFG3L2 Asn432 (**Fig. 1**). By contrast, the H126Q substitution, caused by the 378C>G mutation in exon 4, occurs in the N-terminal part of the mature protein which precedes the 1st transmembrane domain and protrudes into the matrix, a region of unknown functional properties which exhibits high homology (100% identity between residue 113 and residue 133) with rodent AFG3L2 but is not evolutionarily conserved in orthologs from more distantly-related species (data not shown). Predictions on the effects of the substitutions on protein function using the algorithms SIFT[52] and PolyPhen[53] did not give univocal results. Both programs predicted the S674L, R702Q, and H126Q substitutions to be tolerated, and the A694E substitution to affect protein function. By contrast, the E691K change was predicted to be benign by PolyPhen but not tolerated by SIFT. Both programs predicted the N432T not to be tolerated. Possible effects of the mutations on pre-mRNA splicing were assessed using the algorithms ESEfinder[54] (Release 3.0) for changes in exonic splicing enhancers (ESE) and PESX[55] for changes in putative exonic splicing silencers (PESS). None of the mutations is predicted to change putative silencer sequences. No effect on ESE sequences is predicted for the 4 mutations on exon 16. The 1296A>C mutation causing N432T is predicted to alter the

ESE pattern in exon 10 by abolishing one SF/ASF site and creating 3 novel ones. However, RT-PCR analysis of *AFG3L2* transcript in lymphoblastoid cells from patients carrying this mutation or the mutations in exon 16 demonstrated equal dosage of normal and mutant mRNA, with no evidence of aberrant splicing induced by the mutations. Two modest changes were predicted for the 378C>G mutation (H126Q), namely, the mild attenuation of a putative SRp40 ESE sequence along with the creation of a novel similar sequence with a just above the threshold score. Unfortunately, no mRNA source was available from the patient and the effect of the 378C>G mutation (H126Q) on splicing could not be directly tested.

Mutation screening

For mutation screening of the selected patient population, PCR products were analyzed by automated sequencing and/or Denaturing High-Performance Liquid Chromatography (DHPLC)[56,57]. Sequences of the oligonucleotide primers and conditions used for PCR amplification, DNA sequencing, and DHPLC analysis are detailed in **Supplementary Table 2**. For DHPLC analysis on the 3500HT WAVE® system (Transgenomic), melting profiles of each PCR product sequence were predicted using the Navigator 6.4 software (Transgenomic). For each exon, DHPLC mutation analysis was performed at at least two different temperatures (**Supplementary Table 2b**), based on the melting profiles.

PCR products encompassing frequent polymorphic sites or PCR fragments not suitable for DHPLC analysis were directly sequenced.

Structural modeling of AFG3L2 mutations

A three-dimensional model of AFG3L2 was built using the structure of the *Th. thermophilus* (*Tth.*) AAA protease FtsH[11,19] as a template (**Fig. 5**). This protein is a homohexamer (**Fig. 5a**) which adopts a flat-cylinder-like shape divided into two disks (**Fig. 5b**). The lower disk, containing the protease domain, forms a six-fold-symmetric structure with a Zn^{2+} binding site. The upper disk is composed of six AAA+ domains, each of which contains ADP. ***E691K.*** AFG3L2 Glu691 is also a glutamate (Glu537) in *T. thermophilus* FtsH[19], but is not conserved in other orthologs including paraplegin (**Fig. 1**). This residue is at the N-terminus of helix a17 (**Supplementary Figs. 5a** and **6a**) and sits in the middle of the central pore formed by the six subunits surrounding the exit from the pore on the matrix side of the proteolytic domain (**Fig. 5a**-**b** and **Supplementary Figs. 5a**-**b** and **6a**). While overall exposed and therefore not evidently contributing to subunit interactions or fold stability, this residue could be relevant for protease specificity[57]. Substitution of this residue with a lysine as in AFG3L2^{E691K} could have severe consequences on protein function as it drastically changes the electrostatic potential and the chemical characteristics of the pore (**Fig. 5c-g** and **Supplementary Fig. 5c-g**). The change

is evident in the AFG3L2^{WT}-AFG3L2^{E691K} compound homohexamer (**Supplementary Fig. 5e**) but is greatest in both the homohexameric mutant AFG3L2^{E691K}-AFG3L2^{E691K} (**Supplementary Fig. 5d**) and the heterohexameric AFG3L2^{E691K}-paraplegin (**Supplementary Fig. 5g**) in which the charge reversal of E691K is not counteracted by the neutral residue (Gln693) that substitutes AFG3L2 Glu691 in paraplegin.

A694E and ***R702Q***, the other two AFG3L2 mutations which produce a variation in the protein charge, appear to have smaller effects on the electrostatic potential of the protein surface (not shown). Ala694 (Ala540 in FtsH) is also close to the pore and nonconserved. Despite being rather superficial, its side chain points towards the pore inside and is overall rather buried, therefore not influencing significantly the electrostatic potential. Substitution of this alanine with a glutamate as in AFG3L2^{A694E} requires burial of a charged group in the protein interior which can be achieved only at a high energetic cost. We may therefore predict that this mutation would have a strong effect on destabilizing the fold. Arg702 is Arg548 in FtsH. This side chain packs with the next subunit, although it does not appear to establish specific interactions with it. Also in this case, the effect of its replacement by a glutamine in AFG3L2^{R702Q} could be the destabilization of the assembly.

S674L. Ser674 is an alanine (A518) in FtsH. This residue is in a loop region between a16 and 39 and while it is exposed in

the monomer (**Supplementary Fig. 5a**), it is buried in the subunit interface. In FtsH, the side chain of A518 is sandwiched between the conserved T498 and R494 of the adjacent subunit. While a serine can easily substitute the alanine, mutation of this residue in the bulkier leucine as in AFG3L2^{S674L} is expected to destabilize the hexamer assembly.

N432T. N432 is located within the ATPase domain in an evolutionarily conserved region and is absolutely conserved from eubacterial *Tth.* FtsH (N280) to human AFG3L2 (**Fig. 1**). This residue, which lies in the middle of a7, between Walker B and SRH motifs, is relatively exposed in the monomer (46 Å^2 accessible surface area) (**Supplementary Fig. 5a**) and is rather superficial also in the hexameric assembly (**Fig. 5** and **Supplementary Fig. 6b**). The side chain does not seem to form significant specific interactions with the surrounding. Although replacement of Asn432 by threonine in AFG3L2^{N432T} represents an exchange of two amino acids of the same class (uncharged polar), the asparagine side chain could have an important role in forming the required characteristics for substrate recognition and specificity. In the hexameric assembly of *T. thermophilus* FtsH, the side chain of the corresponding residue Asn280 is located in the pore and is near (~6 Å) the conserved Phe229 (Phe381 in AFG3L2) of the alternate monomer (**Supplementary Fig. 6b**). Notably, this phenylalanine is the crucial aromatic residue in the central pore loop motif @XG (pore-1 motif, where @ is an aromatic residue

and X is any residue) that is conserved in all subfamilies of the AAA family[20] and has been proposed to play an essential role for substrate recognition and ATP-dependent translocation of proteins into the proteolytic chamber[27,32].

Expression studies

AFG3L2 and paraplegin yeast expression plasmids

To generate yeast plasmids for heterologous expression of human AFG3L2, the sequence encoding residues 35-797 of human AFG3L2 was amplified by PCR from a full-length human *AFG3L2* cDNA clone (clone IMAGp998I0513535Q1, RZPD Consortium), fused to the sequence encoding the mitochondrial targeting peptide of Yta10p (amino acids 1-63), and cloned into the *Bam*HI/*Xba*I-digested low-copy-number centromeric vector pYC6/CT (Invitrogen) which carries the blasticidin resistance gene (plasmid pYC6/CT^{GAL1}-AFG3L2). To obtain high constitutive levels of AFG3L2 expression under control of the *ADH1* promoter, the glucose/galactose-regulated *GAL1* promoter on pYC6/CT was substituted with the 1-kb region upstream from the *ADH1* translation initiation codon, amplified by PCR and cloned into the *Spe*I/*Bam*HI-digested pYC6/CT^{GAL1}-AFG3L2 plasmid. This plasmid [pYC6/CT^{ADH1}-Yta10p(1-63)-AFG3L2(35-797)-V5/HIS, abbreviated into pYC6/CT^{ADH1}- AFG3L2-V5/HIS] was used in all expression experiments except when differently indicated. For AFG3L2

expression under control of the weaker *YTA10* promoter, plasmid pYC6/CT^{YTA10}-AFG3L2-V5/HIS was likewise generated by replacing the pYC6/CT *GAL1* promoter with a PCR fragment amplified from the 1-kb region upstream from the *YTA10* translation initiation. To investigate dominance of the mutations, plasmid pYC2/CT^{ADH1}- AFG3L2-V5/HIS carrying wild-type AFG3L2 and the *URA3* gene for selection was constructed by subcloning the *Spe*I/*Xba*I fragment [*ADH1*-Yta10p(1-63)-AFG3L2(35-797)] from pYC6/CT^{ADH1}-AFG3L2-V5/HIS into the *Spe*I/*Xba*I-digested centromeric pYC2/CT vector (Invitrogen).

The mutations causing the six substitutions identified in patients (AFG3L2^{H126Q}, AFG3L2^{S674L}, AFG3L2^{E691K}, AFG3L2^{A694E}, AFG3L2^{R702Q}, and AFG3L2^{N432T}) or the control proteolytic substitution AFG3L2^{E575Q} (ref. 13) were introduced into the yeast AFG3L2 expression construct pYC6/CT^{ADH1}-AFG3L2-V5/HIS using the QuikChange XL Site-Directed Mutagenesis Kit (Stratagene) and the following oligonucleotide primer pairs. Mutagenized plasmids were verified by DNA sequencing.

Mutant		Primer pairs (5'->3')
AFG3L2^{E575Q}	Forward Reverse	CTGTGGCATACCACCAAGCAGGCCATGCGG CCGCATGGCCTGCTTGGTGGTATGCCACAG
AFG3L2^{E691K}	Forward Reverse	TATTGGAGAAACCTTACAGTAAAGCCACTGCAAGATTGATAGA TCTATCAATCTTGCAGTGGCTTTACTGTAAGGTTTCTCCAATA
AFG3L2^{H126Q}	Forward Reverse	GGCAAGAAAGTAGATTCTCAGTGGTGGTCCAGGTTTCAGAA TTCTGAAACCTGGACCACCACTGAGAATCTACTTTCTTGCC
AFG3L2^{R702Q}	Forward Reverse	GATGATGAAGTACAAATACTTATTAATGATG CATCATTAATAAGTATTTGTACTTCATCATC
AFG3L2^{A694E}	Forward Reverse	TTACAGTGAAGCCACTGAAAGATTGATAGATGATG CATCATCTATCAATCTTTCAGTGGCTTCACTGTAA
AFG3L2^{S674L}	Forward Reverse	GGTTGGGCAAATCTTATTTGACCTCCCACGTCAGG CCTGACGTGGGAGGTCAAATAAGATTTGCCCAACC
AFG3L2^{N432T}	Forward Reverse	GAGAACACACTCACCCAGCTGCTGGTGGAG CTCCACCAGCAGCTGGGTGAGTGTGTTCTC

For human paraplegin expression, plasmid YCplac111^{ADH1}-Yta10p(1-63)- paraplegin(59-795)-HA (abbreviated into YCplac111^{ADH1}-paraplegin-HA) was used, in which the sequence corresponding to the mature form of paraplegin (amino acids 59-795) is tagged at the C-terminus with the HA epitope, fused to the Yta10p mitochondrial leader peptide (amino acids 1-63), and expressed under control of the *ADH1* promoter[59].

Plasmids and strains generated in this study are available upon request following the execution of an MTA agreement.

Cytochrome *c* oxidase analysis in yeast

For *in-vitro* activity assay of cytochrome *c* oxidase (COX) or immunoblot analysis of its subunits, yeast cells were grown at 28°C in YEP medium supplemented with 2% (wt/vol) galactose-0.1% (wt/vol) glucose[45,46]. Following differential centrifugation of the cells, the resulting mitochondrial pellet was resuspended in 10-mM potassium phosphate buffer and freezed and thawed for three times. COX activity was determined spectrophotometrically at 30°C following for 2 minutes the decrease of absorbance at 550 nm because of oxidation of cytochrome c^{red} (refs. 46,60). Activity was expressed as nanomoles of cytochrome *cred* oxidized per minute per milligram of protein. Protein concentration was determined by Bradford microplate microassay (Bio-Rad) with bovine serum albumin as the standard.

In yeast, COX is composed of 11 subunits, three of which (Cox1p, Cox2p, and Cox3p) are encoded in the mitochondrial genome and form the catalytic core of the enzyme[61]. Immunoblot analysis with antibodies directed against the three mitochondrial-encoded subunits and one nuclear-encoded subunit (Cox4p) demonstrated multi-subunit deficiency, with a drastic reduction (80 - >95%) of Cox1p, Cox2p, and Cox4p protein levels and a milder decrease (40-75%) of Cox3p levels (**Fig. 3b**). Upon co-expression of paraplegin, COX activity (**Fig. 3c**) was partially recovered in mutants AFG3L2^{S674L} (51%), AFG3L2^{A694E} (61%), and AFG3L2^{R702Q} (84%) but remained significantly low (*P* 0.01 *n*=4) in mutants AFG3L2^{E691K} (7%),

AFG3L2^{N432T} (25%), or the control mutant AFG3L2^{E575Q} (ref. 13) (4%), consistently with the observed respiratory phenotypes (**Fig. 2d** and **e**). As illustrated by immunoblot analysis in **Fig. 3d**, COX subunit protein levels paralleled enzyme activity, returning nearly normal in mutants AFG3L2^{S674L}, AFG3L2^{A694E}, and AFG3L2^{R702Q} (**Fig. 3d**, lanes 5, 7, and 8), but remaining significantly low (*P* 0.01 *n*=4) in mutants AFG3L2^{E691K}, AFG3L2^{N432T}, or the control mutant AFG3L2^{E575Q} (**Fig. 3d**, lanes 6, 9, and 3, respectively).

Generation of antibodies against AFG3L2 and paraplegin

To raise rabbit polyclonal antisera against human AFG3L2 and paraplegin, GST fusion proteins were generated with protein fragments of AFG3L2 and paraplegin showing no homology to each other. The regions encoding amino acids 67-305 of AFG3L2 and amino acids 89-304 of paraplegin were PCR amplified from IMAGE clones (clone IMAGp998I0513535Q1 for *AFG3L2* and clone IMAGp998D1211693Q1 for *SPG7*, RZPD Consortium) and subcloned into the pGEX-6P-1 vector (Amersham Biosciences), in order to generate GST-AFG3L2 and GST-paraplegin fusion proteins. Recombinant proteins were expressed in *Escherichia coli* and purified by glutathione affinity chromatography. After preparative SDS-PAGE and electroelution[62], recovered proteins were injected into rabbits (200-300 tg of protein per injection). The anti-AFG3L2 and anti-paraplegin antisera collected from the animals showed no cross-reaction when tested against each protein individually expressed in *yta10Ayta12A* yeast cells (**Supplementary Fig.**

7a) nor when used in Western blot analysis of protein extracts from human cells (**Supplementary Fig. 7b**).

Antibodies generated in this study are available upon request following the execution of an MTA agreement.

SK-N-SH cell culture and confocal immunofluorescence analysis

Human neuroblastoma SK-N-SH cells[63] were grown in Dulbecco's modified Eagle's medium (DMEM) supplemented with nonessential amino acids and 10% fetal bovine serum and plated on coverslip in 12-well plates. Prior to immunofluorescence (**Supplementary Fig. 7**), cells were fixed in 4% (wt/vol) paraformaldehyde for 5 minutes, repeatedly rinsed in phosphatebuffered saline (PBS), and incubated overnight at 4°C with the primary antisera[48] (rabbit polyclonal anti-AFG3L2 or anti-paraplegin, 1:500 dilution). For sequential double-labeling, cells were incubated for 2 hours with Alexa Fluor 546-conjugated goat anti-rabbit IgG (Molecular Probes; 1:2,000 dilution), then with monoclonal anti-prohibitin-1 (PHB1) antibody (Santa Cruz Biotechnology; 1:50 dilution) as mitochondrial marker, followed by Alexa Fluor 488-conjugated goat anti-mouse secondary antibody (Molecular Probes; 1:2,000 dilution). Finally, cells were repeatedly rinsed and coverslipped with Fluorsave (Calbiochem). Immunofluorescence images were acquired on a Radiance

2100 confocal microscope (BioRad) at 1,024 x 1,024-pixel resolution.

Immunoblot analysis of patients' cells

Epstein-Barr-virus-stabilized lymphoblastoid cell lines from patients, their relatives and control subjects were established and cultured as previously described[42]. For Western blot analysis of patients' lymphoblasts (**Supplementary Figs. 8a** and **9**), 50-150 tg of

lymphoblastoid cell lysate from each line were electrophoresed on 10%-15%-SDSpolyacrylamide gels and transferred to a nitrocellulose membrane (Amersham Biosciences) by electroblotting. Filters were probed with polyclonal antibodies as indicated in the text and in the figure legends, and developed by HRP-conjugated secondary antibodies using a chemiluminescent substrate (ECL Kit, Amersham Biosciences) followed by autoradiography. The signals were normalized by probing filters with antibodies directed against tubulin (Santa Cruz Biotechnology) as a loading control protein.

Blue native gel electrophoresis

Blue native polyacrylamide gel electrophoresis (BNE) (**Supplementary Fig. 8b**) was carried out essentially as described[64]. To obtain mitochondria-enriched extracts, lymphoblastoid cell pellets were resuspended in a cold digitonin solution (20-mM MOPS, 250-mM sucrose, pH 7.4, 0.2-mg/ml digitonin), kept on ice for 10 min, and centrifuged at 600 X g for 10 min at 4°C. Supernatants were centrifuged at 7000 x g for 7 min at 4°C. The resulting pellets were solubilized in NativePAGETM Sample Buffer (Invitrogen) with 1% (wt/vol) digitonin, 1-mM ATP, 5-mM E-amino-*n*-caproic acid, and COMPLETETM Protease Inhibitor Cocktail (Roche). The solution was incubated on ice for 90 min and then centrifuged at 125,000 x g for 30 min at 4°C. After addition of NativePAGETM 5%-G-250 Sample Additive (Invitrogen), samples were loaded onto 3-12% NativePAGETM Novex® Bis-Tris Gels (Invitrogen). Electrophoresis was performed at 4°C according to the manufacturer's protocol.

Supplementary Table 1. *AFG3L2* polymorphic variants observed in this study

Nucleotide change[a]	Amino acid change[b]	NCBI SNP Reference Cluster ID[c]	Allele frequency (%) (n=300)
-96G>C		rs12327346	G=97.4; C=2.6
293$^{-61A>G}$		rs8093375	nd[d]
400$^{-95G>A}$		rs2298542	nd[d]
400$^{-14C>G}$		not reported	C=99.4; G=0.6
752$^{+6C>T}$		rs8097342	C=18.4; T=81.6
753$^{-55T>C}$		rs7407640	nd[d]
1026$^{+8G>A}$		rs8091858	G=93.9; A=6.1
1165$^{-21T>A}$		rs9966470	nd[d]
1319$^{-59G>T}$		not reported	G=99.7; T=0.3
1319$^{-55T>G}$		not reported	T=99.1; G=0.9
1389G>A	L463L	rs11080572	G=32; A=68
1650A>G	E550E	not reported	A=18; G=82
1664$^{-39G>A}$		not reported	G=98.1; A=1.9
1664$^{-9T>C}$		not reported	T=99.7; C=0.3
2394G>C		rs1129115	nd[d]

[a]Nucleotide numbering refers to the AFG3L2 cDNA [GenBank accession No. NM_006796.1 (GI:5802969)].

Nucleotides are numbered so that the first nucleotide (nt) of the first in-frame ATG codon is nucleotide +1.

[b]Amino acids are numbered so that methionine encoded by the first in-frame ATG codon is Met1. *c* http://www.ncbi.nlm.nih.gov/projects/SNP/.

[d]nd, not determined.

Supplementary Table 2. Oligonucleotide primers used for PCR amplification, DNA sequencing, and DHPLC analysis of *AFG3L2* exons

2a. DNA sequence analysis

Exon amplicons		Primer pairs (5'->3')	PCR annealing temperature *a*
1	Forward Reverse	TTGAGAGCTTGGGCTCCT GTCATCTCGGCCCAAAAG	57°C
2-3	Forward Reverse	TTATGACCAGGAAATGAAGC CTTTGTTCAGTGGAAACTACC	56°C
4-5	Forward Reverse	AGCCTCCCTGATTGGTAAG GCTGACTGTCACTTCTTTGGT	58°C
6	Forward Reverse	TGGGGGCATCTTTATCTG AGGCAGGTTTTCCTTTCAG	58°C
7	Forward Reverse	AATGAGTGACATTTAATCACC GGACAGAACACAGTGAACC	57°C
8	Forward Reverse	GCCTTTGAAGAACACTTGC TGACCCAAAACGATCCTC	56°C
9	Forward Reverse	AATGTTCTACCATAGCTCAGATG AGCACTCTAGGGGGAAGG	57°C
10	Forward Reverse	GGCCGATTTATTTCATTTCT CCGAAACACACCACTCA	56°C
11-12	Forward Reverse	GCTATGAATTTGCAGTGCTC AGGAAGCCCACAGTAAACAA	56°C
13	Forward Reverse	ACTATGGATTTGGCTGTCC TGGATACACTTTCTTTGCTTCT	57°C
14	Forward Reverse	TTGTGATAGGCAGCTCAGTC CTTTGCAGGAGTGTAGCTTG	58°C
15	Forward Reverse	CCACTAAGGCTGATGAACT TCCTTGCCTAAAAAGCCTAA	57°C
16	Forward Reverse	TGGGATTTGCGTCCTAAC GCAGACAACGAAACATCAGAAC	59°C

17	Forward Reverse	TGGGGTCACCTGTAAATAAAA TCCTGTAGAAAACCATTCCA	56°C

[a]PCR conditions included an initial denaturation step at 95°C for 3 min, followed by 35 cycles of denaturation at 94°C for 1 min, annealing for 45 s at the temperature indicated in the table, and extension at 72°C for 1 min, with a final extension step at 72°C for 10 min.

Supplementary Table 3. *Saccharomyces cerevisiae* strains used in this study

Strain	Relevant genotype [a]	Source
K699 (source: W303)	*MAT***a** *ade2-1 trp1-1 can1-100 leu2-3,112 his3-11,15 ura3-52*	Refs. 43,65
yDDB64 [b]	K699 *yta10::NAT yta12::KanMX6*	This study
yDDB79	yDDB64 (pYC6/CT^{ADH1}-AFG3L2-V5/HIS)	This study
yDDB94	yDDB64 (pYC6/CT^{YTA10}-AFG3L2-V5/HIS)	This study
yDDB 1 1 1b	yDDB64 (pYC6/CT^{YTA10}-AFG3L2-V5/HIS) (YCplac 1 1 1^{YTA10}-paraplegin-HA)	This study
yDDB122	yDDB64 (pYC6/CT^{ADH1}-AFG3L2^{H126Q}-V5/HIS)	This study
yDDB 123	yDDB64 (pYC6/CT^{ADH1}-AFG3L2^{E691K}-V5/HIS)	This study
yDDB124	yDDB64 (pYC6/CT^{ADH1}-AFG3L2^{A694E}-V5/HIS)	This study
yDDB125	yDDB64 (pYC6/CT^{ADH1}-AFG3L2^{R702Q}-V5/HIS)	This study
yDDB126	yDDB64 (pYC6/CT^{ADH1}-AFG3L2^{S674L}-V5/HIS)	This study
yDDB158	yDDB64 (pYC6/CT^{ADH1}-AFG3L2^{N432T}-V5/HIS)	This study
yDDB127	yDDB64 (pYC6/CT*ADH1*-AFG3L2E575Q-V5/HIS)	This study
yDDB 1 09	yDDB64 (pYC2/CT^{ADH1}-AFG3L2-V5/HIS)	This study
yDDB 1 9 0	yDDB64 (pYC6/CT^{ADH1}-AFG3L2^{E691K}-V5/HIS) (pYC2/CT^{ADH1}-AFG3L2-V5/HIS)	This study
yDDB191	yDDB64 (pYC6/CT^{ADH1}-AFG3L2^{A694E}-V5/HIS) (pYC2/CT^{ADH1}-AFG3L2-V5/HIS)	This study

yDDB 1 92	yDDB64 (pYC6/CT^{ADH1}-AFG3L2^{R702Q}-V5/HIS) (pYC2/CT^{ADH1}-AFG3L2-V5/HIS)	This study
yDDB 1 89	yDDB64 (pYC6/CT^{ADH1}-AFG3L2^{S674L}-V5/HIS) (pYC2/CT^{ADH1}-AFG3L2-V5/HIS)	This study
yDDB201	yDDB64 (pYC6/CT^{ADH1}-AFG3L2^{N432T}-V5/HIS) (pYC2/CT^{ADH1}-AFG3L2-V5/HIS)	This study
yDDB138	yDDB64 (YCplac111^{ADH1}-paraplegin-HA)	This study
yDDB 1 65	yDDB64 (pYC6/CT^{ADH1}-AFG3L2-V5/HIS) (YCplac1 1 1^{ADH1}-paraplegin-HA)	This study
yDDB 1 74	yDDB64 (pYC6/CT^{ADH1}-AFG3L2^{R702Q}-V5/HIS) (YCplac111^{ADH1}-paraplegin-HA)	This study
yDDB75b	yDDB64 (pYC6/CT^{ADH1}-AFG3L2^{H126Q}-V5/HIS) (YCplac111^{ADH1}-paraplegin-HA)	This study
yDDB200	yDDB64 (pYC6/CT^{ADH1}-AFG3L2^{A694E}-V5/HIS) (YCplac111^{ADH1}-paraplegin-HA)	This study
yDDB 1 6 6	yDDB64 (pYC6/CT^{ADH1}-AFG3L2^{E691K}-V5/HIS) (YCplac111^{ADH1}-paraplegin-HA)	This study
yDDB 129	yDDB64 (pYC6/CT^{ADH1}-AFG3L2^{E575Q}-V5/HIS) (YCplac111^{ADH1}-paraplegin-HA)	This study
yDDB 1 6 7	yDDB64 (pYC6/CT^{ADH1}-AFG3L2^{S674L}-V5/HIS) (YCplac111^{ADH1}-paraplegin-HA)	This study
yDDB 1 75	yDDB64 (pYC6/CT^{ADH1}-AFG3L2^{N432T}-V5/HIS) (YCplac111^{ADH1}-paraplegin-HA)	This study

[a] See **Supplementary Note** for plasmid description.

[b] *yta10dyta12.* parental strain generated using the one-step PCR strategy (refs. 43,66).

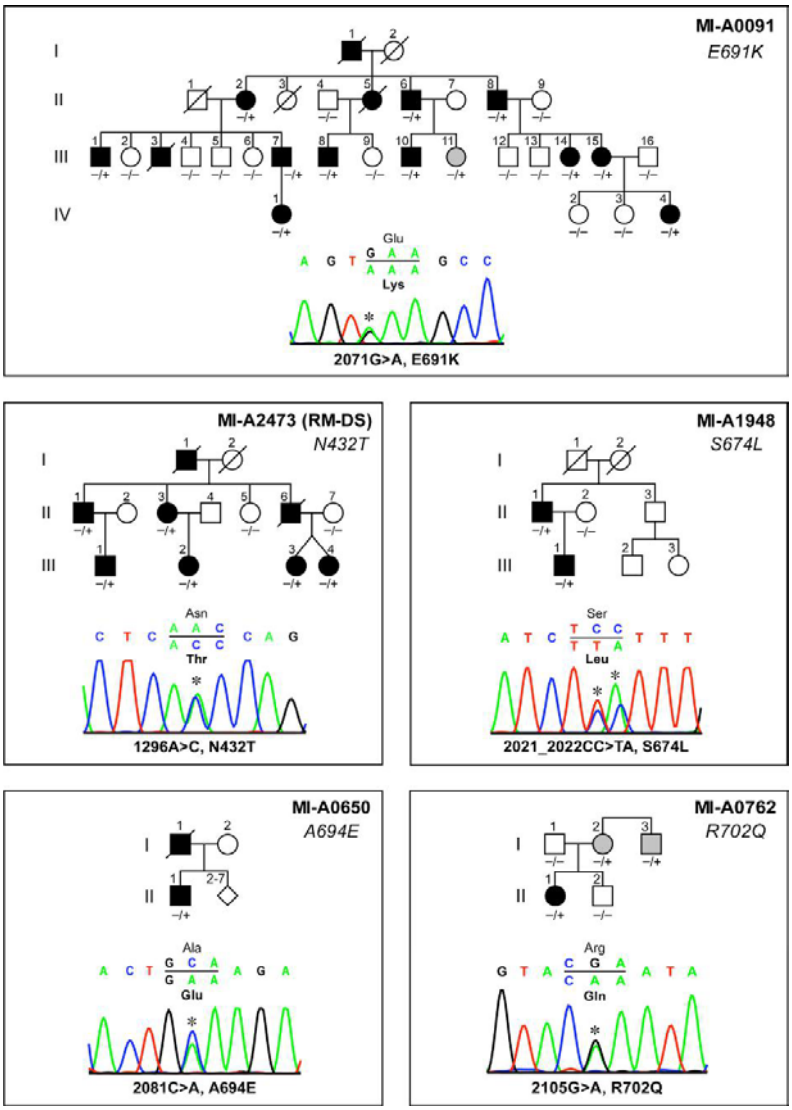

Supplementary Figure 1

Pedigrees and segregation of the mutations detected in *AFG3L2.* Square and circle symbols are male and female individuals, respectively. Symbols filled in black are affected individuals. Symbols filled in gray are asymptomatic or paucisymptomatic individuals carrying an *AFG3L2* mutation.

AFG3L2 genotype is indicated under the symbols of the sampled individuals: - = normal sequence; + = mutation. Electropherograms of mutated *AFG3L2* sequences are shown under each pedigree. Mutated nucleotides are indicated by an asterisk (*). Amino acid changes are indicated in boldface. Nucleotide numbering refers to the AFG3L2 cDNA. Nucleotides are numbered so that the first nucleotide of the first in-frame ATG codon is nucleotide +1. In family MI-A0091, one asymptomatic individual (III-11), previously reported to have the disease haplotype[8], was indeed mutated. Further clinical evaluation demonstrated the presence of nystagmus and very mild cerebellar signs. In family MI-A1948, the S674L substitution (TCC>TTA) was caused by the 2-nt mutation 2021_2022CC>TA. The occurrence of the two changes on the same allele was demonstrated both by segregation in the family (the two nucleotide substitutions were also carried by the affected father) and by sequencing of the subcloned PCR fragment. In family MI-A0762, individuals I-2 and I-3, heterozygous for the R702Q substitution, had a chronic subjective sense of unsteadiness, in the absence of objective neurological signs at clinical examination but with moderate cerebellar atrophy at MRI (see also **Supplementary Fig. 2**).

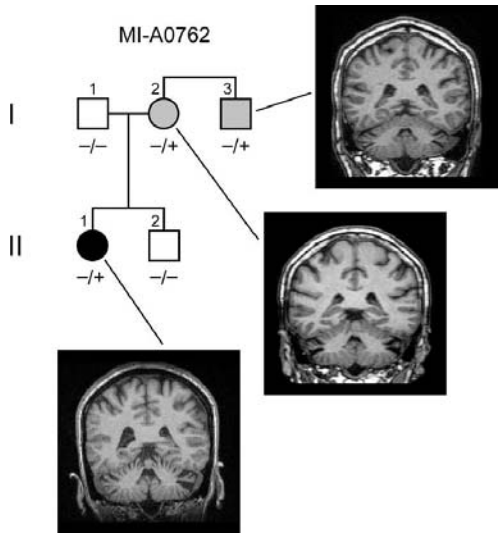

Supplementary Figure 2

Variable expressivity of AFG3L2^{R702Q} in family MI-A0762. Pedigree of family MI-A0762 (see also **Supplementary Fig. 1**) showing segregation of the R702Q substitution. Symbols are as in **Supplementary Fig. 1**. *AFG3L2* genotype is indicated under the symbols of the tested individuals (- = normal sequence; + = mutated sequence). The index case (II-1) is a 40-year-old woman with a full-blown cerebellar phenotype that manifested at 28 years of age with progressive gait and limb ataxia. She now presents severe ataxia and dysarthria, ophthalmoplegia, and pyramidal signs with increased muscle tone, brisk reflexes, and Babinski sign. MRI shows the presence of marked atrophy of the vermis and the cerebellar hemispheres. Her 78-years-old father, who does not carry the AFG3L2^{R702Q} substitution, is completely asymptomatic and does not exhibit any clinical sign at neurological examination. MRI is

negative (not shown). AFG3L2^{R702Q} is carried in heterozygous form by the mother (I2, 76 years old) and the maternal uncle (I-3, 74 years old). Both are negative at neurological examination, exhibiting none of the clinical signs observed in the index case II-1. In particular, there are no abnormalities of gait and speech, and no signs of corticospinal involvement. Despite negative neurological examination, though, both report to have been suffering of a chronic subjective sense of unsteadiness since many years. Interestingly, in both subjects, MRI shows the presence of a moderate cerebellar atrophy in comparison to age-matched controls.

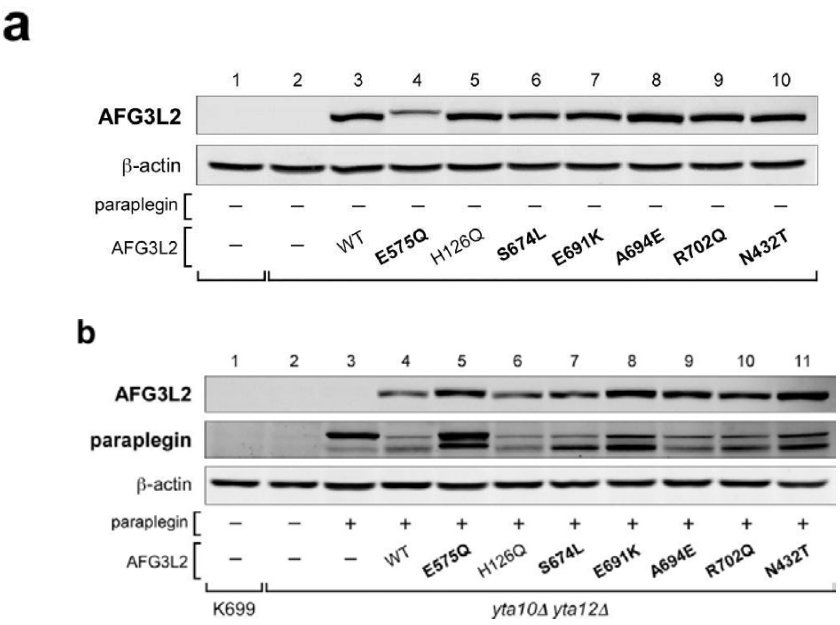

Supplementary Figure 3

Protein levels of heterologous AFG3L2 and paraplegin expressed in yeast cells. Yeast strains and mutants as in **Fig. 4**. Mutations affecting respiration are in bold. (**a**) Fluorescence immunoblot analysis (VersaDoc Imaging System, BioRad) of TCA protein extracts of yeast cells expressing wild-type or mutant human AFG3L2 only. Filters were probed with antibodies against AFG3L2 (upper panel) or the loading control protein *fl*-actin (lower panel). (**b**) Fluorescence immunoblot analysis of TCA protein extracts of yeast cells co-expressing wild-type or mutant human AFG3L2 with human paraplegin. Filters were probed with antibodies against AFG3L2 (upper panel), paraplegin (middle panel), or the loading control protein *fl*-actin (lower panel). The two protein species in the paraplegin panel (middle panel) result

from two-step processing of paraplegin upon import into mitochondria[34].

K699, wild-type yeast strain; *yta10Ayta12A*, yeast strains lacking endogenous *m*-AAA subunits Yta10p and Yta12p.

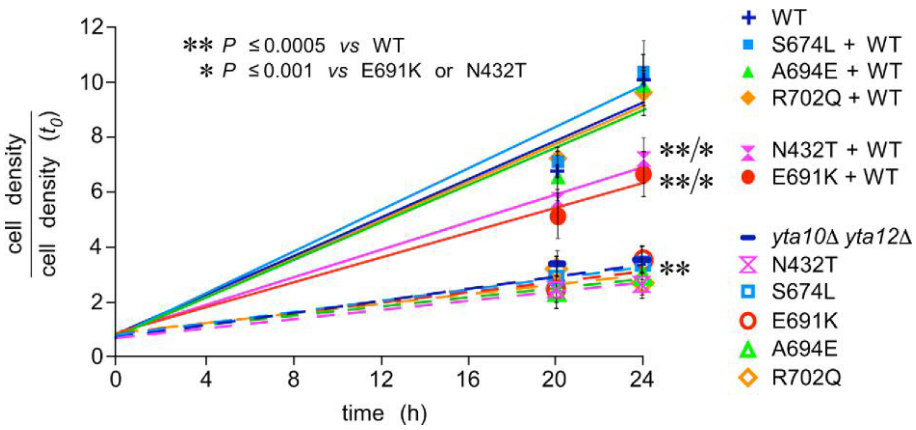

Supplementary Figure 4

Effect of co-expression of normal and mutant AFG3L2 on the growth of *yta10A yta12A* yeast cells. To determine whether the identified *AFG3L2* mutations exert a dominant-negative effect, as observed for AFG3L2^{E691K} (see **Fig. 2c**), the growth rates of *m*-AAA-deficient yeast cells (*yta10Ayta12A*) harboring the different mutant forms of AFG3L2 were analysed both in the absence and in the presence of normal AFG3L2 (WT). The graph shows the growth rates of cells expressing either AFG3L2^{WT} or each mutant or co-expressing both the

normal and the mutant form. Cells were grown for 24 hours with cell counting at 0, 20, and 24 hours. Values on the *y*-axis represent the ratio between cell density (= number of cells/ml) at a given time and cell density at start (*t0*). Growth rates are calculated by linear regression analysis (trend line). Each value represents the mean of four independent experiments. Error bars indicate s.d. Asterisk(s) indicate statistical significance (one asterisk, *P* 0.001; two asterisks, *P* 0.0005) as determined by Student's t-test. Introducing AFG3L2^{WT} into cells carrying mutant AFG3L2^{E691K} or AFG3L2^{N432T} resulted in a limited correction of the *yta10Ayta12A* respiratory phenotype, indicating a dominant-negative effect of these mutations (see also **Fig. 2c**). By contrast, co-expression of AFG3L2^{WT} with mutants AFG3L2^{S674L}, AFG3L2^{A694E}, and AFG3L2^{R702Q} appears to fully rescue the defective growth phenotype, suggesting that haploinsufficiency, rather than a dominant-negative effect, may be the disease-causing mechanism for these mutations.

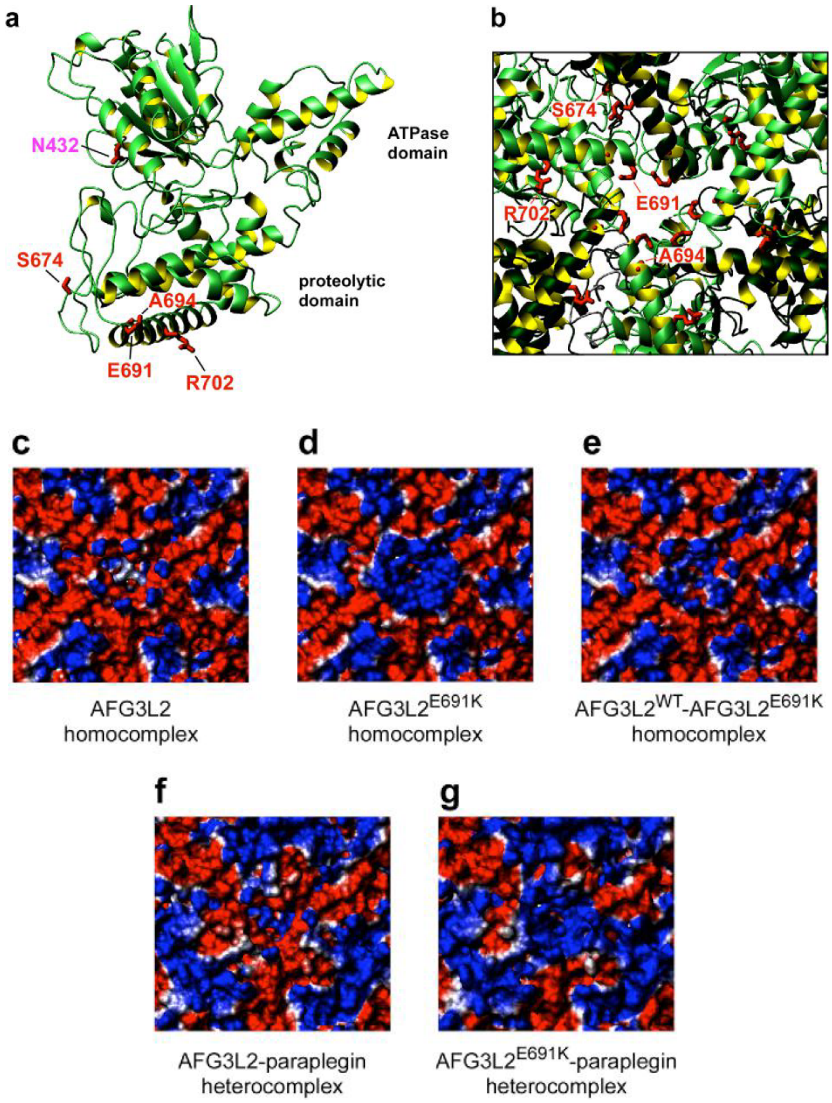

Supplementary Figure 5

Molecular modeling of normal and mutant AFG3L2. The structure of AFG3L2 was built by homology using the coordinates of *T. thermophilus* FtsH (PDB 2DHR) as a template. A similar hetero-oligomeric model was built assuming that AFG3L2 and paraplegin form an alternate heterodimer (**f**,

g). (**a**) The panel shows the structure of one of the subunits corresponding to the monomer boxed in *red* in **Fig. 5b**. The side chains of the residues substituted in the proteolytic domain are indicated in *red* whereas the Asn432, located in the ATPase domain, is highlighted in *magenta*. Residues are labeled using the AFG3L2 numbering. (**b**) A blow-up of the hexameric structure in **Fig. 5a** to show details of the central pore from the matrix side and the location of the amino acid substitutions in the proteolytic domain. (**c**-**g**) Surface representations of the protease side of the homo-oligomeric and heterooligomeric homology models showing the effect of the E691K substitution on the electrostatic potential of the protein. The blow-ups of the structures in **Fig. 5c-g** show a detailed view of the electrostatic changes in the central pore formed by the six subunits surrounding the exit from the pore on the matrix side of the proteolytic domain. (**c**) Electrostatic surface of the homohexamer of AFG3L2; (**d**) homohexamer of AFG3L2^{E691K}; (**e**) homohexamer obtained by alternating wild-type AFG3L2 and mutant AFG3L2^{E691K}; (**f**) heterohexamer obtained by alternating AFG3L2 and paraplegin; (**g**) as in **f** but after substituting Glu691 with a lysine in AFG3L2. The surfaces are coloured according to electrostatic potential with *blue* indicating positive and *red* indicating negative charge. The E691K substitution drastically changes the electrostatic and chemical characteristics of the pore. The change induced by the E->K charge reversal is greatest in the homohexameric mutant (**d**) and in the heterohexameric complex of

AFG3L2^{E691K} and paraplegin (**g**), in which the negatively charged Glu691 of AFG3L2^{WT} is substituted by the neutral Gln693 of paraplegin.

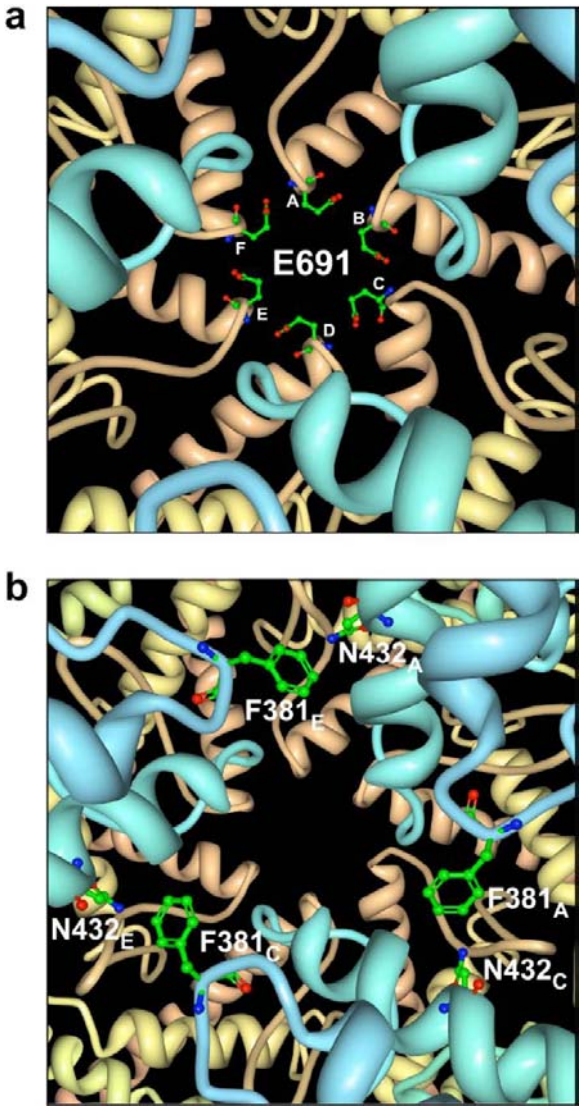

Supplementary Figure 6

Molecular modeling of Glu691 and Asn432 central pore residues substituted in SCA28 patients. The model is based on *T. thermophilus* FtsH structure (PDB 2DHR). The figures are viewed from the ATPase side. (**a**) Wireframe display of Glu691 lining the central pore of the protease ring (*light brown* ribbons). The six monomers are indicated by capital letters from A to F. (**b**) The panel shows the central pore of the ATPase ring (*light blue* ribbons) with wireframe visualization of Asn432 and Phe381. Asn432 is substituted with threonine in patients from family MI-A2473/RM-DS. Phe381 is the crucial aromatic residue in the conserved pore-1 loop motif FVG that protrudes into the central pore and may play an essential function for the ATP-dependent translocation of proteins into the proteolytic cavity[27,32]. The side chain of Asn432 is also located in the pore and is near (~6 Å) Phe381 of the alternate monomer (F381A-N432C, F381C-N432E, F381E-N432A). Atoms are colored as follows: carbon is *green*, oxygen is *red*, and nitrogen is *blue*.

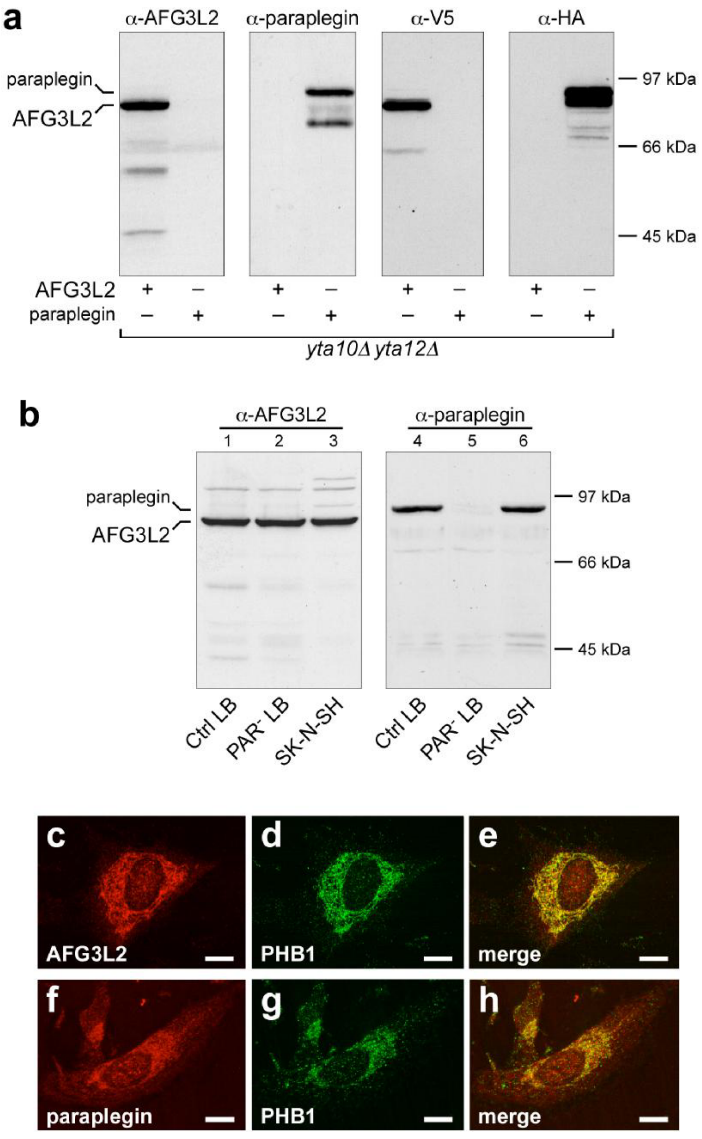

Supplementary Figure 7

Characterization of anti-AFG3L2 and anti-paraplegin antibodies. To investigate expression of the *m*-AAA subunits in normal and diseased human cells and tissue, we raised polyclonal antisera that specifically recognize human AFG3L2 and paraplegin. Western blot analysis shows that the

antibodies exhibit no cross reactivity against the two proteins (**a**, **b**). In both cases, immunofluorescence patterns are consistent with mitochondrial localization of the two proteins (**e** and **h**). (**a**) Immunoblot analysis of extracts from *yta10Ayta12A* yeast cells expressing either AFG3L2^{WT} or paraplegin^{WT} (left panels) or epitope-tagged AFG3L2^{V5} or paraplegin^{HA} (right panels). Blots were probed with anti-AFG3L2 (a-AFG3L2) or anti-paraplegin (a-paraplegin) polyclonal antibodies (left panels), or anti-V5 (a-V5) or anti-HA (a-HA) monoclonal antibodies. (**b**) Immunoblot analysis of AFG3L2 and paraplegin in human cells. Ctrl LB, lymphoblastoid cells from a normal control; PAR^{-} LB, lymphoblastoid cells from a spastic paraplegia patient carrying a homozygous null mutation in the *SPG7* gene; SK-N-SH, human neuroblastoma cells[63]. (**c**-**h**) Confocal immunofluorescence of cultured human neuroblastoma SK-N-SH cells showing the mitochondrial subcellular localization of both AFG3L2 (**c**) and paraplegin (**f**) by double-labeling with either antiAFG3L2 or anti-paraplegin antibodies and antibodies against the mitochondrial marker prohibitin-1 (PHB1; **d**, **g**). Note the high degree of colocalization, as indicated by the yellow signal in the merged images (**e**, **h**). Scale bars: 10 tm.

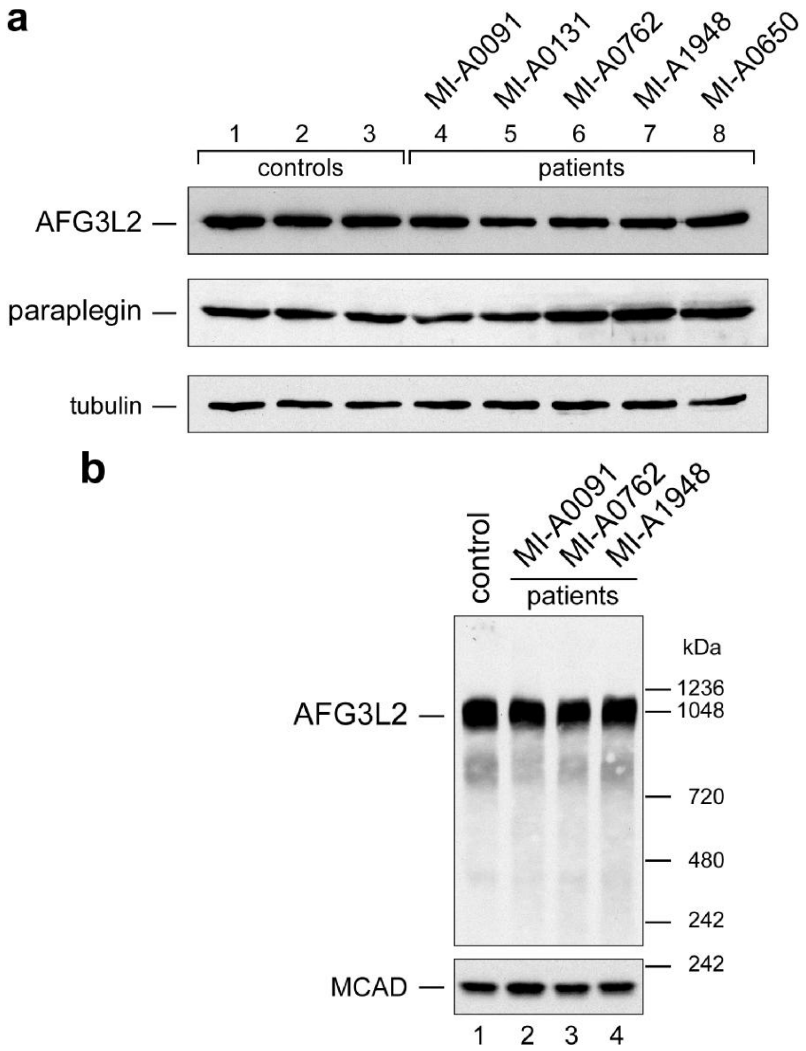

Supplementary Figure 8

Analysis of AFG3L2 and paraplegin protein expression in patients' cells. (**a**) Western blot analysis of lymphoblastoid cell extracts (50 tg) following SDS-PAGE showed normal levels of AFG3L2 and paraplegin in five patients from the four families. Lanes 1-3: control subjects; lanes 4 and 5: probands from family MI-A0091 (AFG3L2^{E691K}); lanes 6-8: probands from families MI-A762 (AFG3L2^{R702Q}) (lane 6), MI-A1948

(AFG3L2^{S674L}) (lane 7), MI-A0650 (AFG3L2^{A694E}) (lane 8). Filters were probed with anti-AFG3L2 or anti-paraplegin antibody and an antibody directed against tubulin as a loading control protein. (**b**) Western blot analysis of lymphoblastoid cell extracts following nondenaturing blue native electrophoresis demonstrated normal levels of a high-molecular-mass immunoreactive protein of approx. 1 MDa, indicating that the substitutions affect neither the amount nor the size of the supramolecular assembly of AFG3L2. Lymphoblastoid cells were solubilized in digitonin and 100 tg of cell protein were loaded on a 3-12% polyacrylamide gradient gel. Immunoblotting was carried out with anti-AFG3L2 antibody or antibody against medium-chain acyl-CoA dehydrogenase (MCAD) as a loading control protein (native molecular mass = ~230 kDa). NativeMarkTM Protein Standard (Invitrogen) were used as molecular weight markers ranging 242-1,236 kDa.

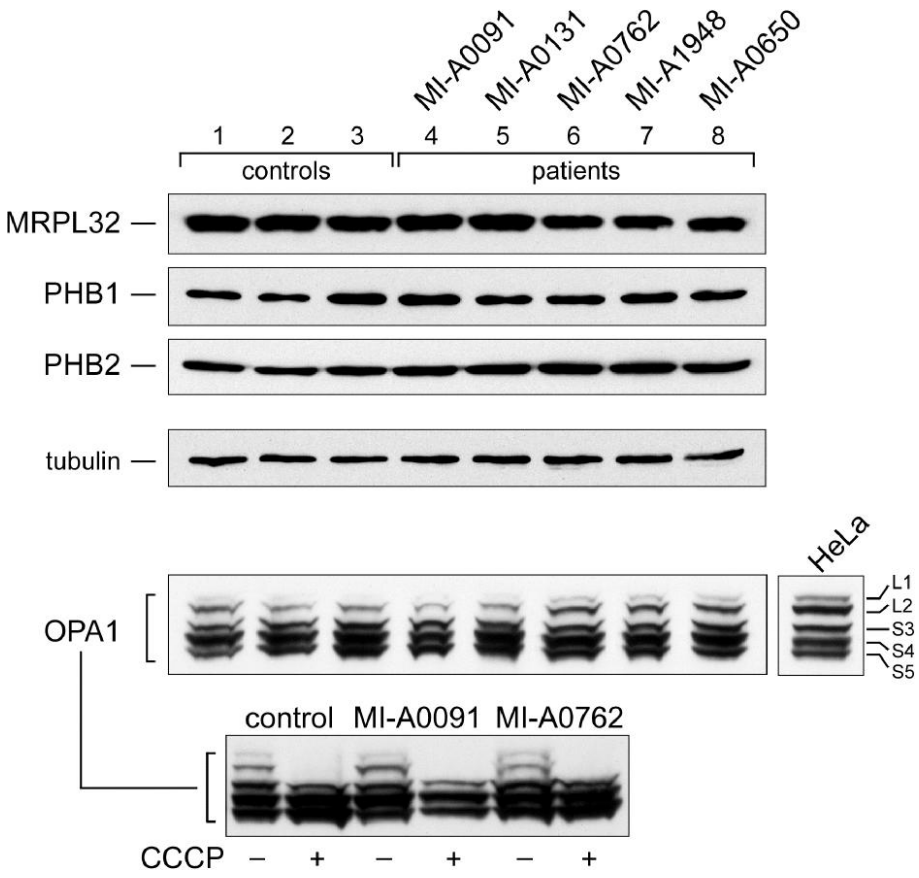

Supplementary Figure 9

Expression analysis of MRPL32, prohibitin 1 and 2, and OPA1 in patients' lymphoblasts. To examine whether mutations affecting AFG3L2 could induce secondary abnormalities of other proteins known for being either partners or substrates of the *m*-AAA complex, we investigated the expression of prohibitin 1 (PHB1) and 2 (PHB2), MRPL32, and OPA1, observing no differences both in the protein levels and in the migration pattern as compared to normal controls. MRPL32 is a subunit of human mitochondrial ribosomes,

homolog of yeast MrpL32, a previously reported substrate of *m*-AAA (ref. 16); prohibitin 1 (PHB1) and 2 (PHB2) have been shown to form ring-shaped assemblies that associate with *m*-AAA in a supercomplex of ~1.2 MDa and modulate *m*-AAA proteolytic activity[12]; OPA1, a dynamin-like GTPase that causes human dominant optic atrophy and functions in mitochondrial fusion and inner membrane remodeling, has been recently proposed to be regulated by the *m*-AAA protease[22,67,68]. Cell extracts were subjected to Western blotting with the antibody indicated. HeLa cell extracts were used as a control for OPA1 processing. Expression of eight OPA1 splice variants and proteolytic processing leads to the formation of at least five different isoforms of OPA1, two long forms designated L1 and L2, which can be proteolytically converted into three short forms, designated S3-S5[67,68]. Dissipation of mitochondrial membrane potential, as that caused by the uncoupler carbonyl cyanide 3-chlorophenylhydrazone (CCCP), stimulates OPA1 processing[67,68] and may thereby reveal impairment of processing, if any.

Supplementary References

52. Ng, P. C. & Henikoff, S. SIFT: Predicting amino acid changes that affect protein function. *Nucleic Acids Res* **31**, 3812-3814 (2003).

53. Ramensky, V., Bork, P. & Sunyaev, S. Human non-synonymous SNPs: server and survey. *Nucleic Acids Res* **30**, 3894-3900 (2002).

54. Cartegni, L., Wang, J., Zhu, Z., Zhang, M. Q. & Krainer, A. R. ESEfinder: A web resource to identify exonic splicing enhancers. *Nucleic Acids Res* **31**, 3568-3571 (2003).

55. Zhang, X. H. & Chasin, L. A. Computational definition of sequence motifs governing constitutive exon splicing. *Genes Dev* **18**, 1241-1250 (2004).

56. Xiao, W. & Oefner, P. J. Denaturing high-performance liquid chromatography: A review. *Hum Mutat* **17**, 439-474 (2001).

57. Takashima, H., Boerkoel, C. F. & Lupski, J. R. Screening for mutations in a genetically heterogeneous disorder: DHPLC versus DNA sequence for mutation detection in multiple genes causing Charcot-Marie-Tooth neuropathy. *Genet Med* **3**, 335-342 (2001).

58. Bieniossek, C. *et al*. The molecular architecture of the metalloprotease FtsH. *Proc Natl Acad Sci U S A* **103**, 3066-3071 (2006).

59. Atorino, L. *et al*. Loss of m-AAA protease in mitochondria causes complex I deficiency and increased sensitivity to oxidative stress in hereditary spastic paraplegia. *J Cell Biol* **163**, 777-787 (2003).

60. Rimoldi, M. *et al*. Cytochrome-*c*-oxidase deficiency in muscles of a floppy infant without mitochondrial myopathy. *J Neurol* 227, 201-207 (1982).

61. Fontanesi, F., Soto, I. C. & Barrientos, A. Cytochrome c oxidase biogenesis: new levels of regulation. *IUBMB Life* **60**, 557-568 (2008).

62. Plumari, M., Gellera, C. & Taroni, F. Production of polyclonal antibodies against protein antigens purified by electroelution from SDS-polyacrylamide gel. *Nat. Protoc.* published online, doi:10.1038/nprot.2010.27 (7 March 2010).

63. Ciccarone, V., Spengler, B. A., Meyers, M. B., Biedler, J. L. & Ross, R. A. Phenotypic diversification in human neuroblastoma cells: expression of distinct neural crest lineages. *Cancer Res* **49**, 219-225 (1989).

64. Schägger, H. Blue-native gels to isolate protein complexes from mitochondria. *Methods Cell Biol* **65**, 231-244 (2001).

65. Nasmyth, K., Adolf, G., Lydall, D. & Seddon, A. The identification of a second cell cycle control on the HO promoter in yeast: cell cycle regulation of SW15 nuclear entry. *Cell* **62**, 631-647 (1990).

66. Longtine, M. S. *et al*. Additional modules for versatile and economical PCR-based gene deletion and modification in Saccharomyces cerevisiae. *Yeast* **14**, 953-961 (1998).

67. Ishihara, N., Fujita, Y., Oka, T. & Mihara, K. Regulation of mitochondrial morphology through proteolytic cleavage of OPA1. *EMBO J* **25**, 2966-2977 (2006).

68. Duvezin-Caubet, S. *et al*. OPA1 processing reconstituted in yeast depends on the subunit composition of the *m*-AAA protease in mitochondria. *Mol Biol Cell* **18**, 3582- 3590 (2007).

Co-immunoprecipitation of human mitochondrial proteases AFG3L2 and paraplegin heterologously expressed in yeast cells

Valentina Fracasso[1], Federico Lazzaro PhD[2] and Marco Muzi-Falconi PhD[2]

1)Lab/Group: Neurodegenerative & Metabolic Disease Lab Fondazione IRCCS Istituto Neurologico Carlo Besta, Milan, Italy
2)DNA Metabolism & Cell Cycle Lab University of Milan, Italy

Nature protocols (2010) DOI: 10.1038/nprot.2010.26
Related Journal & Article Information
Journal: Nature Genetics
Article Title: Mutations in the mitochondrial protease gene AFG3L2 cause dominant hereditary ataxia SCA28

Introduction

AFG3L2 and paraplegin are cognate ATP-dependent metalloproteases that constitute the m-AAA protease complex in the inner mitochondrial membrane. Co-immunoprecipitation (CoIP) is a useful technique for the analysis of protein-protein interaction. Here, we illustrate a protocol to precipitate the complex formed by human epitope-tagged AFG3L2 and paraplegin heterologously expressed in the yeast Saccharomyces cerevisiae. The procedure employs polyclonal anti-AFG3L2 and anti-paraplegin, and monoclonal anti-HA antibodies to investigate the interaction between the two proteins. The protocol can be adapted to the analysis of other protein complexes.

Materials

Reagents

YPD medium for yeast culture

1% (w/v) yeast extract

2% (w/v) Bacto™ Peptone

2% (w/v) D-glucose

10X Phosphate-Buffered Saline (PBS)

1.37 M NaCl, 27 mM KCl, 100 mM Na2HPO4, 17.6 mM KH2PO4, pH 7.4

1X PBS/BSA

1X PBS with 0.1 mg/ml bovine serum albumin (BSA) (keep ice-cold)

Inhibitors Buffer

PBS buffer supplemented with protease and phosphatase inhibitors (keep ice-cold):
30 ml of 1X PBS containing:
1 mM PMSF
1 mM NaVO4
50 mM NaF
1 tablet of COMPLETE™ Protease Inhibitor Cocktail (Roche)
Protein G Resin
10 ml of 50% slurry in 1X PBS/20% ethanol (GenScript Co.)
Loading Buffer
7 ml Stacking Buffer (0.5M Tris-HCl, pH 6.8, 0.4% SDS)
3 ml glycerol
1 g SDS
0.93 g dithiothreitol
1.2 mg bromophenol blue
Equipment
Shaking incubator at 28°C
Refrigerated centrifuges
FastPrep® System (Qbiogene-MP Biomedicals)

Time Taken
Three days

Procedure
Day 1
Inoculate yeast cells from a solid culture (agar plate) into 5 ml of YPD medium or appropriate selective medium

supplemented with 2% (w/v) D-glucose and incubate at 28°C overnight with shaking.

Day 2

A) Cell pellet preparation

1. Transfer overnight culture into 100 ml of YPD and incubate at 28°C with shaking. OD600 nm should be 0.3-0.5 (=1 × 107 cell/ml)
2. Place cells in 50-ml tubes and centrifuge at 3,000g for 4 min at 4°C.
3. Discard the supernatant and resuspend cell pellets by vortexing in 25 ml of sterile H2O. Combine two cell pellets and centrifuge at 3,000g for 2 min at 4°C.
4. Discard the supernatant and resuspend the cell pellet in 1 ml of 1X PBS. Transfer into 2-ml screw-cap eppendorf tube and centrifuge at 2,000g for 2 min at 4°C.
5. Discard the supernatant and store the pellet at -80°C.

B) Resin and pre-saturated tube preparation

1. Pre-saturate Protein G Resin: place 20 µl of Protein G Resin per sample to be immunoprecipitated in one 1.5-ml eppendorf tube and add 1 ml of 1X PBS/BSA. Mix well.
2. Centrifuge at 800g for 2 min at 4°C.
3. Gently remove supernatant and wash three times with 1 ml of 1X PBS/BSA.
4. Resuspend resin with 1 ml of 1X PBS/BSA and incubate overnight at 4°C under gentle shaking.

5. Pre-saturate eppendorf tubes with BSA: aliquot 1 ml of 1X PBS/BSA into 1.5-ml eppendorf tubes (two tubes for each sample) and incubate overnight at 4°C under gentle shaking. Wash with 1 ml of 1X PBS just before use.

Day 3

1. Thaw cell pellets (from step A5 of Day 2) on ice and resuspend each pellet in 1 ml of ice-cold Inhibitors Buffer.
2. Centrifuge at 800g for 2 min at 4°C. Discard the supernatant and resuspend the cell pellet in 500 µl of Inhibitors Buffer.
3. Add 1 g of 425-600-µm glass beads.
4. Homogenize using the FastPrep® System (Qbiogene-MP Biomedicals): shake for 15 sec and then keep on ice for 1 min. Repeat 10 times.
5. Check cell breakage under a microscope.
6. Pierce the tube bottom with a needle.
7. Insert the tube into a new 2-ml eppendorf tube and spin at top speed to transfer the cell extract into the lower tube.
8. Centrifuge at 16,000g for 20 min at 4°C.
9. Transfer the supernatant into a new 1.5-ml eppendorf tube and adjust the volume to 1 ml with Inhibitors Buffer.
10. Determine sample protein concentration.
11. Normalize samples for protein concentration (optimal concentration: 2.5-3 mg/ml). Transfer 1 ml of each sample into the pre-saturated eppendorf tubes washed with 1 ml of 1X PBS (see "Day-2, B-5").

12. Transfer 50 µl of each normalized cellular extract into a new eppendorf tube and add 10 µl of Loading Buffer. Heat samples at 95°C for 5 min. Store at -20°C (**INPUT** sample).
13. Add primary antibody to normalized samples and incubate for 2 hr at 4°C under gentle shaking to allow formation of antigen-antibody complexes. (We use 10 µg of monoclonal anti-HA antibodies).
14. Centrifuge pre-saturated Protein G Resin at 800g for 2 min at 4°C. Gently remove supernatant with pipette.
15. Wash resin twice with Inhibitors Buffer (gently remove supernatant with pipette).
16. Following the second wash, resuspend Protein G Resin 1:1 with 1X PBS.
17. Wash a pre-saturated eppendorf tube with 1 ml of 1X PBS for each sample. In each tube, add 1 ml of 1X PBS and 40 µl of Protein G Resin suspension from previous step.
18. Centrifuge at 800g for 2 min at 4°C. Remove supernatant with pipette.
19. Add 1 ml of antigen-antibody complex (from step 13) and incubate for 2 hr at 4°C under gentle shaking.
20. Centrifuge at 800g for 2 min at 4°C.
21. Transfer 50 µl of supernatant in a new eppendorf tube and add 10 µl of Loading Buffer. Heat samples at 95°C for 5 min. Store samples at -20°C (**IMMUNODEPLETED** sample).
22. Discard the remaining supernatant and wash resin with 1 ml of a freshly prepared Inhibitors Buffer. Shake gently for 2 min and centrifuge at 800g for 2 min at 4°C.

23. Repeat step 22 three times. Remove supernatant with pipette.
24. Add 20 µl of 1:3 diluted Loading Buffer. Heat samples at 95°C for 5 min.
25. Centrifuge at top speed for 5 min at room temperature.
26. Transfer the supernatant into a new 1.5-ml eppendorf tube. Store samples at -20°C [**IMMUNOPRECIPITATED** (**IP**) sample].
27. Analyze samples by SDS-PAGE and immunoblotting (IB) (Figure 1).

Troubleshooting

SDS-PAGE of immunoprecipitates may result in the co-migration of antibody heavy (approx. 50 kDa) and light (approx. 25 kDa) chains with target proteins. To circumvent the issue of IgG chain detection in the immunoblots, it is recommended that antibodies used for co-immunoprecipitation and immunoblotting originate from two different hosts [in the protocol described here: mouse monoclonal (anti-HA) Ab for immunoprecipitation and rabbit polyclonal (anti-AFG3L2 or anti-paraplegin) Ab for immunoblotting (IB)].

Critical Steps

Day 3: keep samples on ice during the entire procedure.
Day 3, Step 21: in the presence of antigen excess (as it occurs when target proteins are overexpressed), immunoprecipitation

may not result in the complete immunodepletion of input sample(s).

Keywords

immunoprecipitation, mitochondria, protease, yeast, Saccharomyces cerevisiae, antibody

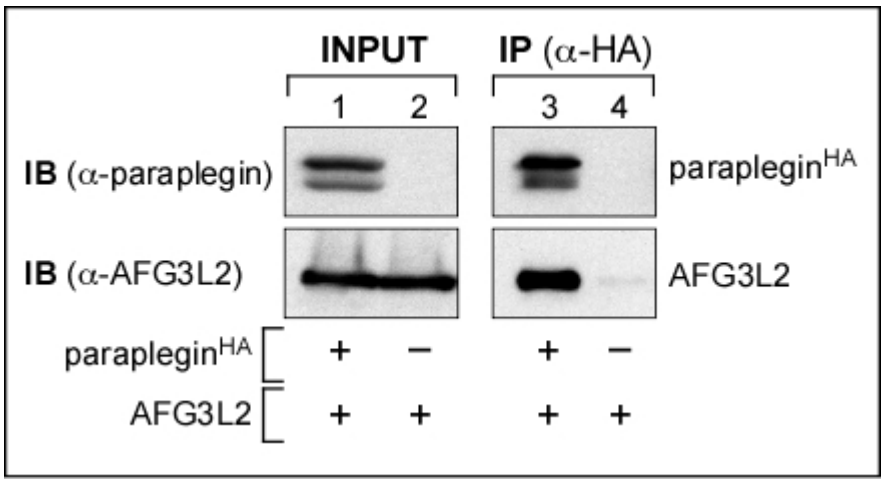

Figure 1

Co-immunoprecipitation of AFG3L2 and HA-tagged paraplegin heterologously expressed in Saccharomyces cerevisiae

HA-tagged paraplegin (parapleginHA) was immunoprecipitated with mouse monoclonal anti-HA antibodies from yeast cells co-expressing AFG3L2 and parapleginHA (lanes 1 and 3) or AFG3L2 alone (lanes 2 and 4). Lanes 1-2: immunoblot analysis of cell extracts before immunoprecipitation (INPUT). Immunoprecipitates (IP) were analyzed by SDS-PAGE and immunoblotting (IB) using rabbit polyclonal anti-paraplegin (α-paraplegin) or anti-AFG3L2 (α-AFG3L2) antibodies. AFG3L2

was detected in the immunoprecipitate from yeast cells co-expressing parapleginHA (lane 3), indicating AFG3L2-paraplegin interaction.

Preparation of yeast mitochondria and in vitro assay of respiratory chain complex activities

Stefania Magri, Valentina Fracasso, Marco Rimoldi and Franco Taroni

Unit of Genetics of Neurodegenerative and Metabolic Diseases
Fondazione IRCCS Istituto Neurologico Carlo Besta, Milan, Italy

Nature protocols (2010) DOI: 10.1038/nprot.2010.25
Related Journal & Article Information
Journal: Nature Genetics
Article Title: Mutations in the mitochondrial protease gene AFG3L2 cause dominant hereditary ataxia SCA28

Introduction

The aim of the protocol is to obtain an enriched fraction of intact mitochondria from the yeast Saccharomyces cerevisiae to perform quantitative determination of the activity of respiratory chain enzymes. All the strains used to perform this protocol are derivatives of W303 (K699: MATa ade2-1 trp1-1 can1-100 leu2-3,112 his3-11,15 ura3-52).

Materials

Reagents

Cell culture

- Selective medium (as appropriate) supplemented with 2% (w/v) D-glucose
- YPGAL medium: YEP medium (1% yeast extract, 2% Bactopeptone) supplemented with 2% (w/v) D-galactose and 0.1% (w/v) D-glucose

Preparation of mitochondria by differential centrifugations

- 10 mM ethylenediaminetetraacetic acid (EDTA)
- Sorbitol Buffer A: 1.2 M sorbitol, 50 mM Tris-HCl, pH7.5, 10 mM EDTA (stored at 4°C), 0.3% (v/v) 2-mercaptoethanol added before use
- Sorbitol Buffer B: 0.7 M sorbitol, 50 mM Tris-HCl, pH 7.5, 0.2 mM EDTA (stored at 4°C)
- Zymolyase-100T (Seikagaku Biobusiness Corporation) 4 mg/ml (stored at -20°C)
- Complete™ Protease Inhibitor Cocktail EDTA-free Tablets (Roche)

Sample preparation

- 10 mM potassium phosphate (PK) buffer, pH 7.4 (stored at -20°C)
- Bradford microplate microassay (Bio-Rad)

Ubiquinol:cytochrome c oxidoreductase assay

- 250 mM potassium phosphate (PK) buffer, pH 7.4 (stored at -20°C)
- 50 mM sodium azide (NaN3) (stored at -20°C)
- 1 mM cytochrome c (freshly prepared)
- 1 mg/ml antimycin A in 50% ethanol (stored at -20°C)
- sodium borohydride (NaBH4)
- decylubiquinone (DB)
- decylubiquinol (DBH2) (stored at 4°C and freshly diluted 1:1 with H2O)

Cytochrome c oxidase assay

- 100 mM potassium phosphate (PK) buffer, pH 7.0 (stored at -20°C)
- 0.8 mM cytochrome c (freshly prepared). Dissolve cytochrome c in H2O containing 10% of 100 mM potassium phosphate buffer, pH 7.0, and reduce it with sodium dithionite)
- 40 mM potassium cyanide (KCN) (stored at -20°C)

ATP synthase assay

- Buffer H-Mg: 10 mM MgSO4 in 100 mM Hepes-KOH, pH 8.0 (stored at -20°C)
- 30 mM NADH (freshly prepared)
- 50 mM phosphoenolpyruvic acid (freshly prepared)
- 10 mg/ml pyruvate kinase

- 5 mg/ml lactate dehydrogenase (stored at 4°C)
- 0.2 mg/ml antimycin A in 50% ethanol (stored at -20°C)
- 25 mM ATP buffered at pH 7.0 with 3M KHCO3 (freshly prepared)
- 0.2 mg/ml oligomycin in 50% ethanol (stored at -20°C)

Equipment

- Shaking incubator at 28°C
- Water bath at 37°C
- Refrigerated centrifuges
- Spectrophotometer

Time Taken

3 days:

- Cell culture: 8h (pre-culture in selective medium) + 20h (overnight culture in YPGAL)
- Preparation of mitochondria by differential centrifugations: 4-6h
- Sample preparation: 1h
- Respiratory chain activity assay: variable, depending on the number of samples

Procedure

Cell culture

1. Pre-inoculate yeast cells in 5 ml of liquid selective medium supplemented with 2% (w/v) glucose with shaking at 28°C for 8h.

2. Harvest cells and inoculate in 200 ml of YPGAL medium. Incubate overnight with shaking at 28°C.
3. Harvest cells by centrifuging when OD600nm of the culture reaches a value of 2.
4. Wash the pellet in 20 ml of sterile H2O. The resulting pellet can be stored at -80°C.

Preparation of mitochondria by differential centrifugations

Yeast cell mitochondria are prepared by differential centrifugations. This protocol is adapted from Ref. 1.
1. Rinse the pellet with 5ml of 10 mM EDTA.
2. Centrifuge at 400g for 3 min.
3. Discard the supernatant and resuspend the pellet in 4.5 ml of ice-cold Sorbitol Buffer A supplemented with 0.3% (v/v) 2-mercaptoethanol.
4. Digest the cell wall with approx. 250 µl of 4 mg/ml Zymolyase-100T (1 mg per g of cells) at 37°C for 45 min.
5. Verify wall digestion under the microscope.
6. Harvest spheroplasts by centrifugation at 1,800g for 15 min at 4°C.
7. Discard the supernatant and resuspend the pellet gently in 7 ml of ice-cold Sorbitol Buffer B.
8. Centrifuge at 2,500g for 15 min at 4°C.
9. Transfer the supernatant in a new tube and centrifuge at 20,000g for 15 min at 4°C.

10. Discard the supernatant and resuspend the pellet by pipetting in 4 ml of ice-cold Sorbitol Buffer B supplemented with EDTA-free Complete™ Protease Inhibitor Cocktail (Roche).
11. Centrifuge at 800g for 5 min at 4°C.
12. Transfer the supernatant in a new tube and centrifuge at 15,000g for 15 min at 4°C.
13. Discard the supernatant and resuspend the pellet by pipetting in 4 ml of ice-cold Sorbitol Buffer B.
14. Centrifuge at 800g for 5 min at 4°C.
15. Transfer the supernatant in a new tube and centrifuge at 15,000g for 15 min at 4°C.
16. Discard the supernatant and resuspend the pellet by pipetting in 1.5 ml of ice-cold Sorbitol Buffer B.
17. Centrifuge at 800g for 5 min at 4°C.
18. Decant the supernatant in a new 2-ml-tube and centrifuge at 15,000g for 15 min at 4°C.
19. Store the pellet at -80°C.

Sample preparation

1. Resuspend the resulting mitochondrial pellet in 300-500 µl of 10 mM PK buffer, pH 7.4.
2. Freeze and thaw three times.
3. Determine protein concentration with Bradford microplate microassay (Bio-Rad).
4. Normalize samples for protein concentration (recommended concentration: between 0.3 and 0.6 µg/µl).

Ubiquinol:cytochrome c oxidoreductase (Complex III) activity assay

The protocol is adapted from Refs. 2 and 3.

A) Chemically reduce decylubiquinone (DB) to decylubiquinol (DBH2)

1. Prepare a 10-mM solution of DB in HCl-acidified ethanol (pH ≤4).
2. Add a few milligrams of sodium borohydride to reduce quinone. Reaction is completed when solution's color changes from yellow to colorless.
3. Add 2 ml of cyclohexane to the reduced solution and stir it.
4. Transfer the upper (organic) phase to a clean tube.
5. Add 2 ml of cyclohexane to the remaining lower phase and stir it. Transfer the upper phase adding it to the previous one.
6. Repeat point 5 another time.
7. Wash the organic fraction with 2 M NaCl.
8. Dry the pellet under nitrogen and resuspend it with a volume of HCl-acidified ethanol (pH ≤4) corresponding to the initial one.

B) Determine ubiquinol:cytochrome c oxidoreductase activity

Activity is determined by measuring spectrophotometrically, at 550 nm at 30°C, the rate of reduction of cytochrome c by ubiquinol. Measure complex III activity at several protein concentrations paying attention to the linearity of the reaction. To determine the reduction of cytochrome c due to the specific activity of complex III, for each sample, perform parallel

measurements of activity in the presence and in the absence of antimycin A, an inhibitor of complex III.

1. Prepare two cuvettes containing 200 µl of 250 mM PK buffer, pH 7.4, 40 µl of 50 mM NaN3, and 50 µl of 1 mM cytochrome c. Add 10 µl of 1 mg/ml antimycin A in one of them and an equal volume of H2O in the other one.
2. Add 2-10 µg of mitochondrial proteins.
3. Adjust the volume to 990 µl with H2O.
4. Record the baseline for 2 min.
5. Start the reaction by adding 10 µl of DBH2.
6. Measure absorbance of the sample at 550 nm for 2 min.
7. Calculate complex III specific activity using the Beer-Lambert law equation (Fig.1). Express the activity as nanomoles of cytochrome c reduced per minute per milligram of protein.

Cytochrome c oxidase (Complex IV) activity assay

Determine cytochrome c oxidase activity by measuring spectrophotometrically at 30°C for 2 minutes the oxidation of cytochrome cred as indicated by the decrease of absorbance at 550 nm (Refs. 2-3). For each sample, measure complex IV activity twice at at least two protein concentrations that ensure the linearity of the reaction.

1. Reduce cytochrome c by adding tiny amounts of sodium dithionite until the absorbance at 550 nm of 100 µl of cytochrome c in 1 ml of H2O is between 1.8 and 1.9.

2. In a cuvette, add 100 µl of 100 mM PK buffer, pH 7.0, 100 µl of reduced cytochrome c and adjust the volume with H2O (800 µl minus sample volume).
3. Incubate the cuvette at 30°C for 2 min.
4. Start the reaction by adding 2-10 µg of mitochondrial proteins.
5. Measure absorbance of the sample at 550 nm for 2 min.
6. Verify the specificity of cytochrome c reduction by inhibiting cytochrome c oxidase activity with 50 µl of 40 mM KCN.
7. Calculate complex IV specific activity using the Beer-Lambert law equation (Fig. 1). Express the activity as nanomoles of cytochrome c oxidised per minute per milligram of protein.

ATP synthase (Complex V) activity assay

Determine complex V activity by measuring spectrophotometrically at 30°C for 2 minutes the oxidation of NADH as indicated by the decrease of absorbance at 340 nm (Refs. 2-3). Repeat each measurement twice at at least two protein concentrations that ensure the linearity of the reaction.
1. In a cuvette add 500 µl of Buffer H-Mg, 10 µl of 30 mM NADH, 50 µl of 50 mM phosphoenolpyruvic acid, 5 µl of 10 mg/ml of pyruvate kinase, 10 µl of 5 mg/ml of lactate dehydrogenase, and 10 µl of antimycin A.
2. Add 2-10 µg of mitochondrial proteins.
3. Adjust the volume to 900 µl with H2O.
4. Incubate the cuvette at 30°C for 2 minutes
5. Record the baseline for 2 min.

6. Start the reaction by adding 100 µl of 25 mM ATP.

7. Measure absorbance of the sample for 2 min (ΔAbs340nmwithout oligomycin)

8. Add 10 µl of oligomycin.

9. Measure absorbance for 2min (ΔAbs340nmwith oligomycin).

10. Calculate complex V specific activity using the Beer-Lambert law equation (Fig. 1). Express complex V activity as nanomoles of NADH oxidised per minute per milligram of protein.

Critical Steps

Preparation of mitochondria by differential centrifugations

Keep samples on ice during the entire procedure.

Following wall digestion, resuspend the pellets by gentle pipetting (not vortexing) to avoid mitochondria fragmentation.

References

1. Lemaire, C. & Dujardin, G. Preparation of respiratory chain complexes from Saccharomyces cerevisiae wild-type and mutant mitochondria: activity measurement and subunit composition analysis. Methods Mol Biol 432, 65-81 (2008).

2. Rimoldi, M. et al. Cytochrome-c-oxidase deficiency in muscles of a floppy infant without mitochondrial myopathy. J Neurol 227, 201-207 (1982).

3. Dionisi-Vici, C. et al. Fulminant Leigh syndrome and sudden unexpected death in a family with the T9176C mutation of the mitochondrial ATPase 6 gene. J. Inherit Metab Dis 21, 2-8 (1998).

Keywords

yeast, Saccharomyces cerevisiae, mitochondria, respiratory chain complexes, ATP synthase, cytochrome c oxidase, ubiquinol:cytochrome c oxidoreductase

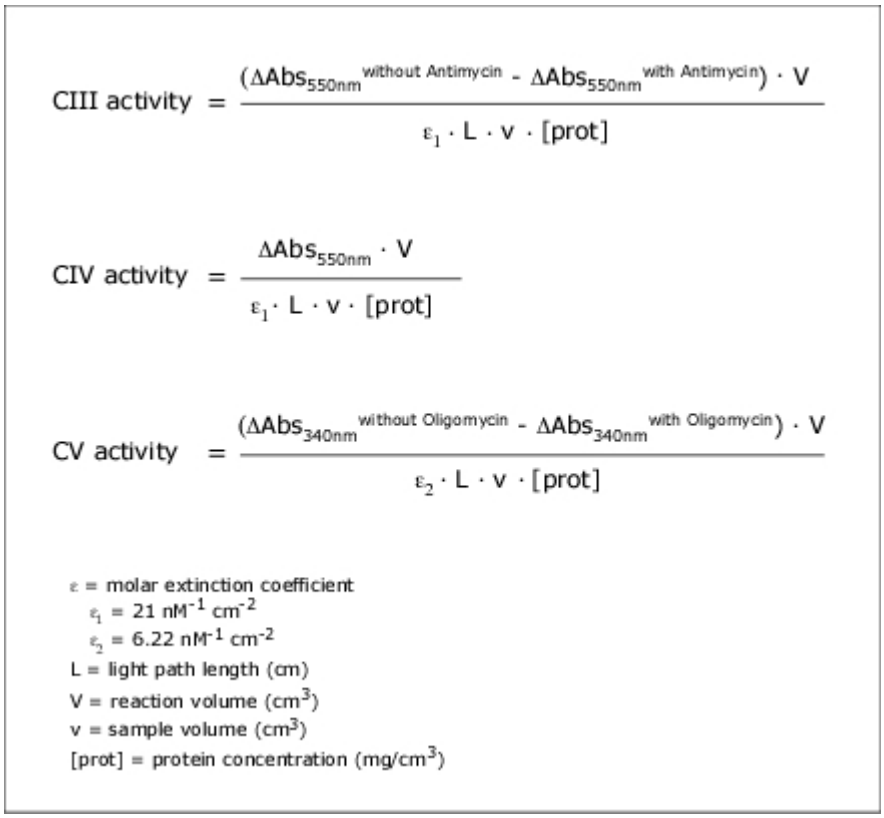

Figure 1

Formulae to calculate Complex III, Complex IV, and Complex V activity

Formulae are derived from the Beer-Lambert law equation. Activities are expressed as nanomoles per minute per milligram of protein.

Chapter 3:

Spinocerebellar ataxia type 28: identification and functional analysis of novel AFG3L2 mutations

V. Fracasso[1], S. Magri[1], M.Plumari[1], P. Giunti,[2] S. Boesch,[3] M. Muzi-Falconi[4], F. Lazzaro[4], D. Di Bella[1], and F. Taroni[1*]

[1]Unit of Genetics of Neurodegenerative and Metabolic Disease, Fondazione IRCCS Istituto Neurologico "Carlo Besta", Milan, Italy

[2]Institute of Neurology and The National Hospital for Neurology and Neurosurgery, London, UK

[3]Department of Neurology, Innsbruck Medical University, Innsbruck, Austria

[4]Department of Biomolecular Sciences and Biotechnology, University of Milan, Milan, Italy

Submitted

Abstract

Autosomal dominant spinocerebellar ataxias (SCAs) are a clinically and genetically heterogeneous group of diseases caused by progressive degeneration of the cerebellum and its afferent and efferent paths. We have recently identified missense mutations in the *AFG3L2* gene (ATPase Family Gene 3-Like 2) as the cause of spinocerebellar ataxia type 28 (SCA28). AFG3L2 and paraplegin are components of the inner mitochondrial membrane metalloprotease AAA (*m*-AAA). This protease complex is known to exert chaperon-like activity and to participate in protein quality control. We screened 233 individuals with ataxia for mutations in the *AFG3L2* gene. We identified 4 heterozygous missense mutations and 2 small in-frame deletions, establishing a minimum frequency of 2.5% for patients with a SCA phenotype. The respiratory competence and the proteolytic activity of these mutations were analyzed in a yeast cellular model confirming the pathogenic role of the amino acid substitutions identified in AFG3L2.

Introduction

Cerebellar ataxias are a heterogeneous group of diseases caused by progressive degeneration of the cerebellum which leads to a complex movement disorder, whose principal symptoms are the progressive loss of motor coordination and difficulties in executing voluntary movements. Autosomal dominant spinocerebellar ataxias (SCAs) are clinically and genetically heterogeneous [Dürr, 2010]. Thirty-one SCA loci are currently known (http://neuromuscular.wustl.edu/ataxia/domatax.html). These diseases may be caused by expansions of tri- or pentanucleotide repeats or deletions, missense, nonsense or frameshift mutations in the corresponding genes [Taroni and DiDonato, 2004]. We have recently identified missense mutations in the gene encoding the mitochondrial protease AFG3L2 (ATPase Family Gene 3-Like 2) as the cause of spinocerebellar ataxia type 28 (SCA28) [Di Bella et al., 2010]. Mutations in the *AFG3L2* gene are interesting because no dominant ataxia has been thus far associated with mitochondrial dysfunction, and because its partner protein is paraplegin. Mutations in the *SPG7* gene encoding paraplegin cause an autosomal recessive form of hereditary spastic paraparesis [Casari et al., 1998]. Both AFG3L2 and paraplegin are metalloproteases that are components of the mitochondrial AAA (*m*-AAA) protease complex. These proteases belong to the family of the AAA proteins (ATPases Associated with

different cellular Activities). In the subfamily AAA^+, proteins have a common structural domain composed by one AAA-domain with ATPase activity followed by a highly conserved proteolytic domain. They exert chaperone-like activity and are implicated in the degradation of macromolecular structures involved in different cellular processes. Studies in the yeast *Saccharomyces cerevisiae* have demonstrated a dual role for the *m*-AAA protease [Tatsuta and Langer 2008]. First, it is implicated in the quality control of mitochondrial inner membrane proteins selectively degrading improperly folded or unassembled polypeptides [Koppen and Langer, 2007). Second, it plays a regulatory role in mitochondrial protein synthesis participating in the processing and maturation of some mitochondrial proteins including cytochrome *c* peroxidase (Ccp1) in yeast [Esser et al., 2002] and the ribosomal subunit Mrpl32 in both yeast and mammals cells [Nolden et al., 2005]. The importance of *m*-AAA in humans is underlined by the evidence that mutations in both genes are responsible for important neurodegenerative diseases. *m*-AAA is well characterized in yeast. Yeast *m*-AAA is composed of Yta10p and Yta12p which show high homology with AFG3L2 and paraplegin, respectively [Arlt et al., 1996; Banfi et al., 1999].

Here, we report the AFG3L2 variations identified in the genetic study of a new cohort of affected individuals with ataxic phenotype. We also describe the results of a functional study using a yeast cellular model to evaluate the functional effects and the pathogenic role of the amino acid substitutions

identified in AFG3L2. Functional analysis of the respiratory competence and the proteolytic activity of human mutant AFG3L2 expressed in yeast *Saccharomyces cerevisiae* represents a necessary tool to discriminate between real pathogenic mutations and rare/unique polymorphic variants.

Results

Mutation analysis

Two hundred and thirty-three unrelated individuals with a chronic progressive ataxic phenotype were screened for *AFG3L2* mutations. In this patient series, 153 index cases were Italian (108 with autosomal dominant inheritance and 45 sporadic cases) whereas other probands came from European collaborating groups: 75 were British (with positive family history), 2 were Austrian (from 2 unrelated families), and 3 were Spanish (from 3 unrelated families). All affected individuals showed a progressive ataxic phenotype and cerebellar atrophy variably associated with additional features such as pyramidal signs and minor abnormalities in ocular movements, consistent with a SCA28 phenotype [Cagnoli et al., 2010; Mariotti et al., 2008]. The 17 coding exons of the *AFG3L2* gene were analysed by denaturing high performance liquid chromatography (dHPLC) and direct sequencing. We identified 7 heterozygous AFG3L2 missense substitutions and 2 heterozygous small in-frame deletions in 9 affected individuals.

Most AFG3L2 variations are located in functional domains of the protein involving highly conserved residues: 2 variations (T444A and I473V) are located in a portion of the AAA-domain encoded by exon 11, 5 variations (K569del, M666V, R679C, K687T, and L772F) are located in the proteolytic domain, whereas only 2 variations (82N_84Kdel and A86P) were found in exon 3 in a region of the protein with unknown function (**Figs. 1** and **2**). The affected individual with the R679C substitution presented another variation, a transition T>C at position c.1779+2C changing the splice donor site from GT to GC. The two mutations are likely to be on distinct alleles since RT-PCR analysis of total RNA from this patient demonstrated the presence of the R679C variant only, which suggests that transcript from the c.1779+2C-carrying allele is degraded. The substitution M666V identified in this analysis has also been observed in two previously reported families [Cagnoli et al., 2010].

None of the substitutions identified in this study are reported as polymorphisms in the dbSNP database (http://www.ncbi.nlm.nih.gov/projects/SNP/) nor were they found in >400 control chromosomes. *In silico* prediction by PolyPhen (http://genetics.bwh.harvard.edu/pph/) and SIFT (http://blocks.fhcrc.org/sift/SIFT.html) of the effects of the substitutions on protein structure/function did not give univocal results. Both programs predicted as benign the substitutions A86P, T444A, and I473V, and as probably damaging the M666V and R679C. By contrast the substitutions K687T and

L772F were predicted to be benign by PolyPhen but not tolerated by SIFT. Computational analysis by ESE Finder (ESE, exonic splicing enhancers) (http://rulai.cshl.edu/cgi-bin/tools/ESE3/esefinder.cgi?process=home), FAS-ESS web server (ESS, exonic splicing silencers) (http://genes.mit.edu/fas-ess/), and RESCUE-ESE web server (http://genes.mit.edu/burgelab/rescue-ese/) of the possible effects of the mutations on splicing excluded the formation of ESS in all cases but gave nonunivocal results regarding the generation or abolition of exon splicing enhancers.

As for the mutations described previously [Cagnoli et al., 2010; Di Bella et al., 2010], most of the substitutions identified are located in exons, mostly in exon 16, that encode the proteolytic domain, indicating that this region of AFG3L2 is a hot spot for mutations (**Fig. 1**). Fewer mutations were located in the ATPase domain.

The SPG7 gene encoding paraplegin was also sequenced in all patients. Interestingly, two patients were found to be positive for mutations in this gene. An Italian patient heterozygous for the A86P mutation in *AFG3L2* also carried a homozygous nonsense mutation (R457X) in SPG7 exon 10, which is predicted to result in a truncated protein. Western blot analysis of paraplegin in the patient's peripheral blood lymphocytes showed the absence of the protein (not shown). In a second patient of British origin, SPG7 sequence analysis revealed heterozygosis for a frameshift mutation (c.1052dupC)

in exon 8, which is predicted to cause premature termination of the protein (G352RfsX43) encoded by the mutant allele.

Respiratory competence of AFG3L2 variants in yeast model

We have used a yeast *(Saccharomyces cerevisiae)* cellular model to evaluate the functional effects and to validate the pathogenic role of the amino acid substitutions identified in AFG3L2. Yeast *YTA10*/*YTA12*-defective strains have been widely used in previous studies on the characterization of the *m*-AAA protease [Di Bella et al., 2010; Koppen et al., 2007]. Yeast cells lacking either Yta10 (*yta10*Δ) or Yta12 (*yta12*Δ) grow on glucose but exhibit impaired growth on a nonfermentable carbon source such as glycerol, indicating a respiratory defect (OXPHOS phenotype) [Arlt et al., 1996]. Yta10p and Yta12p exhibit high homology with AFG3L2 and paraplegin, respectively [Banfi et al., 1999]. Complementation studies in yeast have shown that human AFG3L2 homocomplex or AFG3L2/paraplegin heterocomplex, but not paraplegin homocomplex, if any, are able to functionally replace the Yta10p/Yta12p complex and to restore the respiratory competence of the yeast cell [Koppen et al., 2007]. The functional effects of the 9 substitutions identified in the present study and of 5 mutations identified by a collaborating group [Cagnoli, et al, 2010] were analysed by expressing normal and mutant AFG3L2 under the control of the strong yeast *ADH1* promoter. We evaluated the human AFG3L2 substitutions for their ability to support respiration in an *m*-AAA-defective strain

(double-deletion mutant *Δyta10/Δyta12*) (**Figs. 3** and **4**). All transformants exhibited normal growth in glucose-containing medium (YPD). When glycerol was the only carbon source, three mutants (AFG3L2^{T444A}, AFG3L2^{I473V}, and AFG3L2^{L772F}) were able to grow, suggesting that these variations may represent rare AFG3L2 polymorphic variants. Some mutants (AFG3L2^{82N_84Kdel}, AFG3L2^{A86P}, AFG3L2^{K569del}, and AFG3L2^{K687T}) were partially able to rescue respiration, showing a slower growth than the strain carrying normal AFG3L2 (AFG3L2^{WT}). By contrast, the other amino acid substitutions in the highly-conserved proteolytic domain (AFG3L2^{T654I}, AFG3L2^{M666R}, AFG3L2^{M666T}, AFG3L2^{M666V}, AFG3L2^{G671E}, AFG3L2^{G671R} , and AFG3L2^{R679C}) were not able to restore respiratory competence of *Δyta10/Δyta12* cells (**Fig. 3a**). These results clearly indicate a pathogenic role for these mutations. Results at 28°C and 37°C (not shown) were comparable. To better evaluate the intermediate growth of strains AFG3L2^{82N_84Kdel}, AFG3L2^{A86P}, AFG3L2^{K569del}, and AFG3L2^{K687T}, growth rate was measured in liquid medium for 24h at 28°C. The results confirmed the data obtained on solid medium showing a statistically significant slower growth as compared with AFG3L2^{WT}. However, quantitative analysis of growth in liquid medium allowed to further divide AFG3L2 mutants associated with intermediate growth rate into two groups that differed in a statistically significant fashion (P <0,0005): I1 (intermediate group 1, slow-growing strains; AFG3L2 $^{82N\_84Kdel}$, AFG3L2^{A86P}) and I2 (intermediate group 2,

slower-growing strains; AFG3L2^{K569del} and AFG3L2^{K687T}) (**Fig. 3b**).

In human, the *m*-AAA exist as homo-oligomeric AFG3L2 complexes as well as hetero-oligomeric complexes composed of AFG3L2 and paraplegin subunits [Koppen et al., 2007]. We analyzed the phenotype of strains carrying mutant AFG3L2 also in the presence of normal human paraplegin. When AFG3L2 and paraplegin were coexpressed, cells harboring AFG3L2^{T444A}, AFG3L2^{I473V}, and AFG3L2^{L772F} maintained respiratory competence, as expected. By contrast, the strains (AFG3L2^{82N_84Kdel}, AFG3L2^{A86P}, AFG3L2^{K569del} and AFG3L2^{K687T}) showing intermediate growth when carrying AFG3L2^{mut} alone, were fully rescued by paraplegin coexpression.

As regards the AFG3L2 substitutions that abolished respiration competence when expressed alone, coexpression of paraplegin resulted in four respiratory phenotypes. All the experiments were carried out at 28°C, but similar results were obtained at 37 °C (not shown). A full rescue of respiratory competence was observed in the case of AFG3L2^{G671R} while a partial rescue (intermediately reduced growth rate) was the effect of paraplegin coexpression in the case of AFG3L2^{M666V}, AFG3L2^{M666T}, AFG3L2^{G671E}, and AFG3L2^{R679C} (**Fig. 4a**). These strains with intermediate growth phenotype were further characterized in liquid medium, which allowed to further identify two subgroups: I1 (intermediate group 1, slow-growing strains; AFG3L2^{M666T}, AFG3L2^{R679C}) and I2 (intermediate group 2,

slower-growing strains; AFG3L2^{M666V}, AFG3L2^{G671E}) (**Fig. 4b**). For all these mutants, the mutation mechanism is likely to be haploinsufficiency or a weak dominant negative effect, resulting in variably reduced penetrance or expressivity in affected people. In the last group of mutants, coexpression of paraplegin did not rescue the defective phenotype (AFG3L2^{T654I}, AFG3L2^{M666R}) suggesting a dominant-negative effect of the mutations (**Fig. 4a**).

Notably, different amino acid substitutions at the same residue may lead to different phenotypes. In the case of glycine 671 (G671), substitution with the negatively-charged glutamic acid (G671E) leads to a respiratory phenotype with slower growth than substitution with the positively-charged arginine (G671R) that results in the complete recovery of the respiratory phenotype following paraplegin coexpression. The substitution of methionine 666 with arginine (M666R) is particularly interesting since it leads to a total loss of respiration, while the other two substitutions identified (threonine, M666T, and valine, M666V) result in I1 and I2 phenotypes, respectively (**Fig. 4b**).

Proteolytic activity of AFG3L2 variants

To determine the proteolytic competence of AFG3L2 substitutions, we analysed the processing of two mitochondrial precursor proteins: MrpL32 and cytochrome *c* peroxidase (Ccp1). Lack of *m*-AAA, as in *Δyta10/Δyta12* cells, causes respiratory defect and also completely abolishes the processing of MrpL32 and Ccp1 with accumulation of unprocessed

precursor proteins [Nolden et al., 2005; Esser et al., 2002]. MrpL32 is a ribosomal protein, encoded by nuclear genome, whose maturation is necessary for ribosome assembly and subsequent protein synthesis within mitochondria, thus controlling the assembly of respiratory complexes in the inner membrane. MrpL32 is known to be matured by the yeast as well as the mammalian *m*-AAA protease [Nolden et al., 2005]. Ccp1 is localized to mitochondrial intermembrane space and it is required for peroxide and toxic radical scavenging. In yeast, Ccp1 precursor (pCcp1) contains a bipartite N-terminal targeting sequence which is sequentially processed to an intermediate form (iCcp1) by the *m*-AAA protease and to a mature form by the intramembrane rhomboid protease Pcp1 [Esser et al., 2002]. Recent studies, however, have shown that the major role of *m*-AAA in the maturation of Ccp1 is the ATP-dependent dislocation of the pCcp1 precursor from the inner mitochondrial membrane rather than its processing to an intermediate form iCcp1 [Tatsuta et al., 2007].

We evaluated the human AFG3L2 substitutions for their ability to support proteolytic activity in the *m*-AAA-defective strain (*Δyta10/Δyta12*). AFG3L2 proteolytic competence is expressed as the ratio of precursor protein level (p) to total protein level (p + m; m=mature) for both proteins [Di Bella et al., 2010]. Data are summarized in **Table 1**. We observed a good correlation between the respiratory competence of the cells and the maturation of MrpL32, both when AFG3L2^{mut} was expressed alone and when was coexpressed with paraplegin

(**Fig. 5**). Notably, the two strain subgroups (I1 and I2) with intermediate growth phenotype resulted in two distinct proteolytic phenotypes: in the first subgroup (I1, blue bars), MrpL32 processing was not statistically significantly different from that in AFG3L2^{WT} strain. By contrast, processing of MrpL32 precursor was significantly impaired in I2 strains (yellow bars).

In the set of experiments where paraplegin was coexpressed with AFG3L2, all transformed strains showed higher levels of pMrpL32, suggesting either increased MrpL32 expression in cells expressing both heterologous proteins or reduced processing by AFG3L2/paraplegin heterocomplex as compared with that by AFG3L2 homocomplex.

For Ccp1, the results indicated that some mutant strain harbouring mutant AFG3L2 homocomplex or AFG3L2/paraplegin heterocomplex (AFG3L2^{R679C}, AFG3L2^{M666T}/paraplegin, AFG3L2^{M666V}/paraplegin, and AFG3L2^{G671E}/paraplegin) showed a dissociation between respiratory growth and processing of the substrate. Surprisingly, Ccp1 was processed in the strain harbouring mutant AFG3L2^{R679C}, which exhibited respiratory deficiency (see **Fig. 3**). On the contrary, proteolysis of Ccp1 was impaired in strains carrying AFG3L2^{M666T}/paraplegin, AFG3L2^{M666V}/paraplegin, or AFG3L2^{G671E}/paraplegin which exhibited an intermediate growth phenotype (see **Fig. 4**).

Discussion

In this work, we screened a large series of patients with a SCA-like chronic-progressive ataxic phenotype [Dürr, 2010] to identify novel mutations in the *AFG3L2* gene and to evaluate the frequency of *AFG3L2* mutations in this large group of people with ataxia. Moreover, we wanted to characterize the function of the protein involved in the pathogenesis of this new form of dominant spinocerebellar ataxia.

We have identified six novel heterozygous mutations in AFG3L2 in individuals with ataxic phenotype, further confirming that mutations in AFG3L2 cause spinocerebellar ataxia SCA28. Most mutations are located in the proteolytic domain, one mutation in exon 14 ($AFG3L2^{K569del}$) and three mutations in exon 16 ($AFG3L2^{M666V}$, $AFG3L2^{R679C}$ and $AFG3L2^{K687T}$), confirming that this region is a mutational hot spot for SCA28 and underlining the crucial importance of the peptidase domain for *m*-AAA activity. Notably, two mutations ($AFG3L2^{82N\_84Kdel}$ and $AFG3L2^{A86P}$) are located in exon 3 where mutations have not been thus far reported. Since they occur in a region outside functional domains, it was necessary to assess their functional effects in a suitrable cellular system.

No mutation was found in the metal-binding motif HEXGH. In this study, for the first time we have identified two small in-frame deletions in addition to missense mutations. All the mutations identified, except for $AFG3L2^{M666V}$, are novel and have not been

found in previous studies [Di Bella et al., 2010; Cagnoli et al., 2010; Edener et al., 2010].

The pathogenicity of the identified mutations is suggested by the following: 1) in families with more than one affected subject, the identified mutation segregated with the disease and was not present in healthy members of the family; 2) the mutations were not found in more than 400 control chromosomes; and 3) the mutations affect residues that are highly conserved or occur in regions with high degree of conservation through evolution. However, most mutations occurred only in a single patient/family and, in some cases, segregation could not be adequately assessed due to the limited size of the family. Thus, the possibility exists that, at least in some cases, the identified substitutions represent very rare or private polymorphic variants. Functional studies are ultimately necessary to confirm the pathogenicity of the identified amino acid substitutions. The yeast *S. cerevisiae* has been previously used as an *in vivo* model to validate the pathogenic significance of mutations in genes involved in mitochondrial diseases, thanks to the similarity of orthologous yeast *vs.* human OXPHOS-related genes, and the ability of the yeast to survive in spite of mitochondrial dysfunction, provided that a fermentable carbon source is made available [Fontanesi et al., 2009]. In addition to functional proof of pathogenicity, expression studies may provide clue to genotype-phenotype correlations. Finally, the interesting question of negative dominance *vs.* haploinsufficiency of mutations can be defined

by using yeast heteroallelic strains that contain both the mutant and the wild-type allele, thus mimicking the human diploid condition.

Human AFG3L2 and paraplegin have high homology with Yta10p and Yta12p yeast proteins, respectively. Complementation studies in yeast have shown that human *m*-AAA is able to restore the respiratory competence in *m*-AAA-deficient cells Δ*Yta10*/Δ*Yta12* [Koppen et al., 2007]. In order to provide a complete picture of the functional effects of AFG3L2 mutations causing SCA28, we functionally tested the 9 substitutions identified in the present study as well as the 5 mutations previously reported by a collaborating group [Cagnoli, et al, 2010]. Expression studies of mutant AFG3L2 in yeast cells lacking *m*-AAA showed that all the substitutions analysed, except T444A, I473V and L772F, were not able to restore a functional *m*-AAA. These data strongly suggested that the substitutions 82N_84Kdel, A86P, K569del, T654I, M666R, M666T, M666V, G761E, G671R, R679C and K687T are pathogenic mutations while substitutions T444A, I473V, and L772F are likely to be rare/unique benign variants. Interestingly, these apparently nonpathogenic substitutions are also located in the crucial functional regions of the protein, two (T444A and I473V) in the AAA (ATPase) domain and one (L772F) in the proteolytic domain. It was also interesting to find one patient who carried a homozygous nonsense paraplegin mutation (R457X) along with the relatively milder A86P mutation in AFG3L2. Although this patient can be classified as both SPG7

and SCA28, clinical manifestations were dominated by cerebellar dysfunction and cerebellar atrophy with marginal pyramidal dysfunction. Further clinical investigations are required to elucidate the contribution of either genotype to the clinical picture in this patient.

Some interesting results were provided from coexpression of mutant AFG3L2 and its partner paraplegin. Analysis of the respiratory phenotype of cells coexpressing both proteins showed three respiratory phenotypes: 1) a full restore of respiratory competence; 2) a partial rescue of respiratory phenotype, that we call intermediate growth rate with subgroups I1 and I2; and 3) no rescue of the defective phenotype. Altogether, these phenotypes suggest that two classes of AFG3L2 mutations exist. The majority of mutations are “paraplegin-responsive”, namely 82N_84Kdel, A86P, K569del, M666T, M666V, G761E, G671R, R679C, and K687T. In these cases, the mechanism is likely to be haploinsufficiency, which may result in variably reduced penetrance and/or expressivity in affected people. Two mutations (T654I and M666R) are not rescued by paraplegin coexpression. These variants behave as dominant-negative mutations with a likely full penetrance in the family. Segregation of the T654I mutation in the family pedigree lends support to this hypothesis [Cagnoli et al. 2010]. The M666R mutation exhibited the most severe phenotype in yeast, with the highest impairment of MrpL32 and Ccp1 processing. Interestingly, this mutation was identified in a very small family with early onset of the disease (6 and 8 years of age) and

severe clinical features [Cagnoli et al. 2010]. Structural modeling of the M666R mutation had showed significant decrease of the electrostatic potential difference between the inner mitochondrial membrane side and the matrix side of the hexamer [Cagnoli et al. 2010].

The proteolytic competence of AFG3L2 variants was assessed analysing the processing of two known substrates, MrpL32 and Ccp1. MrpL32 is a component of the large mitochondrial ribosomal particle 54S. The correct assembly of mitochondrial ribosomes is required for the translation of proteins encoded by mitochondrial DNA, including the core subunits of the respiratory chain. The correct maturation of MrpL32 is therefore crucial for the control of mitochondrial protein synthesis, in particular for the assembly of respiratory chain and F_1F0-ATP-synthase complexes [Nolden et al., 2005]. Overall, our data on processing of MrpL32 in strains harboring $AFG3L2^{mut}$ correlate well with the respiratory phenotype, consistent with the other results described above. The different processing ability of the strains with intermediate growth indicates that a small amount of the mature protein is sufficient to ensure aerobic growth in yeast. However, this might not be sufficient for nerve cells. Neurons, in particular the cerebellar Purkinje cells, large cells with long axons where AFG3L2 is highly and selectively expressed [Di Bella et al., 2010], need high and constant levels of energy to perform their activities. Therefore, they could particularly suffer of the energy deficit and undergo a degenerative process such as that occurring in

affected individuals. Moreover, if functionality of the *m*-AAA complex is lost, even partially, several mitochondrial proteins may not be correctly processed and/or degraded creating an accumulation of unassembled/undegraded polypeptides potentially toxic for the cell.

Interestingly, some mutant strains showed inconsistency between respiratory growth and processing of the substrate. Thus, Ccp1 was processed in the respiratory-deficient mutant strain AFG3L2^{R679C}. On the contrary, processing of Ccp1 was impaired in strains carrying AFG3L2^{M666T}/paraplegin, AFG3L2^{M666V}/paraplegin, or AFG3L2^{G671E}/paraplegin which exhibited an intermediate growth phenotype. Altogether, these results raise the intriguing possibility that the mutations may differentially affect distinct and specialized functions of the *m*-AAA complex.

In conclusion, we identified 9 substitutions in AFG3L2 in patients with autosomal dominant spinocerebellar ataxia and nalyzed the functional effects of them. The discovery of the genetic cause of SCA28 is extremely important for the diagnosis of SCA allowing a molecular diagnosis of the disease. Our data allow to establish a minimum frequency of AFG3L2 mutations of ~2.5% (6/233) in a raw series of patients with chronic progressive neurodegenerative ataxia negative for the most common SCA mutations (SCA1, SCA2, SCA3, SCA11, and SCA17). Functional data have clearly shown the pathogenic role of AFG3L2^{82N_84Kdel}, AFG3L2^{A86P}, AFG3L2^{K569del}, AFG3L2^{M666V}, AFG3L2^{R679C} and AFG3L2^{K687T}

and have instead suggested that the AFG3L2^{T444A}, AFG3L2^{I473V}, and AFG3L2^{L772F} represents a rare benign variants of the gene AFG3L2. Our results demonstrate that the yeast *Saccharomyces cerevisiae* is an appropriate and useful functional model for assessing the pathogenicity of substitutions, particularly in the critical cases of mutations identified in sporadic cases or small families where segregation analysis is not informative.

MATERIALS AND METHODS

Patients and DNA samples

We studied 233 unrelated index cases with a diagnosis of ataxia. 153 individuals (108 with autosomal dominant inheritance, and 45 sporadic cases) were selected from a large cohort of patients referred to our Centre from throughout Italy. The other individuals were selected by European collaborating group: 75 British, 2 Austrian, 3 Spanish. Inclusion criteria were the presence of a progressive ataxic phenotype and cerebellar atrophy variably associated with additional features such as pyramidal signs and minor abnormalities in ocular movements, in according with SCA28 phenotype. Control subjects were individuals who presented for work-up of unrelated neurologic conditions. Genomic DNA was prepared from peripheral-blood lymphocytes using standard procedures as previously described [Gellera et al., 2007]. Written informed consent was obtained from each individual providing a biological sample. All procedures involving human subjects were approved by the Institutional Review Board of the Fondazione IRCCS Istituto Neurologico “Carlo Besta”, Milan, Italy.

Mutation analysis

For mutation screening of the selected patient population, PCR products were analyzed by automated sequencing and/or Denaturing High-Performance Liquid Chromatography (DHPLC). Sequences of the oligonucleotide primers and

conditions used for PCR amplification, DNA sequencing, and DHPLC analysis are as previously described [Di Bella et al., 2010].

Except when noted differently, nucleotides were numbered so that the first nucleotide of the first in-frame ATG codon was nucleotide +1. Amino acids were numbered so that methionine encoded by the first in-frame ATG codon was Met1.

AFG3L2 and paraplegin yeast expression plasmids

Plasmids for heterologous expression of human AFG3L2 and paraplegin in yeast were generated as previously described [Di Bella et al.2010]. Seven of the nine mutations identified in our patients (AFG3L2^{T444A}, AFG3L2^{L772F}, AFG3L2^{I473V}, AFG3L2^{K569del} AFG3L2^{K687T}, AFG3L2G6^{M666V}, AFG3L2^{K687T}) were introduced into the yeast AFG3L2 expression construct pYC6/CT*ADH1*-AFG3L2-V5/HIS using the QuikChange XL Site-Directed Mutagenesis Kit (Stratagene) (**Supplementary Table 1**).The other two mutations (AFG3L2^{A86P}, AFG3L2$^{82-84del}$,) were obtained by Gene Synthesis Service (Eurofins MWGoperon); the gene region between EcoRI and AspI carring these mutation were synthesised and subsequently subcloned into our plasmid. Mutagenized plasmids were verified by DNA sequencing. The yeast AFG3L2 expression construct carring the five mutations previously described in [Cagnoli et al., 2010], (AFG3L2^{T654I}, AFG3L2^{G671R}, AFG3L2^{G671E}, AFG3L2^{M666T} AFG3L2^{M666R}), were performed by

Brusco Lab using the QuikChange XL Site-Directed Mutagenesis Kit (Stratagene).

For human paraplegin expression, plasmid YCplac111*ADH1*-Yta10(1-63)-paraplegin(59-795)-HA (abbreviated into YCplac111*ADH1*-paraplegin-HA) was used as previously described [Di Bella et al., 2010].

Yeast strains and growth conditions

All the strains used in this study are derivatives of W303 (K699, *MATa ho ade2-1 trp1-1 can1-100 leu2-3,12 his3-11,15 ura3 ssd1*) (**Supplementary Table 2**). Deletions of *YTA10* and *YTA12* (*yta10yta12* strain) were generated using the one-step PCR system [Longtine et al., 1998]. Standard genetic procedures were followed for strain generation [Adams et al. 1997]. Yeast strains were transformed with the described vectors. Cells were grown at 28°C on YEP medium (1%-yeast extract, 2%-peptone, 2%-agar for plates) or selective medium supplemented with 2% (wt/vol) glucose according to standard procedures. Blasticidin-resistant transformants were selected on YEP medium supplemented with 50 µg of blasticidin S per ml. For complementation experiments, equal amounts of five-fold serial dilutions of cells from exponentially grown cultures were spotted onto YEP plates containing 2% (wt/vol) glucose (YPD) or 2% (wt/vol) glycerol (YPG) and incubated at 28°C or 37°C.

For growth rate analysis, we precultured overnight yeast cells in selective medium supplemented with 2% (wt/vol)

galactose and 0.1% (wt/vol) glucose and then cultured them in YEP medium supplemented with 2% (wt/vol) glycerol for 24 h, inoculated at a standard density of approximately 1×10^6 cells/ml. We removed samples at 0, 20 and 24h and determined cell density spectrophotometrically, expressed as OD_{600}.

For Western blot analysis yeast cells were cultured overnight in selective medium supplemented with 2% (wt/vol) galactose and 0.1% (wt/vol) glucose and normalized spectrophotometrically at OD_{600}.

Antibodies

Polyclonal antisera directed against human AFG3L2 and paraplegin were raised in rabbit as previously described [Di Bella et al., 2010]. Anti-yeast MrpL32 and anti-Ccp1 [Koppen et al., 2007] were as previously reported. Anti-ßactin antibody was from Abcam.

Protein blot analysis

For Western blot analysis of yeast cells, trichloroacetic acid (TCA) protein extracts were prepared as described [Muzi-Falconi et al., 1993]. Protein extracts were separated by SDS-PAGE in 10% or 15% acrylamide gels and transferred to a PVDF membrane (Immobilon LF, Millipore). Filters were probed with anti-yMrpL32 and anti-Ccp1 (1:1,000 dilution) [Koppen et al., 2007], and anti-ßactin antibodies (1:1,500 dilution) and revealed by Alexa Fluor®647-coniugated goat anti-rabbit IgG (H+L) and antibody and Alexa Fluor®488-coniugated goat anti-

mouse IgG (H+L) antibody (Molecular probes). Fluorescence signals were acquired using G:BOX iChemi (Syngene); quantification was performed using Gene Tools software (Syngene) on four independent Western Blots normalizing the signals to the ß-actin loading control.

Supplementary Material

Supplementary Table 1. Oligonucleotide primers used for site-directed mutagenesis of *AFG3L2* cDNA

Mutant		**Primer pairs (5'->3')**
AFG3L2^{T444A}	Forward	GAGATGGATGGTTTTAATACACAACAAATGTCGTCATTTTGG
	Reverse	CCAAAATGACGACATTTGTTGTGTATTAAAACCATCCATCTC
AFG3L2^{L772F}	Forward	GGATGAGGACACCTCATTTCCAGAAGGCCTTAA
	Reverse	CTTAAGGCCTTCTGGAAATGAGGTGTCCTCATC
AFG3L2^{I473V}	Forward	CGTTTCGACAGGCAGGTCTTTATTGGACCAC
	Reverse	GTGGTCCAATAAAGACCTGCCTGTCGAAACG
AFG3L2^{K687T}	Forward	ACATGGTATTGGAGACACCTTACAGTGAAGCC
	Reverse	GGCTTCACTGATAGGTGTCTCCAATACCATGTC
AFG3L2^{K569del}	Forward	GCCTGAGGAGAAGACTGTGGCATACCAC
	Reverse	GTGGTATGCCACAGTCTTCTCCTCAGGC
AFG3L2^{M666V}	Forward	CCAATTGTTCAGTTTGGCGTGAATGAAAAGGTTGGGC
	Reverse	GCCCAACCTTTTCATTCACGCCAAACTGAACAATTGG
AFG3L2^{R679C}	Forward	CTTTGACCTCCCATGTCAGGGGGACATG
	Reverse	ATGTCCCCCTGACATGGGAGGTCAAAGG

Supplemenatry Table 2. *Saccharomyces cerevisiae* strains used in this study

Strain	Relevant genotype	Origin
K699	*MATa ho ade2-1 his3-11,15 leu2-3,112 trp1-1 ura3-52 can1-100 ssd1*	Ref. (Nasmyth et al., 1990]
yDDB64	*MATa ade2-1 his3-11,15 leu2-3,112 trp1-1 ura3-52 can1-100 yta10::NAT yta12::KanMX6*	Ref. [Di Bella 2010]
yDDB79	*MATa ade2-1 his3-11,15 leu2-3,112 trp1-1 ura3-52 can1-100 yta10::NAT yta12::KanMX6* pYC6/CT^{ADH1}-Yta10(1-63)-AFG3L2(66-797)-V5/HIS	Ref. [Di Bella 2010]
yDDB165	*MATa ade2-1 his3-11,15 leu2-3,112 trp1-1 ura3-52 can1-100 yta10::NAT yta12::KanMX6* pYC6/CT^{ADH1}-Yta10(1-63)-AFG3L2(66-797)-V5/HIS YCpLac111^{ADH1}-Yta10(1-63)-paraplegin(59-795)-HA	Ref. [Di Bella 2010]
yDDB159	*MATa ade2-1 his3-11,15 leu2-3,112 trp1-1 ura3-52 can1-100 yta10::NAT yta12::KanMX6* pYC6/CT^{ADH1}-Yta10(1-63)-AFG3L2(66-797)^{T444A}-V5/HIS	This study
yDDB176	*MATa ade2-1 his3-11,15 leu2-3,112 trp1-1 ura3-52 can1-100 yta10::NAT yta12::KanMX6* pYC6/CT^{ADH1}-Yta10(1-63)-AFG3L2(66-797) ^{T444A}-V5/HIS YCpLac111^{ADH1}-Yta10(1-63)-paraplegin(59-795)-HA	This study
yDDB193	*MATa ade2-1 his3-11,15 leu2-3,112 trp1-1 ura3-52 can1-100 yta10::NAT yta12::KanMX6* pYC6/CT^{ADH1}-Yta10(1-63)-AFG3L2(66-797)^{L772F}-V5/HIS	This study

Strain	Relevant genotype	Origin
yDDB195	*MATa ade2-1 his3-11,15 leu2-3,112 trp1-1 ura3-52 can1-100 yta10::NAT yta12::KanMX6* pYC6/CT^{ADH1}-Yta10(1-63)-AFG3L2(66-797)^{L772F} -V5/HIS YCpLac111^{ADH1}-Yta10(1-63)-paraplegin(59-795)-HA	This study
yDDB226	*MATa ade2-1 his3-11,15 leu2-3,112 trp1-1 ura3-52 can1-100 yta10::NAT yta12::KanMX6* pYC6/CT^{ADH1}-Yta10(1-63)-AFG3L2(66-797)^{A86P}-V5/HIS	This study
yDDB222	*MATa ade2-1 his3-11,15 leu2-3,112 trp1-1 ura3-52 can1-100 yta10::NAT yta12::KanMX6* pYC6/CT^{ADH1}-Yta10(1-63)-AFG3L2(66-797)^{A86P} -V5/HIS YCpLac111^{ADH1}-Yta10(1-63)-paraplegin(59-795)-HA	This study
yDDB232	*MATa ade2-1 his3-11,15 leu2-3,112 trp1-1 ura3-52 can1-100 yta10::NAT yta12::KanMX6* pYC6/CT^{ADH1}-Yta10(1-63)-AFG3L2(66-797)^{I473V}-V5/HIS	This study
yDDB223	*MATa ade2-1 his3-11,15 leu2-3,112 trp1-1 ura3-52 can1-100 yta10::NAT yta12::KanMX6* pYC6/CT^{ADH1}-Yta10(1-63)-AFG3L2(66-797)^{I473V} -V5/HIS YCpLac111^{ADH1}-Yta10(1-63)-paraplegin(59-795)-HA	This study
yDDB220	*MATa ade2-1 his3-11,15 leu2-3,112 trp1-1 ura3-52 can1-100 yta10::NAT yta12::KanMX6* pYC6/CT^{ADH1}-Yta10(1-63)-AFG3L2(66-797)$^{82.84del}$-V5/HIS	This study
yDDB221	*MATa ade2-1 his3-11,15 leu2-3,112 trp1-1 ura3-52 can1-100 yta10::NAT yta12::KanMX6* pYC6/CT^{ADH1}-Yta10(1-63)-AFG3L2(66-797)$^{82.84del}$-V5/HIS YCpLac111^{ADH1}-Yta10(1-63)-paraplegin(59-795)-HA	This study
yDDB162	*MATa ade2-1 his3-11,15 leu2-3,112 trp1-1 ura3-52 can1-100 yta10::NAT yta12::KanMX6* pYC6/CT^{ADH1}-Yta10(1-63)-AFG3L2(66-797)^{K687T}-V5/HIS	This study

Strain	Relevant genotype	Origin
yDDB179	*MATa ade2-1 his3-11,15 leu2-3,112 trp1-1 ura3-52 can1-100 yta10::NAT yta12::KanMX6* pYC6/CT^{ADH1}-Yta10(1-63)-AFG3L2(66-797)^{K687T} -V5/HIS YCpLac111^{ADH1}-Yta10(1-63)-paraplegin(59-795)-HA	This study
yDDB146	*MATa ade2-1 his3-11,15 leu2-3,112 trp1-1 ura3-52 can1-100 yta10::NAT yta12::KanMX6* pYC6/CT^{ADH1}-Yta10(1-63)-AFG3L2(66-797)^{T654I}-V5/HIS	This study
yDDB149	*MATa ade2-1 his3-11,15 leu2-3,112 trp1-1 ura3-52 can1-100 yta10::NAT yta12::KanMX6* pYC6/CT^{ADH1}-Yta10(1-63)-AFG3L2(66-797)^{T654I} -V5/HIS YCpLac111^{ADH1}-Yta10(1-63)-paraplegin(59-795)-HA	This study
yDDB203	*MATa ade2-1 his3-11,15 leu2-3,112 trp1-1 ura3-52 can1-100 yta10::NAT yta12::KanMX6* pYC6/CT^{ADH1}-Yta10(1-63)-AFG3L2(66-797)^{K659del}-V5/HIS	This study
yDDB204	*MATa ade2-1 his3-11,15 leu2-3,112 trp1-1 ura3-52 can1-100 yta10::NAT yta12::KanMX6* pYC6/CT^{ADH1}-Yta10(1-63)-AFG3L2(66-797)^{K659del}-V5/HIS YCpLac111^{ADH1}-Yta10(1-63)-paraplegin(59-795)-HA	This study
yDDB148	*MATa ade2-1 his3-11,15 leu2-3,112 trp1-1 ura3-52 can1-100 yta10::NAT yta12::KanMX6* pYC6/CT^{ADH1}-Yta10(1-63)-AFG3L2(66-797)^{G671R}-V5/HIS	This study
yDDB154	*MATa ade2-1 his3-11,15 leu2-3,112 trp1-1 ura3-52 can1-100 yta10::NAT yta12::KanMX6* pYC6/CT^{ADH1}-Yta10(1-63)-AFG3L2(66-797)^{G671R}-V5/HIS YCpLac111^{ADH1}-Yta10(1-63)-paraplegin(59-795)-HA	This study
yDDB147	*MATa ade2-1 his3-11,15 leu2-3,112 trp1-1 ura3-52 can1-100 yta10::NAT yta12::KanMX6* pYC6/CT^{ADH1}-Yta10(1-63)-AFG3L2(66-797)^{G671E}-V5/HIS	This study

Strain	Relevant genotype	Origin
yDDB153	*MATa ade2-1 his3-11,15 leu2-3,112 trp1-1 ura3-52 can1-100 yta10::NAT yta12::KanMX6* pYC6/CT^{ADH1}-Yta10(1-63)-AFG3L2(66-797)^{G671E}-V5/HIS YCpLac111^{ADH1}-Yta10(1-63)-paraplegin(59-795)-HA	This study
yDDB161	*MATa ade2-1 his3-11,15 leu2-3,112 trp1-1 ura3-52 can1-100 yta10::NAT yta12::KanMX6* pYC6/CT^{ADH1}-Yta10(1-63)-AFG3L2(66-797)^{R679C}-V5/HIS	This study
yDDB178	*MATa ade2-1 his3-11,15 leu2-3,112 trp1-1 ura3-52 can1-100 yta10::NAT yta12::KanMX6* pYC6/CT^{ADH1}-Yta10(1-63)-AFG3L2(66-797)^{R679C}-V5/HIS YCpLac111^{ADH1}-Yta10(1-63)-paraplegin(59-795)-HA	This study
yDDB144	*MATa ade2-1 his3-11,15 leu2-3,112 trp1-1 ura3-52 can1-100 yta10::NAT yta12::KanMX6* pYC6/CT^{ADH1}-Yta10(1-63)-AFG3L2(66-797)^{M666V}-V5/HIS	This study
yDDB151	*MATa ade2-1 his3-11,15 leu2-3,112 trp1-1 ura3-52 can1-100 yta10::NAT yta12::KanMX6* pYC6/CT^{ADH1}-Yta10(1-63)-AFG3L2(66-797)^{M666V}-V5/HIS YCpLac111^{ADH1}-Yta10(1-63)-paraplegin(59-795)-HA	This study
yDDB143	*MATa ade2-1 his3-11,15 leu2-3,112 trp1-1 ura3-52 can1-100 yta10::NAT yta12::KanMX6* pYC6/CT^{ADH1}-Yta10(1-63)-AFG3L2(66-797)^{M666T}-V5/HIS	This study
yDDB150	*MATa ade2-1 his3-11,15 leu2-3,112 trp1-1 ura3-52 can1-100 yta10::NAT yta12::KanMX6* pYC6/CT^{ADH1}-Yta10(1-63)-AFG3L2(66-797)^{M666T}-V5/HIS YCpLac111^{ADH1}-Yta10(1-63)-paraplegin(59-795)-HA	This study
yDDB145	*MATa ade2-1 his3-11,15 leu2-3,112 trp1-1 ura3-52 can1-100 yta10::NAT yta12::KanMX6* pYC6/CT^{ADH1}-Yta10(1-63)-AFG3L2(66-797)^{M666R}-V5/HIS	This study

Strain	Relevant genotype	Origin
yDDB152	*MATa ade2-1 his3-11,15 leu2-3,112 trp1-1 ura3-52 can1-100 yta10::NAT yta12::KanMX6* pYC6/CT^{ADH1}-Yta10(1-63)-AFG3L2(66-797)^{M666R}-V5/HIS YCpLac111^{ADH1}-Yta10(1-63)-paraplegin(59-795)-HA	This study

References

- Adams A, Gottschling DE, Kaiser CA, Stearns T. 1997. Methods in Yeast Genetics. A Cold Spring Harbor Laboratory Course Manual (Cold Spring Harbor Laboratory Press, Cold Spring Harbor, NY).
- Arlt H, Tauer R, Feldmann H, Neupert W, Langer T. 1996. The YTA10-12 complex, an AAA protease with chaperone-like activity in the inner membrane of mitochondria. Cell 85:875-885.
- Banfi S et al. 1999. Identification and characterization of AFG3L2, a novel paraplegin-related gene. Genomics 59:51-58.
- Cagnoli C et al. 2010. Missense Mutations in the AFG3L2 Proteolytic Domain Account for ~1.5% of European Autosomal Dominant Cerebellar Ataxias. Hum Mutat 31:1117–1124.
- Casari G et al. 1998. Spastic paraplegia and OXPHOS impairment caused by mutations in paraplegin, a nuclear-encoded mitochondrial metalloprotease. Cell 93:973-983.
- Di Bella D et al. 2010. Mutations in the mitochondrial protease gene AFG3L2 cause dominant hereditary ataxia SCA28. Nat Genet 42:313-321.
- Dürr A. 2010. Autosomal dominant cerebellar ataxias: polyglutamine expansions and beyond. Lancet Neurol 9:885-894.
- Esser K, Tursun B, Ingenhoven M, Michaelis G, Pratje E. 2002. A novel two-step mechanism for removal of a mitochondrial signal sequence involves the mAAA complex and the putative rhomboid protease Pcp1. J Mol Biol 323:835-843.
- Fontanesi F, Diaz F, Barrientos A. 2009. Evaluation of the mitochondrial respiratory chain and oxidative phosphorylation system using yeast models of OXPHOS deficiencies. Curr Protoc Hum Genet Chapter 19:Unit19.5.
- Gellera C et al. 2007. Frataxin gene point mutations in Italian Friedreich ataxia patients. Neurogenetics 8:289-299.

- Koppen M, Langer T. 2007. Protein degradation within mitochondria: versatile activities of AAA proteases and other peptidases. Crit Rev Biochem Mol Biol 42:221-242.
- Koppen M, Metodiev MD, Casari G, Rugarli EI, Langer T. 2007. Variable and tissue-specific subunit composition of mitochondrial m-AAA protease complexes linked to hereditary spastic paraplegia. Mol Cell Biol 27:758-767.
- Longtine MS et al. 1998. Additional modules for versatile and economical PCR-based gene deletion and modification in Saccharomyces cerevisiae. Yeast 14:953-961.
- Mariotti C et al. 2008. Spinocerebellar ataxia type 28: A novel autosomal dominant cerebellar ataxia characterized by slow progression and ophthalmoparesis. Cerebellum 7:184-188.
- Muzi-Falconi M et al. 1993. De novo synthesis of budding yeast DNA polymerase alpha and POL1 transcription at the G1/S boundary are not required for entrance into S phase. Proc Natl Acad Sci USA 90:10519-10523.
- Nolden M et al. 2005. The *m*-AAA protease defective in hereditary spastic paraplegia controls ribosome assembly in mitochondria. Cell 123:277-289.
- Taroni F, DiDonato S. 2004. Pathways to motor incoordination: the inherited ataxias. Nature Rev Neurosci 5:641-655.
- Tatsuta T, Augustin S, Nolden M, Friedrichs B and Langer T. 2007. *m*-AAA protease-driven membrane dislocation allows intramembrane cleavage by rhomboid in mitochondria. EMBO J 26:325-335.
- Tatsuta T, Langer T. 2008. Quality control of mitochondria: protection against neurodegeneration and ageing. EMBO J. 27:306–314.

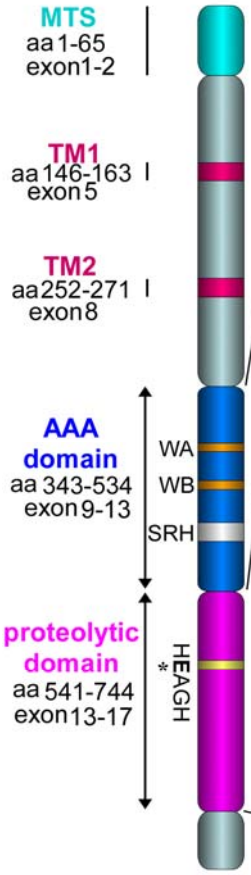

Variant	Exon location	Reference
N82_K84del	3	This study
A86P	3	This study
H126Q	4	Di Bella 2010
N432T	10	Di Bella 2010
T444A	11	This study
I473V	11	This study
K569del	14	This study
T654I	15	Cagnoli 2010
M666R	16	Cagnoli 2010
M666T	16	Cagnoli 2010
M666V	16	This study - Cagnoli 2010
G671E	16	Cagnoli 2010
G671R	16	Cagnoli 2010
S674L	16	Di Bella 2010
R679C	16	This study
K687T	16	This study
E691K	16	Di Bella 2010
A694E	16	Di Bella 2010
E700K	16	Edener 2010
R702Q	16	Di Bella 2010
L772F	17	This study

Figure 1

All variations identified in the *AFG3L2* gene

The domain structure of human AFG3L2 is shown in the left part of the figure. MTS, mitochondrial targeting sequence; TM1 and TM2, transmembrane domains 1 and 2, respectively, AAA domain with WA (Walker-A motif), WB (Walker-B motif) SRH (second region of homology). Proteolytic domain with the protease catalytic site (HEAGH motif). Variations (in blue, variations in the AAA domain; in magenta, variations in the proteolytic domain), exon location, and reference are reported in the right part of the figure.

Figure 2

Amino acid conservation

ClustalW2 multiple alignment (http://www.ebi.ac.uk/Tools/clustalw2/index.html) of variations of human AFG3L2 with members of the *m*-AAA family from different organisms: Human AFG3L2, Mouse afg3l2, Mouse afg3l1, *Dr. mel.* (*Drosophila melanogaster*); *C. el.* (*Caenorhabditis elegans*); *S. cer.* (*Saccharomyces cerevisiae*) Yta10p; *Human paraplegin*, *S. cer.* (*Saccharomyces cerevisiae*) Yta12p; *Th. therm*. (*Thermus thermophilus*) FtsH.

The nucleotide position, nucleotide change and mutated residues are indicated above the alignment.

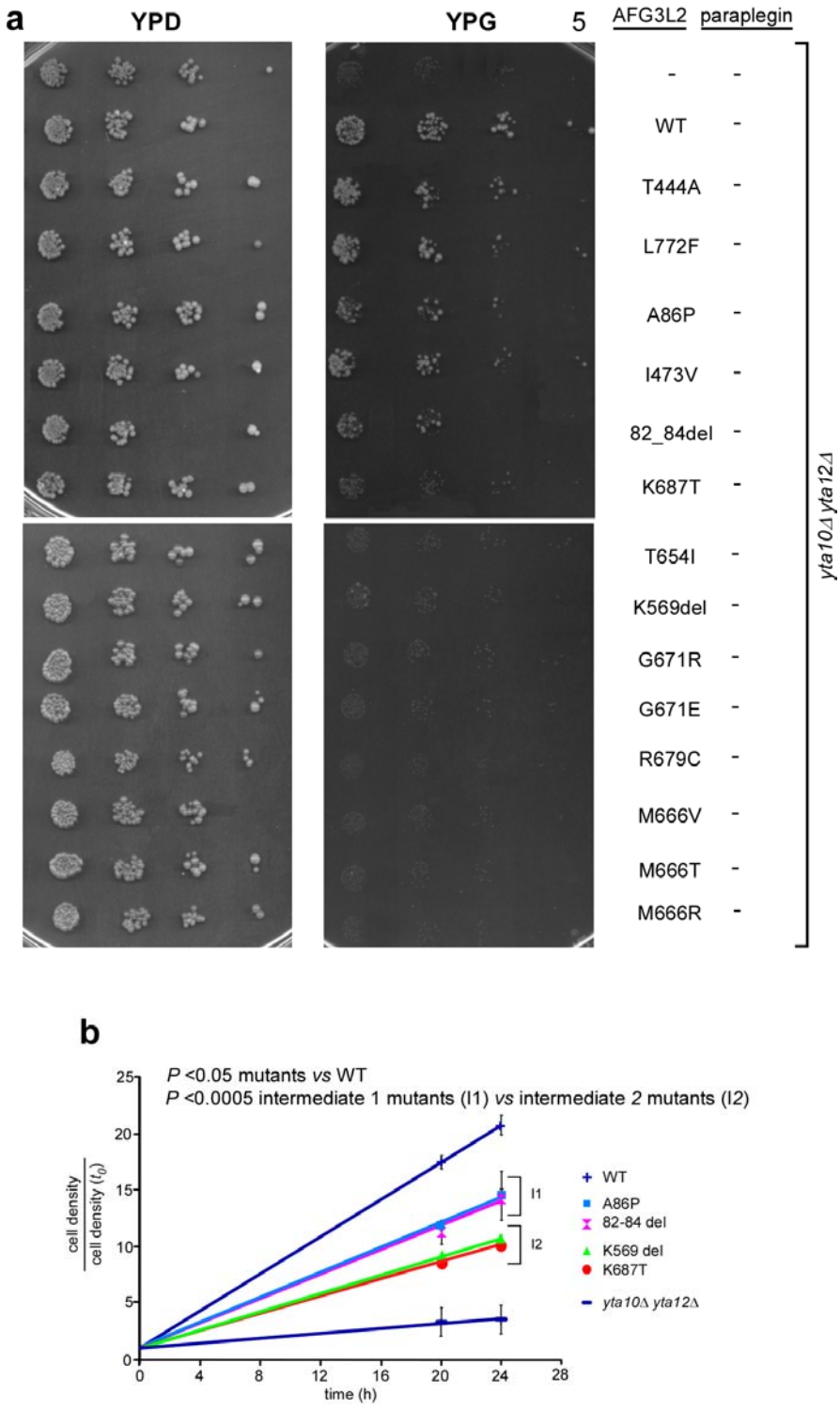
a
YPD
YPG
5
AFG3L2
paraplegin
-
WT
T444A
L772F
A86P
I473V
82_84del
K687T
T654I
K569del
G671R
G671E
R679C
M666V
M666T
M666R
yta10Δ yta12Δ
b
P <0.05 mutants vs WT
P <0.0005 intermediate 1 mutants (I1) vs intermediate 2 mutants (I2)
cell density
cell density (t0)
time (h)
I1
I2
WT
A86P
82-84 del
K569 del
K687T
yta10Δ yta12Δ

Figure 3

Complementation studies in *Saccharomyces cerevisiae*

(**a**) Serial dilutions of cells from exponentially grown cultures were spotted onto YEP plates containing either 2%(wt/vol) glucose (left panels, YPD) or 2%(wt/vol) glycerol (right panels, YPG) and they are incubated at 28°C. Respiratory competence is deduced by the ability to grow on glycerol (YPG). We analyse the respiratory phenotype of yta10Δyta12Δ cells expressing either normal (WT) or mutant human AFG3L2 at 28°C.

(**b**) The graph show the growth rates of cells expressing either $AFG3L2^{WT}$ or some mutants. Cells were grown in YEP medium supplemented with 2% (wt/vol) galactose-0.1% (wt/vol) glucose for 24 hours at 28°C. Values on the *y*-axis represent the ratio between cell density (= number of cells/ml) at a given time and cell density at start (*t0*). The cells are counted at 0, 20, and 24 hours. Each value represents the mean of five independent experiments. Error bars indicate s.d.. Statistical significance, determined by Student's t-test, is $P < 0.05$ for mutants vs WT and $P < 0.0005$ for intermediate subgroup 1 mutants (I1) *vs.* intermediate subgroup 2 mutants (I2). Growth rates are calculated by linear regression analysis (trend line).

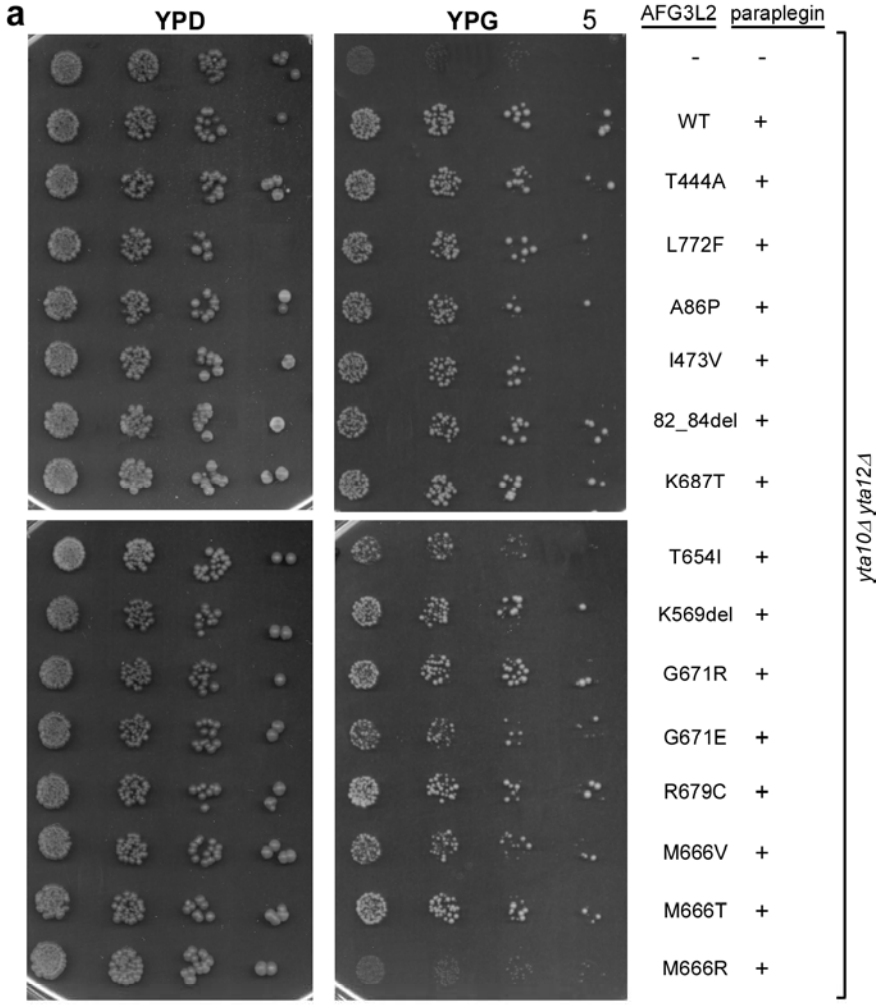
a
YPD
YPG
5
AFG3L2
paraplegin
-
-
WT
+
T444A
+
L772F
+
A86P
+
I473V
+
82_84del
+
K687T
+
T654I
+
K569del
+
G671R
+
G671E
+
R679C
+
M666V
+
M666T
+
M666R
+
yta10Δ yta12Δ

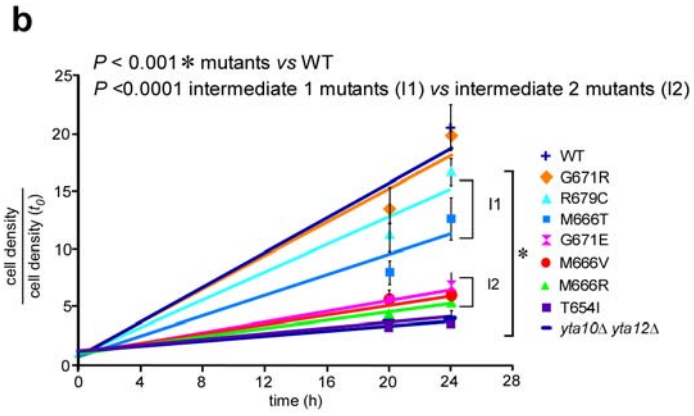
b
P < 0.001 * mutants vs WT
P <0.0001 intermediate 1 mutants (I1) vs intermediate 2 mutants (I2)
cell density / cell density (t0)
time (h)
I1
I2
*
WT
G671R
R679C
M666T
G671E
M666V
M666R
T654I
yta10Δ yta12Δ

Figure 4

Complementation studies in *Saccharomyces cerevisiae*

(**a**) Serial dilutions of cells from exponentially grown cultures were spotted onto YEP plates containing either 2% (wt/vol) glucose (left panels, YPD) or 2%(wt/vol) glycerol (right panels, YPG). and they are incubated at 28°C. Respiratory competence is deduced by the ability to grow on glycerol (YPG). Respiratory phenotype of *yta10*Δ*yta12*Δ cells coexpressing either normal or mutant human AFG3L2 with human paraplegin at 28°C.

(**b**) The graphs show the growth rates of cells coexpressing either normal or some mutants human AFG3L2 with human paraplegin. Cells were grown in YEP medium supplemented with 2% (wt/vol) galactose-0.1% (wt/vol) glucose for 24 hours at 28°C. Values on the *y*-axis represent the ratio between cell density (= number of cells/ml) at a given time and cell density at start (*t0*). The cells are counted at 0, 20, and 24 hours. Each value represents the mean of five independent experiments. Error bars indicate s.d.. Asterisk indicate statistical significance, determined by Student's t-test. For strains grow at 28°C is $P < 0.001$ for mutants vs WT and $P < 0.0001$ for intermediate subgroup 1 mutants (I1) *vs.* intermediate subgroup 2 mutants (I2). Growth rates are calculated by linear regression analysis (trend line).

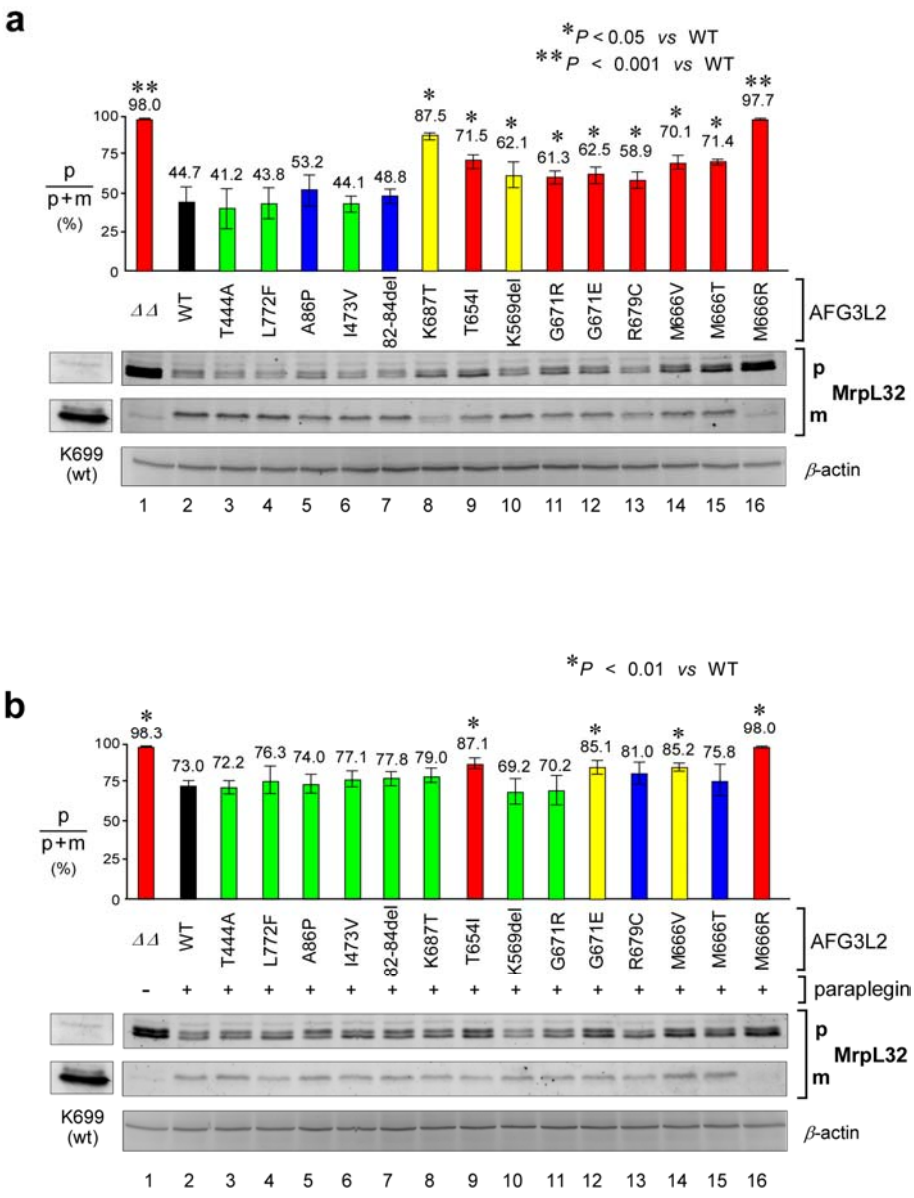

Figure 5

Proteolytic activity of normal and mutant AFG3L2 expressed in yeast

(**a**) Fluorescence immunoblot analysis with anti-MrpL32 in yeast cells expressing mutant AFG3L2. Immunoblotting was

performed using polyclonal antisera directed against MrpL32. p (precursor form); m (mature form). AFG3L2 proteolytic competence is expressed as the ratio of pMrpL32 level to total (p + m) MrpL32 level. MrpL32 levels were normalized to the loading control protein β-actin. Histogram above immunoblot reports quantitative results and it represents the mean of four experiments. The colours of histograms symbolize the respiratory growth: wt in black, grow strains in green, slow strains in blue, slower strains in yellow and no grow strainsin red. Error bars indicate s.d.. Asterisks indicate a statistically significant (P <0.05 or P <0.001) difference from AFG3L2^{WT} as determined by Student's *t*-test.

(**b**) Proteolytic activity of normal and mutant AFG3L2 in the presence of paraplegin coexpression. Analysis performed under the same conditions described above. In these experiments statistically significant difference from AFG3L2^{WT} is P <0.01)

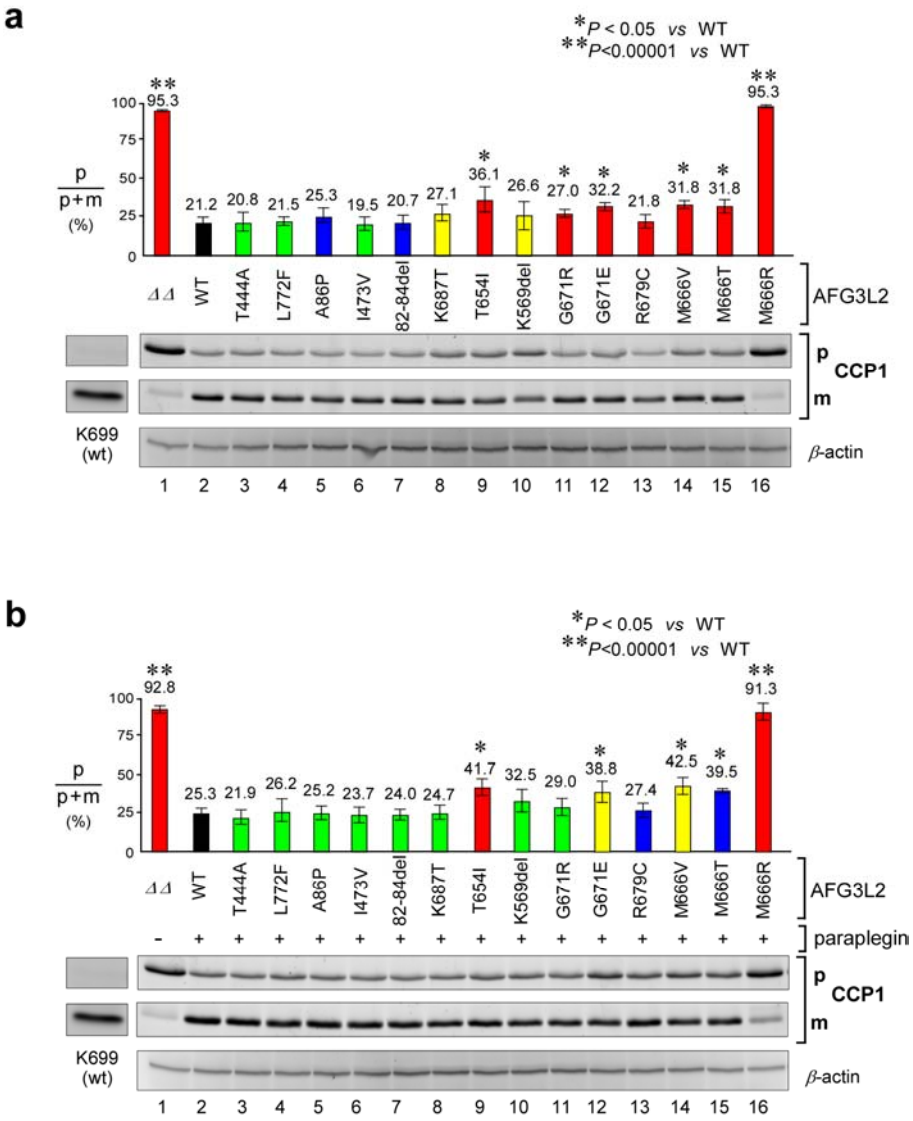

Figure 6

Proteolytic activity of normal and mutant AFG3L2 expressed in yeast

(**a**) Fluorescence immunoblot analysis with anti-Ccp1 in yeast cells expressing mutant AFG3L2. Immunoblotting was performed using polyclonal antisera directed against Ccp1. p (precursor form); m (mature form). AFG3L2 proteolytic competence is expressed as the ratio of p Ccp1level to total (p + m) Ccp1 level. Ccp1 levels were normalized to the loading control protein β-actin. Histogram above immunoblot reports quantitative results and it represents the mean of five experiments. Error bars indicate s.d. Asterisks indicate a statistically significant (P <0.05 or P <0.00001) difference from $AFG3L2^{WT}$ as determined by Student's t-test.

(**b**) Proteolytic activity of normal and mutant AFG3L2 in the presence of paraplegin coexpression. Analysis performed under the same conditions described above.

AFG3L2 genotype	AFG3L2			AFG3L2 + paraplegin		
	respiratory growth	MrpL32 processing	Ccp1 processing	respiratory growth	MrpL32 processing	Ccp1 processing
ΔΔ	-	-	-	-	-	-
WT	+++	+	+	+++	+	+
T444A	+++	+	+	+++	+	+
L772F	+++	+	+	+++	+	+
A86P	++	+	+	+++	+	+
I473V	+++	+	+	+++	+	+
82-84del	++	+	+	+++	+	+
K687T	+	-	-	+++	+	+
T654I	-	-	-	-	-	-
K569del	+	-	-	+++	+	+
G671R	-	-	-	+++	+	+
G671E	-	-	-	+	-	-
R679C	-	-	+	++	+	+
M666V	-	-	-	+	-	-
M666T	-	-	-	++	+	-
M666R	-	-	-	-	-	-

Table 1. Respiratory growth: (**+++**) indicates growth similar to AFG3L2 ^{WT}, (**++**) indicates intermediate growth I1, (**+**) indicates intermediate growth I2 and (-) indicates absence of growth. Processing activity: (**+**) indicates proteolytic activity with no statistically significant difference from that of AFG3L2^{WT}, (**-**) indicates a statistically significant difference ($P \leq 0.05$) between proteolytic activity of mutant AFG3L2 and that of AFG3L2^{WT}.

Chapter 4

Summary, conclusions and future perspectives

In my PhD project, I focussed on two main aspects. First, I wanted to demonstrate that mutations in *AFG3L2* cause dominant SCA type 28. I have screened for mutations the *AFG3L2* gene in a large sample of ataxic patients. The second aspect has regarded the functional characterization of the mutations involved in SCA28 pathogenesis with the validation of their pathogenic role.

Autosomal dominant spinocerebellar ataxias (SCAs) are a clinically and genetically heterogeneous group of diseases caused by progressive degeneration of the cerebellum which leads to a complex movement disorder, whose principal symptoms are the progressive loss of motor coordination and difficulties in executing voluntary movements. Thirty-one SCA loci are currently known. The diseases are caused by both expansion of tri- or pentanucleotide repeats and deletions, missense, nonsense or frameshift mutations in the corresponding genes (http://neuromuscular.wustl.edu/ataxia/domatax.html) (Taroni, F. & Di Donato, 2004). Linkage analysis previously conducted in the Laboratory of Genetics of Neurodegenerative and Metabolic Disease of Carlo Besta Neurologic Institute, where I carried out my PhD project, allowed us to map a new SCA locus on chromosome region 18p11.22–q11.2.99, called

SCA28. Chromosome 18 has never been associated with hereditary cerebellar ataxias (Cagnoli, C. et al., 2006).

Genetic analysis of the critical region of the SCA28 locus has been conducted in the family positive to linkage analysis. All the affected subjects are characterized by a missense mutation (E691K) in the exon 16 of the *AFG3L2* gene demonstrating that *AFG3L2* is the causative gene for SCA28.

In total, we have screened 570 individuals with progressive ataxic phenotype consistent with a SCA28 clinical features. We have identified 13 heterozygous *AFG3L2* missense mutations and 2 heterozygous small in-frame deletions in affected individuals that were absent in >400 control chromosomes. Notably, most of the substitutions affect highly conserved functional domains of AFG3L2. Nine variations were located in the proteolytic domain, the majority of them in exon 16, except for one mutation in exon 14 (K569del) and one in exon 17 (L772F). Three variations are located in the AAA-domain. Only three substitutions have been identified outside the functional domains: two in exon 3 and one in exon 4. The identified mutations confirmed that *AFG3L2* is the disease-gene responsible for spinocerebellar ataxia type 28.

AFG3L2 and its protein partner paraplegin are metalloproteases that are components of the mitochondrial AAA (*m*-AAA) protease. These two proteins form a hexameric complex located on the inner mitochondrial membrane and active on its matrix side (Casari et al.,1998). The *m*-AAA protease carries out protein quality control by degrading non-assembled or

damaged inner-membrane proteins and participates in processing and maturation of some mitochondrial proteins (Koppen, M. & Langer, T., 2007). The importance of *m*-AAA in humans is underlined by the evidence that mutations in both genes are responsible for important neurodegenerative diseases: an autosomal recessive form of hereditary spastic paraparesis (SPG7) is caused by mutations in the *SPG7* gene encoding paraplegin (Casari et al.,1998) while autosomal dominant spinocerebellar ataxia type 28 (SCA28) is caused by mutations in the *AFG3L2* gene. Notably, dominant ataxia has never been associated with mitochondrial dysfunction. Moreover, most of the diseases caused by mutations in nuclear genes encoding mitochondrial proteins are usually recessive as in the case of SPG7/paraplegin.

Expression studies in an *m*-AAA–deficient *S. cerevisiae* strain (*yta10*Δ *yta12*Δ) allowed to establish the functional role of the amino acid variants discriminating between real mutations and rare/unique benign variants. Analysis of the respiratory phenotype of cells AFG3L2^{mut} suggests that four substitutions are rare/unique benign variants (AFG3L2^{H126Q}, AFG3L2^{T444A}, AFG3L2^{I473V}, and AFG3L2^{L772F}), four substitutions are possibly pathogenic (AFG3L2^{82N_84Kdel}, AFG3L2^{A86P}, AFG3L2^{K569del} and AFG3L2^{K687T}), and twelve substitutions are certainly pathogenic (AFG3L2^{N432T}, AFG3L2^{T654I}, AFG3L2^{M666R}, AFG3L2^{M666T}, AFG3L2^{M666V}, AFG3L2^{G671E}, AFG3L2^{G671R}, AFG3L2^{S674LR}, AFG3L2^{R679C}, AFG3L2^{E691K}, AFG3L2^{A694E} and AFG3L2^{R702Q}). Among the pathogenic mutations only one is located outside

the proteolytic domain, the N432T mutation located in the ATPase domain.

The co-expression of paraplegin or AFG3L2^{WT} with AFG3L2^{mut} allowed to discriminate further pathomechanisms of pathogenic mutations. Analysis of the respiratory phenotype of these strains suggested that two classes of *AFG3L2* mutations exist: the majority of mutations (AFG3L2^{M666T}, AFG3L2^{M666V}, AFG3L2^{G671E}, AFG3L2^{G671R}, AFG3L2^{S674LR}, AFG3L2^{R679C}, AFG3L2^{A694E} and AFG3L2^{R702Q}) are "paraplegin-responsive" and, if coexpressed with AFG3L2^{WT}, showed a full rescue of defective growth phenotype. In these cases, the mechanism is likely to be haploinsufficiency, or weak dominant negative. These mutations may result in variably reduced penetrance and/or expressivity in affected people. This hypothesis is confirmed by analysis of some family pedigrees. The second group of mutations (AFG3L2^{N432T}, AFG3L2^{T654I}, AFG3L2^{M666R} and AFG3L2^{E691K}) are dominant negative both in homo-oligomeric and hetero-oligomeric complex. These four mutations are expected to be highly penetrant, and the number of affected subjects observed in three of these families is consistent with this hypothesis.

The second part of this project concerned the function of the protein involved in the pathogenesis of SCA28. We analyzed two aspects: first, to better understand the respiratory phenotype, we have investigated the respiratory chain activity, in particular cytochrome *c* oxidase activity (COX, complex IV). Second, AFG3L2 proteolytic activity was investigated by

evaluating the processing of specific substrates such as MrpL32 and Ccp1. We have shown a clear correlation between both respiratory deficiency and the severe defect of respiratory chain complex IV and respiration and proteolytic competence of AFG3L2. The yeast strains with deficient respiratory phenotype showed a reduced level of COX activity and also of some of the subunits that compose the complex. The processing of MrpL32 was also deficient. If the functionality of the complex is lost, even only partially, several mitochondrial proteins could not be degraded correctly. The nervous cells, which need high and constant energy levels to carry out their activity, could be particularly susceptible to this energy deficit and prone to a degenerative process as that observed in the disease affecting these patients.

We investigated the expression of MrpL32 in lymphoblasts of some patients, finding no change compared with healthy control subjects. The expression of OPA1, another possible substrate of mammalian *m*-AAA, and prohibitin-1 (PHB1) and prohibitin-2 (PHB2), two ancillary proteins associated with *m*-AAA complex, was also normal. Naturally, lymphoblasts are not the most appropriate cells to perform biochemical analysis as they might not be particularly affected by a mutation on one single allele.

AFG3L2 and paraplegin proteins and transcripts were found to be highly and selectively expressed in cerebellar Purkinje cells. In contrast expression analysis of AFG3L2 and paraplegin indicates a lower expression of AFG3L2 relative to

paraplegin in the human motor system. These results are in accordance with the differences observed in the phenotypes of individuals affected by mutations in SPG7 or *AFG3L2* gene: mutations in paraplegin cause a progressive spasticity and axonopathy of the corticospinal tract while in patients with mutations *AFG3L2* pyramidal dysfunction is clinically modest.

In conclusion, the data establish AFG3L2 as the molecular cause of the autosomal dominant spinocerebellar ataxia known as SCA28. They also indicate a previously unknown essential role of mitochondrial AFG3L2 homocomplex in protecting the human cerebellum against neurodegeneration. The study has also expanded the spectrum of AFG3L2 mutations allowing to establish a minimum frequency of ~2.5% in patients wit ataxia of unknown origin. The results also indicate that mutations can act through distinct pathomechanisms at the molecular level with a different role in shaping homo- and hetero-mAAA complex activity. Once again, these results indicate the crucial importance of functional studies to validate the pathogenic role of mutations that are not found in large control populations but for which there are insufficient data on segregation in the family. Identification of mutations in AFG3L2 represents an important goal for the diagnosis of SCA because it allows to have a definite diagnosis in a highly clinically and genetically heterogeneous disease. Understanding the pathogenetic mechanisms of neurodegeneration in spinocerebellar ataxias should lead to the identification of potential therapeutic targets. Next experiments

will focus on the identification of specific substrates of the *m*-AAA proteases and may identify novel therapeutic targets for the associated diseases.

- Cagnoli, C. et al. SCA28, a novel form of autosomal dominant cerebellar ataxia on chromosome 18p11.22-q11.2. *Brain* **129**, 235-242 (2006).
- Casari, G. et al. Spastic paraplegia and OXPHOS impairment caused by mutations in paraplegin, a nuclear-encoded mitochondrial metalloprotease. *Cell* **93**, 973-983 (1998).
- Koppen, M. & Langer, T. Protein degradation within mitochondria: versatile activities of AAA proteases and other peptidases. *Crit Rev Biochem Mol Biol* **42**, 221-242 (2007).
- Taroni, F. & Di Donato, S. Pathways to motor incoordination: the inherited ataxias. *Nature Rev Neurosci* **5**, 641-655 (2004).

Chapter 5

Publications

- ***Mutations in the mitochondrial protease gene AFG3L2 cause dominant hereditary ataxia SCA28***
  Di Bella D., Lazzaro F., Brusco A., Plumari M., Battaglia G., Pastore A., Finardi A., Cagnoli C., Tempia F., Frontali M., Veneziano L., Sacco T., Boda E., Brussino A., Bonn F., Castellotti B., Baratta S., Mariotti C., Gellera C., **Fracasso V**., Magri S., Langer T., Plevani P., Di Donato S., Muzi-Falconi M., Taroni F.
  Nature Genetics. 2010 Apr;42(4):313-21

- ***Spinocerebellar ataxia type 28: identification and functional analysis of novel AFG3L2 mutations***
  Fracasso V., Magri S., Plumari M., Muzi-Falconi M., Lazzaro F., Di Bella D.,Taroni F.
  Submitted

- ***Co-immunoprecipitation of human mitochondrial proteases AFG3L2 and paraplegin heterologously expressed in yeast cells***
  Fracasso V., Lazzaro F., Muzi-Falconi M.
  Nature Protocols (2010) DOI: 10.1038/nprot.2010.26

- ***Preparation of yeast mitochondria and in vitro assay of respiratory chain complex activities***
  Magri S., **Fracasso V**., Rimoldi M. and Taroni F.
  Nature Protocols (2010) DOI: 10.1038/nprot.2010.25